University of Nottingham



School of Mathematics

A Study of the Properties of Mesoscopic Consensus Clusters that Arise Due to Ising Dynamics on Graphs

Karthik Sowdi R.B.

A thesis submitted to the University of Nottingham for the degree of

Philosophiæ Doctor

July 2016

ABSTRACT

We studied the impact of graph structure and temperature has on the sizes and lifetimes of crowds (mesoscopic clusters of consensus) that form when due to Ising Spin dynamics. Spin models have proven successful in modelling the formation of global consensus in opinion for large groups of people. We focus on the case where lots of small groups form consensuses but no global consensus forms. Our results can be interpreted in the light of consumer opinion and give an explanation for fads and brand reputation.

Data was obtained by performing Monte Carlo simulations of the Ising Model on various graphs, our key control parameter was the inverse temperature $\beta = 1/k_B T$. In the Ising Model each vertex chooses an opinion -1 or $+1$ each time step based on the opinions of its neighbours. Low $\beta \ll 1$ exhibit as vertices behaving noisily (flipping opinion often), while $\beta \to 1$ tend to be quieter (flipping rarely). Interactions between neighbours creates feedback loops which determine crowd properties. The simulations we perform start with $\beta = 0$ for $0 \leq t < 500$, then the temperature is sharply quenched to a value $\beta_q \geq 0$ and kept constant for $t \in (500, 15000]$. We analyse the data in the time period $13000 \leq t \leq 15000$. The simulations were performed on the 2-d rectangular

lattice (RL), K-degree 1-d circular lattice (CL), Erdős-Rényi (ER), and 1-d Watts-Strogatz (WS) graphs.

We conclude that crowds with multiple unique feedback loops are more robust against noisy vertices and crowd-crowd interactions. On the CL many feedback loops use the same paths which makes it easy for noisy vertices to disrupt the loops simultaneously. However 1-d structure limits crowd-crowd interactions making crowds strong against absorption by their neighbours. On the RL there are many paths between vertices, thus feedback loops can be easily rerouted around noisy vertices and crowds are robust against noise. On weakly connected ER graphs many feedback loops share the same paths and thus crowds are extremely susceptible to noisy vertices. Disorder in the 1-d lattice structure in WS graphs reduces the number of feedback loops in certain regions, this makes some crowds weak against both noisy vertices and neighbouring crowds.

On the RL, CL and WS graphs we observe that size of crowds changes like an anomalous diffusion process. The anomalous diffusion exponent α was determined by plotting the root mean square change in crowd size $\sqrt{\langle \Delta \mathcal{P}^2 \rangle}$ as a function of the crowd lifetime $\mathcal{L}$. On the RL changes in crowd size were super-diffusive for $0.35 \lesssim \beta \lesssim 0.65$; crowds grew very large in short periods of time, however such crowds also had short lifetimes as they were constantly replaced by new crowds. This behaviour is similar to the coming and going of fads. For $0.65 \lesssim \beta \lesssim 1$ crowd sizes changed sub-diffusively, crowds grew in very small amounts to very large sizes over long time periods, this is analogous to the spread of reputation through word of mouth.

ACKNOWLEDGEMENTS

Foremost I would like to thank my supervisors' Prof. Keith Hopcraft and Prof. Simon Preston for their advice and insight during the entirety of my Ph.D study.

My friend David Kirby has my deepest gratitude for his endless optimism and belief in me and my work. I thank him especially for making sure I did not spend all my time in front of a computer.

Finally I thank my parents and my sister for continuing to listen even when they did not understand what I was saying. My parents deserve a great deal of thanks for their support throughout all my life and during the writing period.

CONTENTS

1 INTRODUCTION AND LITERATURE REVIEW 14

1.1 Graph Theory 16

1.1.1 Definitions and Notation Pertaining to Graphs 17

1.1.2 Properties of Graphs 20

1.1.3 Generating Graphs 31

1.1.4 Rectangular Lattice 32

1.1.5 Circular Lattice 36

1.1.6 Erdős-Rényi Graphs 40

1.1.7 Watts-Strogatz Graphs 44

1.2 Spin Models of Voting Behaviour 48

1.2.1 Ising Spin Model 50

1.2.2 Potts Model 54

1.2.3 Consensus Formation 57

1.3 Community Structure in Complex Graphs 60

2 FURTHER DEFINITIONS AND VALIDATION OF SIMULATION 64

2.1 Introduction 64

2.2 Crowds 65

2.2.1 Pre-Processing Spin Data 69

2.2.2 Models of Crowd Population Dynamics 73

2.3 Properties of the Graphs Studied by Simulation 77

2.4 Validation of Ising Model Implementation 82

3 DYNAMICS OF CROWD POPULATIONS 91

3.1 Introduction 91

3.2 Rectangular Lattice 92

3.3 Circular Lattice 100

3.4 Erdős–Rényi Graphs 106

3.5 Watts-Strogatz Graphs 109

3.6 Discussion and Summary 114

4 POPULATION SIZE FREQUENCY DENSITIES 117

4.1 Introduction 117

4.2 Rectangular Lattice 118

4.3 Circular Lattice 122

4.4 Erdős-Rényi Graphs 126

4.5 Watts-Strogatz Graphs 131

4.6 Discussion and Summary 134

5 LIFETIME FREQUENCY DENSITIES 137

5.1 Introduction 137

5.2 Rectangular Lattice 139

5.3 Circular Lattice 144

5.4 Erdős-Rényi Graphs 150

5.5 Watts-Strogatz Graphs 155

5.6 Discussion and Summary 161

6 MAXIMUM POPULATIONS AND LIFETIMES 164

6.1 Introduction 164

6.2 Rectangular Lattice 165

6.3 Circular Lattice 167

6.4 Erdős-Rényi Graphs 170

6.5 Watts-Strogatz Graphs 172

7 CORRELATIONS 176

7.1 Introduction 176

7.2 Initial Crowd Population Size and Lifetime 177

7.3 Current Crowd Population Size and Remaining Lifetime 182

8 CONCLUSION AND FUTURE WORK 187

8.1 Thesis Summary 187

8.2 Recommendations for Future Work 191

8.2.1 Alternative Regular Graph Structures 191

8.2.2 Alternative Modelling Approaches 192

8.2.3 Real World Data 192

Appendices 194

A THE HURST EXPONENT 195

A.1 Introduction 195

A.2 Results for the Rectangular Lattice 197

B GRAPH GENERATION ALGORITHMS 200

B.1 Rectangular Lattice 200

B.2 Circular Lattice 203

B.3 Erdős-Rényi 204

B.4 Watts-Strogatz Graphs 205

C GRAPH ANALYSIS ALGORITHMS 206

C.1 Breadth First Search 206

C.2 Girvan-Newman 210

C.3 CNM 211

D ISING MODEL AND CROWD ALGORITHMS 213

D.1 Ising Model 213

D.2 Crowd Extraction 217

NOMENCLATURE

α	The diffusion exponent
$\bar{\boldsymbol{Z}}$	A matrix containing the moving averages over time of the vertex spin states
β_c	The critical inverse temperature
β_q	The inverse temperature after quenching
β_s	The inverse temperature before quenching (normally 0)
$\boldsymbol{\mathcal{F}}$	A matrix of the proportion of flips in opinion a vertex makes in a time period w
$\boldsymbol{A}$	The adjacency matrix of a graph
$\boldsymbol{D}$	The degree matrix
$\boldsymbol{J}^{\text{int}}_{N\times n}$	A matrix of the interaction strengths between vertices
$\boldsymbol{K}^{\text{in}}$	The matrix of in degrees
$\boldsymbol{K}^{\text{out}}$	The matrix of out degrees
$\boldsymbol{Z}_{N\times T}$	A matrix where each column t represents the spin configuration of a graph at time step t

$\delta(x, y)$ Kronecker delta function

$\Delta\mathcal{L}$ The remaining lifetime of a crowd

$\Delta\mathcal{P}(C, \tau)$ The change in a crowd C's population size from its initial size at τ time steps after forming

$\gamma_{\mathcal{P}}$ The exponent of a power law fit of a population size frequency distribution

$\gamma_{\mathcal{L}}$ The exponent of the power law fit of a lifetime frequency distribution

$\gamma_{\mathcal{L}}$ The exponent of the power law fit of a lifetime frequency distribution

$\hat{\boldsymbol{Z}}$ The matrix of pre-processed opinion states

$\hat{\rho}$ A simple path

$\langle\langle M\rangle_T\rangle_C$ The configuration average for the magnetisation of a graph

$\langle M\rangle_T$ The time averaged magnetisation of a graph

$\mathcal{L}(C)$ The lifetime of a crowd C

$\mathcal{L}^{\max}$ The lifetime of the crowd which survives for the longest period of time

$\mathcal{P}(C, \tau)$ The population of a crowd C at τ time steps after forming

$\mathcal{P}^0$ The initial population size of a crowd

$\mathcal{P}^{\max}$ The population size of the crow with the most vertices

$\mathcal{P}^t$ The population size of a crowd at t time steps after it forms

μ The magnetic moment

$\bar{l}$ The average shortest path length

$\Phi(K_1, K_2)$ The similarity between components K_1 and K_2

ρ An ordered set of vertices describing a path on a graph

$\rho^*(i, j)$ The shortest path between vertices i and j

ρ_{cw} A closed walk

ρ_{sc} A simple cycle

Σ The ordered set of spin configuration states of a system

σ^t The spin configuration state of a system at time step t

σ_i^t The spin state of a vertex i at time step t

τ_B Kendall's rank correlation coefficient

$\theta_{\mathcal{P}}$ The exponent of an exponential fit of a population frequency distribution

$\theta_{\mathcal{L}}$ The exponent of the exponential fit of a lifetime frequency distribution

B_e The edge-betweeness of an edge e

C A crowd; consists of a set of spin-clusters

$C(G)$ The clustering coefficient of a graph G

$C_i(G)$ Clustering coefficient of a vertex i

$C_{ER}(p_w)$ Clustering coefficient for the Erdős-Rényi graph

$C_{WS}(p_{rw})$ The clustering coefficient for a Watts-Strogatz graph

$D(G)$ The diameter of the graph G

E A set of edges

$G(V, E)$ A graph consisting of the set of vertices V and set of edges E

G_{RL} A rectangular lattice graph

$H(\sigma)$ The energy of a system with spin configuration σ

J_i^{ext} The interaction strength of a vertex i with an external magnetic field

k_B The Boltzmann constant

k_i The degree of vertex i

l The path length

$M(\sigma^t)$ The magnetisation of a graph with spin configuration σ^t

N The number of vertices in a graph

$P(k)$ The degree distribution

p_c The critical (re)wiring probability

p_w The Erdős-Rényi graph's wiring probability

p_{rw} The rewiring probability for the Watts-Strogatz graph

Q The modularity of a graph

S_i^t The number of neighbours of vertex i that are in the same spin state at time t

$S_i^t(\psi)$ The number of neighbour of vertex i that are in spin state ψ at time t

V A set of vertices

z The wiring exponent $p_w \sim N^z$

z_c The critical wiring exponent for Erdős-Rényi graphs

CL Circular Lattice

ER Erdős-Rényi

RL Rectangular Lattice

WS Watts-Strogatz

1

INTRODUCTION AND LITERATURE REVIEW

Everyone has an opinion. As individuals how they form an opinion varies is a result of a complicated process: consequently modelling such processes accurately is difficult. On the other hand in a group the interactions between people that influence opinion are relatively simple and can be represented by simple models. This has lead to a large inter-disciplinary field of study in *consensus* and *norm* formation, i.e. how opinions or common behaviours gain dominance over others in a group of people. Naturally psychologists, sociologists and economists have a vested interested in how people behave alone and together. To mathematicians, physicists and computer scientists it is the complex emergent behaviours arise from these simple models which excite us.

One of the approaches to encapsulate the system mathematically is to model social connections as a graph with other dynamics running on top of it. The social environment is extremely important in the structure of social networks: within a University its students form lots of clusters with varying amount of links between clusters; whereas in a corporate or military environment relation-

ships can be modelled as hierarchically. Correctly choosing the graph structure and understanding its properties is extremely important in being able to analyse the social interactions that occur on a graph. With this in mind these approaches have been successful in modelling how epidemics spread [1, 2], which is similar to how memes (extremely catchy ideas) spread through social networks [3, 4] and importantly how consensuses of opinion and norms form [5–7].

These models focus on how a consensus form across an entire network, these are good models of collective behaviour such as during elections [8]. However the question remained if the mesoscopic features [9] that arise in simple voting models [10–13] before a global consensus is formed could be of interest in understanding opinions. Knowing how groups form opinions can allow us to develop methods of influencing opinions on small and large scales [14, 15].

In this thesis we investigate the mesoscopic clusters of consensus that form due to the Ising spin dynamics [16] by performing Monte Carlo simulation on a variety of graphs. Tracking the hundreds and thousands of consensus clusters which form, interact and die is not an easy task and is fraught with ambiguity. To make the analysis easier we provide a strict definition for what constitutes a consensus cluster and a method of tracking them as they change.

Chapter 1 will provide an overview of the literature required to understand graphs and the Ising spin model. In the second chapter we provide our definitions and validation of our implementation of the Ising model. Within the third, fourth, fifth, sixth and seventh chapters we present the results of our simulations and the analysis of the behaviour of the consensus clusters as the inverse

temperature parameter is altered. The eighth chapter summarises the work and offers suggestions for future work. Implementations of the algorithms and models used in the thesis can be found at https://github.com/karthiksowdirb.

1.1 GRAPH THEORY

The idea of graphs has penetrated the common knowledge of the general public over the years. Colloquially graphs are referred to as networks. Initially they entered the public lexicon due to the popularisation of the "six degrees of separation" concept. People were amazed that a chain of acquaintances consisting of around 6 people could link any 2 people on the planet. In more recent years the emergence of social networks such as MySpace, Facebook, Twitter, and Google+ have further educated the public on social networks. For researchers this information has been a boon in studying graphs with non-trivial structures.

Throughout the world we have physical examples of graphs such as rivers [17–19]; water, gas and oil pipes; electrical grids; neurons; atoms and molecules in a solid; and the physical internet [20]. There has also been great success in modelling abstract systems as graphs. These include the researcher collaboration network [21], protein-protein interactions networks [22], the food web and the afore mentioned social networks [23].

Our goal is to model opinion making processes of people when they are influenced by friends, family or acquaintances. Graphs allow us to describe these social connections in a way that can be incorporated into our opinion

model which is discussed later in section 1.2. To do this we shall first provide an overview of how graphs are defined and their associated notation. Then define the properties used to categorise graphs and finally the algorithms used to generate graphs with specific properties.

1.1.1 *Definitions and Notation Pertaining to Graphs*

Mathematically graphs are a way of representing the relationships between objects in a system. The objects are represented as a set of vertices V and the relationships which connect them are described by a set of edges E. Together the sets form a graph $G(V, E) = \{V, E\}$ [24]. Two vertices that have an edge between them are said to be *adjacent* or *nearest neighbours* in the graph.

Consider using a graph $G(V, E)$ to represent the family trees in a town, where individuals are considered related if they are parent and child. If individuals i and j live in the town then there exists corresponding vertices $i, j \in V$. Should j be a child of i then there exists an edge $\{i, j\} \in E$. Edges have a source vertex and a termination vertex thus the order a vertex appears in an edge matters. $\{j, i\}$ would indicates that i is a child of j. $\{i, j\}$ and $\{j, i\} \in E$ are *conjugates*.

For systems where the relationships between objects are not mutual we can represent the system as a *directed graph*. In such graphs the existence of an edge does not imply anything about the existence of its conjugate $\{i, j\} \in E \not\Longleftrightarrow \{j, i\} \in E$. We use $\Longleftrightarrow$ to indicate a mutual implication and $\not\Longleftrightarrow$ to indicate

that there no implication of any kind between statements. On the other hand if the relationships are mutual their graphs are referred to as *undirected*. In which case the existence of one edge guarantees the existence of its conjugate $\{i,j\} \in E \iff \{j,i\} \in E$.

In this thesis we restrict out graphs such that vertices can not have *duplicate edges*. Thus if we write $E = \{e_1, e_2, ..., e_n\}$ then $e_x \neq e_y \forall x, y \in [1,n] \, | x \neq y$. Note that $\{i,j\} \neq \{j,i\}$ so undirected graphs are still allowed. We shall also not allow graphs with *loops* where a loop is an edge which connects a vertex to itself i.e., $\forall i \in V \nexists \{i,i\} \in E$. *Simple graphs* are those without loops and or multiple edges.

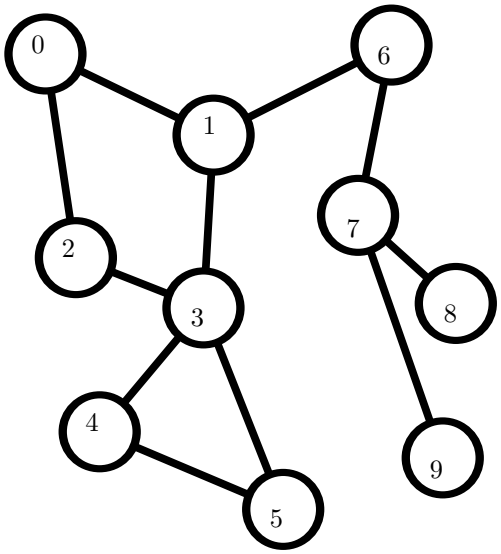
At times we may simplify the notation for ease of reading and drop the bracketed terms such that $G(V,E)$ will be referred to as G. We also may use short cuts for relationships where we might state that $i \in G$ by which we mean that there exists a vertex $i \in V$ where $V \in G(V,E)$. Similarly if an edge exists in a graph, $\{i,j\} \in G$, it would mean $\exists \{i,j\} \in E$ where $E \in G(V,E)$. If there are multiple graphs we shall use a superscript $G^x(V^x, E^x)$ to differentiate between them.

We will also quite frequently be working with subgraphs, which are graphs that are identical to a portion (or whole) of another graph.

Definition 1. *A graph $S(V', E')$ is a subgraph of a graph $G(V,E)$ if*

- $V' \subseteq V$.
- $E' = \{\{i,j\} \, | \exists i, j \in V' \wedge \exists \{i,j\} \in E\}$.

We use the notation $S \subseteq G$ to denote that S is a subgraph of G, where the bracketed terms have been dropped.



$$\begin{bmatrix} 0 & 1 & 1 & 0 & 0 & 0 & 0 & 0 & 0 & 0 \\ 1 & 0 & 0 & 1 & 0 & 0 & 1 & 0 & 0 & 0 \\ 1 & 0 & 0 & 1 & 0 & 0 & 0 & 0 & 0 & 0 \\ 0 & 1 & 1 & 0 & 1 & 1 & 0 & 0 & 0 & 0 \\ 0 & 0 & 0 & 1 & 0 & 1 & 0 & 0 & 0 & 0 \\ 0 & 0 & 0 & 1 & 1 & 0 & 0 & 0 & 0 & 0 \\ 0 & 1 & 0 & 0 & 0 & 0 & 0 & 1 & 0 & 0 \\ 0 & 0 & 0 & 0 & 0 & 0 & 1 & 0 & 1 & 1 \\ 0 & 0 & 0 & 0 & 0 & 0 & 0 & 1 & 0 & 0 \\ 0 & 0 & 0 & 0 & 0 & 0 & 0 & 1 & 0 & 0 \end{bmatrix}$$

Figure 1.: On the left is a graph. Circles are vertices and lines are edges. On the right is its matrix representation.

Set theory provides the machinery for defining graphs while its matrix representation is useful for manipulating and analysing a graph computationally [25]. A square matrix $\boldsymbol{A}$ with its elements defined as

$$\boldsymbol{A}_{ij} = \begin{cases} w_{ij} & \text{if } \{i,j\} \in G\left(V,E\right) \\ 0 & \text{otherwise} \end{cases} \tag{1}$$

is called the adjacency matrix of $G\left(V,E\right)$, where A_{ij} is the element in the matrix which is at the intersection of its $i-th$ row and $j-th$ column. Also w_{ij} is the weight of the edge $\{i,j\} \in E$. Weights can be used to represent many things primarily $w_{ij} = 0$ means no edge exists between vertices i and j and $w \neq 0$ means an edge exists. For example the graph of motorways between cities, where each vertex is a city and edges are the motorways connecting them.

The edge weights could be the motorway length in kilometres. Unless otherwise stated it will be safe to assume $w_{ij} = w = 1 \forall \{i, j\} \in G$ in the thesis.

At times we shall be required to deal with powers of matrices $\boldsymbol{A^n}$ and the subscript notation can cause confusion. To prevent this we say that $\boldsymbol{A^n_{ij}}$ is the $ij-th$ element of $\boldsymbol{A}$ to the power n and $[\boldsymbol{A}^n]_{ij}$ is the $ij-th$ element of the matrix $\boldsymbol{A^n}$.

As edges in an undirected graph are identical then so are their weights $w_{ij} = w_{ji}$. It follows then that the adjacency matrix of an undirected graph must be symmetric. Adjacency matrices of directed graphs may be symmetric but not necessarily so. The relationship chosen to be modelled can decide the weights and consequently whether it is directed or undirected. The graph of a river network is directed for water flow (in a simple river model) but is undirected for human traffic.

1.1.2 *Properties of Graphs*

Real world graphs can be characterised by the context in which we find them. The graphs describing the network of websites and the hyperlinks between them as well as the physical network of routers and servers can both be referred to as the 'internet'. The researcher collaboration network and Facebook friends network fall under the banner of 'social networks'. This can be an intuitive way to classify types of graphs as it describes their uses. The graphs representing these networks can have similar properties at a structural level consequently

differentiating them no longer makes sense. In this section we will describe and define some of the properties that are used to differentiate graphs into regular, random, small-world and scale-free.

Paths [24, 26, 27]

We have used transportation networks as an example of types of graph in prior sections with vertices and edges describing locations and the roads respectively. Consider a person starting from their home, travelling to their place of work then visiting the supermarket before returning home. We describe the *path* taken by a person by the vertices they visit in the order they visited them. The order in which vertices are visited is important: a path that starts at vertex i, that goes to vertex j and ends at k is different from its reverse k to j to i. Consequently we use ordered sets to provide a mathematical definition of paths. In an ordered set the order in which elements appear matters, e.g. the ordered sets $\{i, j, k\}$ and $\{k, j, i\}$ are not equal.

Definition 2. *Path: an ordered set of vertices in the same graph. Vertices i and $i+1$ in the path must be connected by an edge, i.e. be adjacent.*

Expressing this mathematically a path between vertices v_0 and v_l is

$$\rho\left(v_0, v_n\right) = \left\{v_0, \ldots, v_i, v_{i+1}, \ldots, v_l | \exists \left\{v_i, v_{i+1}\right\} \in G \forall i \in (0, n]\right\}. \tag{2}$$

Including the starting node the path ρ contains $l+1$ vertices, we define this as the *path length*.

Definition 3. *Path Length: the number of edges traversed while visiting every vertex in a path.*

Mathematically the path length $l = |\rho(v_0, v_n)| - 1$, where the operator $|\cdot|$ returns the number of elements in the set they surround. We can also define paths such that they only visit any vertex once.

Definition 4. *Simple Path: A path where each vertex in the chain is unique.*

$$\begin{aligned}\hat{\rho}(v_0, v_n) = &\{v_0, \ldots, v_i, \ldots, v_j, \ldots, v_l| \\ &\exists \{v_i, v_{i+1}\} \in G, v_i \neq v_j \forall i \neq j \in (0, n]\}.\end{aligned} \tag{3}$$

Consider a graph containing vertices and 0 edges: there can be no path between any of the vertices as there are no edges connecting them. It stands to reason that a path need not exist between any two vertices in a graph; if a path does exist between vertices then they are *reachable* from one another. This concept is the basis for defining *graph components* in the next sub-section.

Definition 5. *Reachable: a vertex j is reachable from vertex i if a path $\rho(i, j)$ exists.*

A path can form *closed walks* and *simple cycles*. A closed walk is a path $\rho_{cw}(v, v)$, it starts at a vertex v and ends at the same vertex v.

$$\begin{aligned}\rho_{cw}(v_0, v_n) = &\{v_0, \ldots v_i, \ldots, v_n | v_0 = v_n \\ &\text{and } \exists \{v_i, v_{i+1}\} \in G \forall i, j \in (0, n]\}.\end{aligned} \tag{4}$$

There are no restrictions on a closed walk containing repeated vertices or edges. In such a path one can return to the same vertex multiple times. Whereas in a simple cycle vertices can be visited only once, thus $\rho_{sc}(v, v)$ is a path defined by

$$\rho_{sc}(v_0, v_n) = \{v_0, \dots v_i, \dots, v_j, \dots, v_n | \exists \{v_i, v_{i+1}\} \in G \text{ and } \nexists v_i = v_j \forall i \neq j \in [1, n]\}. \tag{5}$$

The powers of the adjacency matrix have an interesting property. The $ij-th$ element of the $l-th$ power of the adjacency matrix, $\left[\boldsymbol{A}^l\right]_{ij}$, is the number of walks from vertex i to vertex j with a path length of l [24]. The consequence of this is that when $l = 3$ the diagonal elements are all simple cycles of length 3, otherwise known as *triangles*. The number of triangles in a graph is an important indicator of how clustered the vertices are. Clustering is covered in further detail later in the section.

Graph Components [24, 26, 27]

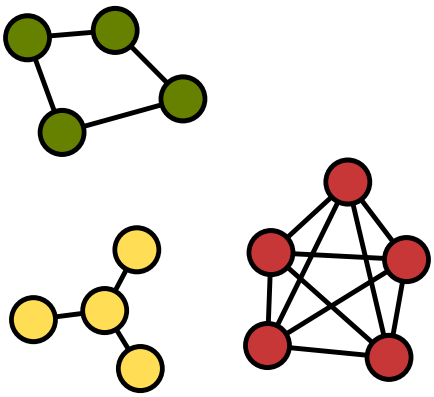


Figure 2.: All the vertices and edges pictured are in the same graph. Note that green and yellow vertices are not reachable from red ones and vice versa. This is a graph which consists of 3 components.

In the previous Section 1.1.2 we introduced the idea of vertices being reachable from to another. The concept of reachability can be applied to entire graphs or subgraph. When every vertex in a (sub)graph is reachable from every other it is considered a *connected* (sub)graph.

Definition 6. *Connected (sub)graph: a (sub)graph G is connected if every pair of vertices $i, j \in G$ there exists a path $\rho(i,j)$ such that every vertex in the path $k \in \rho(i,j)$ is also a vertex in G, i.e. $\forall i, j \in G \; \exists \rho(i,j) = \{i, \ldots, k, \ldots, j \mid \exists k \in G\}$.*

We now need to introduce the concept of *maximality* of graphs and subgraphs. What this means is that given a (sub)graph G which has been defined by some set of rules is maximal if there does not exist another (sub)graph G' defined by the same set of rules such that G' is a supergraph of G.

Definition 7. *Let $G(V,E)$ be a (sub)graph such that $V = \{i | \phi(i) \leq 0\}$, where $\phi(i)$ is a mathematical expression which describes the criteria that the vertex i is judged by to be included in the set V. The function $\Phi(i)$ returns 'true' if i meets the criteria and 'false' otherwise. Then $G(V,E)$ is maximal $\iff \nexists G'(V',E') \supset G(V,E) : V' = \{i | \Phi(i)\}$.*

We can apply maximality to connectedness to define *components* which are maximally connected (sub)graphs,

Definition 8. *A subgraph $C(G)$ of a graph G is a component if it is maximally connected.*

1. *Is a subgraph: $C(G) \subseteq G$.*

2. *Is connected:* $\forall i, j \in C(G)\, \exists \rho_C(i, j)$.

3. *Is maximal:* $\nexists C'(G) \supset C(G) : C'(G)$ *and* $C(G)$ *are both connected.*

Where the subscript notation in $\rho_G(i, j)$ *is used to denote the graph on which the path is valid.*

If a component $C(G) \equiv G$ then the graph G is a connected graph. Such graphs consist of only 1 component. Any graph with more than 1 component is a *disconnected* graph.

Average Path Length and Diameter

When it came to whether vertices were reachable we only cared that a path existed or not. However in real life applications the path taken through a graph can be extremely important. In the case of 6 degrees of separation it is the shortness of the average path length that is interesting.

The average path length of a connected graph G is the average of all the shortest paths between every pair of vertices. Let $\rho^*(i, j)$ be the shortest path between vertices i and j. The average path length is

$$\bar{l} = \frac{1}{N(N-1)} \sum_{i=1}^{N} \sum_{j>i}^{N} |\rho^*(i, j)| \tag{6}$$

where N is the number of vertices in the graph. The sum in the equation considers every shortest path between vertices once, thus as there are N vertices and each of those has $N-1$ shortest paths we must divide the sum by $N(N-1)$ to get the average.

The *diameter* of a graph is the longest of all the shortest paths in a graph.

$$D\left(G\right) = \max\left(\left\{\left|\rho^{*}\left(i,j\right)\right| \; \left|i,j \in G\right\}\right). \tag{7}$$

Both the average path length and diameter measure the size of the graph in different manner than counting the number of vertices. These measures are important in differentiating between random graphs and small world graphs.

Degree Distribution

The degree of a vertex is the number of edges attached to it. We define a *degree matrix* $\boldsymbol{K}$ as having the degrees of the vertices along its diagonal.

$$\boldsymbol{K}_{ij} = \begin{cases} k_i & \text{if } i = j. \\ 0 & \text{otherwise.} \end{cases} \tag{8}$$

where k_i is the degree of vertex i.

A vertex v in a directed graph has an *out-degree*, the number of edges directed away from it, which is defined as $k_v^{\text{out}} = \sum_{j=1}^{N} \boldsymbol{A}_{vj}$ where $\boldsymbol{A}$ is the adjacency matrix of the graph. We use a superscript to indicate that a degree matrix, $\boldsymbol{K}^{\text{out}}$, has out-degrees along its diagonal. Similarly the *in-degree* of vertex v, the number of edges directed towards it, is $k_v^{\text{in}} = \sum_{i=1}^{N} \boldsymbol{A}_{iv}$ with a corresponding in-degree matrix K^{in}. For directed graphs k_i^{in} and k_i^{out} may differ.

Edges of a vertex i in an undirected graph are both the 'in' and 'out' edges. This is reflected as symmetry in the adjacency matrix. The in-degree and out-

degree of an undirected graph are equal. As such it is sufficient to say that the degree of vertex v is $k_v = \sum_{j=1}^{N} \boldsymbol{A}_{vj}$ with $\boldsymbol{D}$ as the degree matrix.

The degree distribution of a graph is the frequency distribution of the degrees of its vertices. It is one of the main methods of differentiating between types of graphs. Infinitely large *regular* graphs contain vertices that have the same degree k, this is expressed as a delta function about k in the degree distribution. Complex graphs such as Erdős-Rényi and Watts-Strogatz have Poisson degree distributions. These graphs and their properties will be discussed later in this chapter.

If a graph's degree distribution is $P(k) = \delta(N-1)$, where N is the number of vertices in the graph, then every vertex has an edge to every other vertex such graphs are considered *complete*.

Definition 9. *Complete Graph: every vertex is adjacent (a neighbour) to every other vertex.*

Clustering Coefficient

The clustering coefficient is a measure of how many neighbours are shared by vertices in a graph. One such measure is the ratio between the number of *triangles* and *triplets* a vertex is part of. We define a triplet as

Definition 10. *Triplet: a group of* 3 *vertices. At least* 1 *of the vertices is connected to the other* 2*.*

Definition 11. *Triangle: a group of* 3 *vertices. Each vertex is connected to the others by an edge. .*

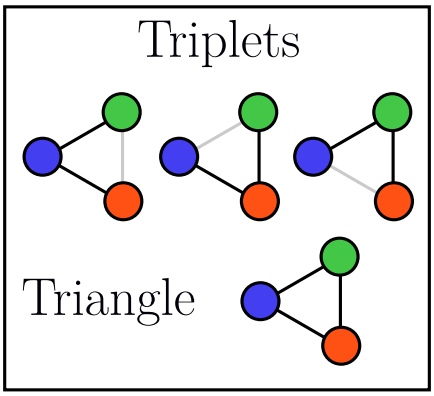


Figure 3.: A triplet consists of 3 vertices where 1 vertex is connected to the 2 others. A triangle consists of 3 vertices where each vertex is connected to the other two. The triangle consists of the union of the 3 triplets.

These definitions can be expressed mathematically with the definition of a triplet being,

$$\tau = \{i, j, k | \exists \{i, j\}, \{i, k\} \in E\}, \tag{9}$$

and for triangles,

$$\theta = \{i, j, k | \exists \{i, j\}, \{i, k\}, \{j, k\} \in E\}. \tag{10}$$

Comparing the equations we can see that 10 is a stronger version of 9. Thus any set of three vertices which satisfy equation 10 will also satisfy 9, as illustrated in figure 3.

Using equations 9 and 10 we can define that $\Theta(G)$ and $T(G)$ as the sets of all triangles and triplets respectively in a graph G. As all triangles are also triplets it follows that the set of triangles is a subset of the set of triplets, $\Theta \subseteq T$. The set T can also be thought of as a set of potential triangles in the graph. To compute the clustering coefficient we require the sizes of Θ and T.

Let $T_i \subset T$ be the set of triplets a vertex i for which it is the centre vertex. The size of set of triplets $|T| = \sum |T_i|$. Computing $|T_i|$ is easy given the degrees of the vertices,

$$|T_i| = \frac{k_i \left(k_i - 1\right)}{2}. \tag{11}$$

Where k_i is the degree of vertex i. However each triplet is counted twice thus we had to divide by a factor of 2.

As was discussed while defining paths $\left[\boldsymbol{A}^3\right]_{ii}$ is the number of simple cycles of length 3 starting and ending at a vertex i. However both paths going forward and backwards along the path are counted. The number of triangles a vertex i is a part of is then given by,

$$|\Theta_i| = \frac{\left[\boldsymbol{A}^3\right]_{ii}}{2}. \tag{12}$$

Thus using equations 11 and 12 we can define the clustering coefficient of a vertex i as

$$\begin{aligned} C_i\left(G\right) &= \frac{\text{Number of unique Triangles}}{\text{Number of unique Triplets}} && (13)\\ &= \frac{\left[\boldsymbol{A}^3\right]_{ii}}{2} \frac{2}{k_i \left(k_i - 1\right)} && (14)\\ &= \frac{\left[\boldsymbol{A}^3\right]_{ii}}{k_i \left(k_i - 1\right)} && (15) \end{aligned}$$

A graph's clustering coefficient of a graph is the average clustering coefficient of its vertices,

$$C(G) = \frac{1}{N}\sum_{i=1}^{N}\frac{\left[\boldsymbol{A}^3\right]_{ii}}{k_i\left(k_i-1\right)}. \tag{16}$$

This measure is used in many methods of identifying communities in graphs. Communities and their identification will be discussed later in this chapter.

Cliques

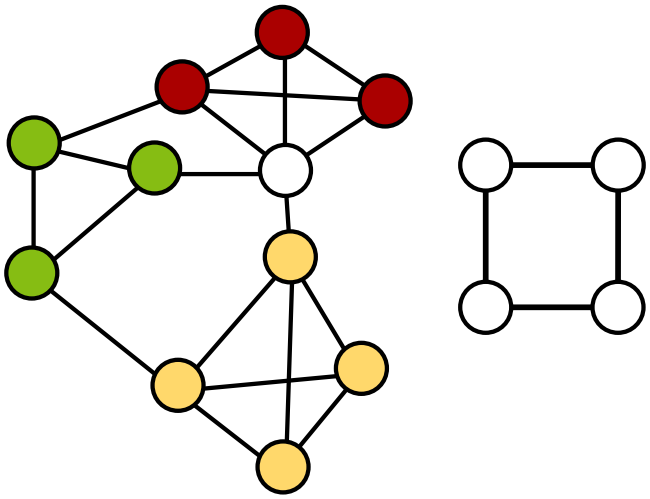


Figure 4.: This is a graph consisting of 2 components. The triangle on the left (green vertices) and the square at the bottom (yellow vertices) are maximal cliques. While the triangle at the top (red vertices) is a non-maximal clique. The square on the right is a separate component but does not contain a clique.

Subgraphs which are complete, definition 9, are referred to as *cliques*,

Definition 12. *Clique: a subgraph $G^* \subseteq G$ is a clique if $\forall i, j \in G^* \exists \{i, j\} \in G$.*

From this definition we can surmise that if G^* is a clique then $G^* \cup \{i\}$ is also a clique iff $i \in G \backslash G^*$ and $\exists \{i, j\} \in G \forall j \in G^*$. Cliques to which vertices can not be added to make larger cliques are *maximal* cliques.

Definition 13. *Maximal Clique: a clique G^* is a maximal clique $\hat{G}^* = G^*$ if $\nexists S^* \supset G^* : S^*$ is a clique.*

A maximal clique is a complete subgraph which can not be increased in size by adding another vertex and remaining complete. Cliques are one of the numerous structural properties that can be used to define communities in graphs.

1.1.3 *Generating Graphs*

In the previous subsection we discussed a few of the inherent properties by which we differentiate graphs. It is possible to generate graphs which have specific properties. In this section we shall introduce several graphs with specific properties and the motivation behind algorithms which generate them.

Our motivation is to understand how the crowd dynamics and properties are influenced by the graph structure. As the dynamics aim to model social interactions we shall require graphs which do and do not have properties associated with social networks. For a model of social networks we choose to use graphs which exhibit small-world characteristics which have very short path lengths. The rectangular lattice, the ring lattice and the Erdős-Rényi graphs are not small-world but are good comparative models as each has some but not

all of the characteristics of the Watts-Strogatz graph. Each graph has distinct structural differences which should impact the opinion dynamics and allow us to gain insight into how different properties of social networks affects opinion formation.

Pseudo-code and descriptions of the algorithms used to generate the graphs discussed in this section can be found in the appendix B. Implementations of the code in C++ can be found at https://github.com/karthiksowdirb.

1.1.4 *Rectangular Lattice*

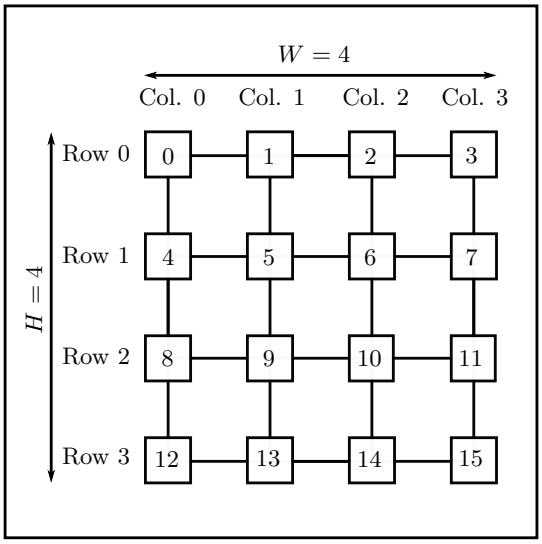


Figure 5.: A non-periodic rectangular lattice graph. It has a height $H = 4$ and a width $W = 4$. The total number of vertices are $N = WH = 16$. Each vertex is labelled from 0 to $N - 1$.

The Ising Spin model, see Section 1.2.1, we use in the main body of this thesis first arose as description of magnetism, it is no surprise that some the earliest graph structures studied where those of magnetic materials. The simplest structure is known as simple cubic which where the entire crystal consists

of repeated cubes. An atom thick layer of an infinitely large crystal would be a lattice consisting of square units. Due to its regular structure it is homogeneous as every vertex has the same degree, clustering coefficient and average shortest path. In other words every vertex is essentially the same. Thus it is a graph on which the opinion dynamics are almost entirely independent of the graph structure.

In figure 5 we illustrate the vertices as arranged in a Cartesian grid pattern. This is an accurate depiction of a potential rectangular graph. It has H rows and W columns of vertices and there are HW vertices in total. By inspection we can see it is not homogeneous as the vertices on the edges and corners of the lattice have different degrees to each other and those in the centre. If a graph is small the structural differences on the edges of the lattice can effect the opinion dynamics of the whole graph. The opinion dynamics would not be independent of graph structure. While if a graph is large there is still some effect on vertices some distance from the edges of the lattice. What we want is a graph without such effects.

As we can not generate infinitely large graphs we shall make do by using a common trick. We need to get rid of the lattice edges. By setting periodic boundary conditions we allow vertices on the lattice edges to become neighbours with those on the opposite edges. Doing this also makes the lattice homogeneous as ever vertex has the same degree. Topologically the shape of such a lattice is a torus. We still can not have small (*periodic*) rectangular lattice graphs as there is a chance that a vertex could influence itself over a periodic boundary. This

would mean the network structure is still influencing the outcome of the opinion forming dynamics - which we do not want. However a very large periodic rectangular lattice graph would not have such effects. It would be difficult to distinguish vertices in a very large periodic rectangular lattice and an infinitely large rectangular lattice based on their behaviour as it should be the same.

We use the following procedure to connected vertices to form a rectangular lattice without periodic boundary conditions,

1. Set $x = 0$ and $y = 0$.
2. If $x - 1 \geq 0$ then set $\boldsymbol{A}_{vw} = 1 : v = y \cdot W + x, w = y \cdot W + (x - 1)$.
3. If $x + 1 < W$ then set $\boldsymbol{A}_{vw} = 1 : v = y \cdot W + x, w = y \cdot W + (x + 1)$.
4. If $y - 1 \geq 0$ then set $\boldsymbol{A}_{vw} = 1 : v = y \cdot W + x, w = (y - 1) \cdot W + x$.
5. If $y + 1 < H$ then set $\boldsymbol{A}_{vw} = 1 : v = y \cdot W + x, w = (y + 1) \cdot W + x$.
6. Set $x = x + 1$.
7. If $x < W$ then go to step 2, otherwise continue.
8. Set $x = 0$ and $y = y + 1$.
9. If $y < H$ then go to step 2, otherwise stop.

This algorithm works by mapping coordinates of a $W \times H$ Cartesian grid to the vertex ids, where a point (x, y) is mapped to a vertex $v = y * W + x$. The algorithm then create edges between two vertices v and w if they are separated by a unit distance according to their Cartesian grid coordinates.

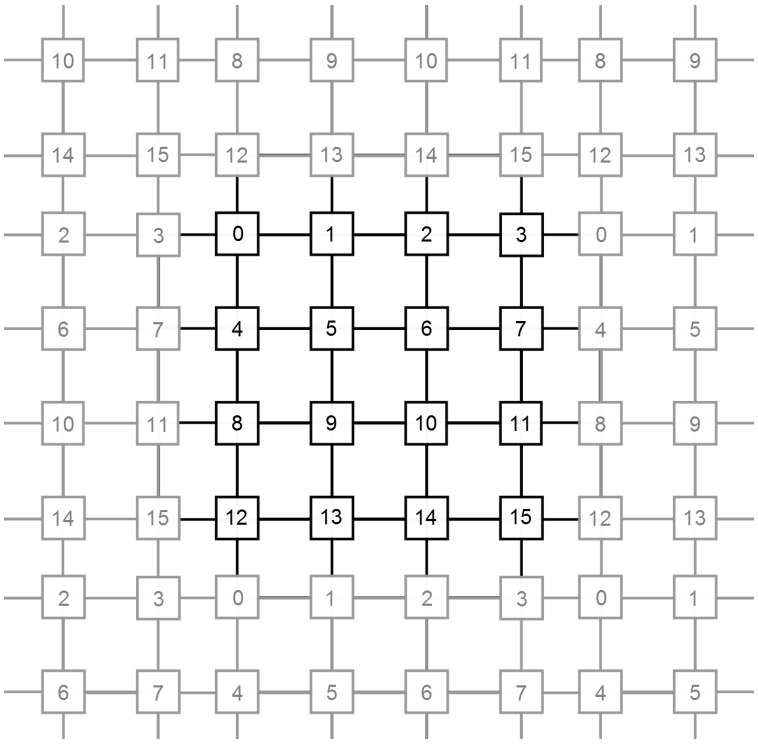


Figure 6.: A periodic rectangular lattice graph is illustrated here as a non-periodic graph (black edges and vertices) repeated an infinite number of times in all directions (grey edges and vertices).

As we can create both periodic and non-periodic graphs we shall cover the properties of both. The path length of any shortest path between two vertices is the number of horizontal steps plus the vertical steps we can say that the diameter of a non-periodic rectangular lattice is,

$$D\left(H,W\right)=H+W. \tag{17}$$

This is true as the longest of the shortest path lengths is from the vertex at $(0,)$ to $(W-1,H-1)$. In the case of a periodic rectangular lattice the vertices

which are furthest from each other are the corner nodes from the central. While the diameter of the periodic rectangular lattice is given by,

$$D\left(H,W\right)=\frac{H+W}{2}-\frac{1}{2}\cdot H\left(\mathrm{mod}\ 2\right)-\frac{1}{2}\cdot W\left(\mathrm{mod}\ 2\right). \tag{18}$$

The rectangular lattice always consists of 1 component. The normalized degree distribution for the non-periodic rectangular lattice is

$$\begin{aligned}\rho\left(k\right)=&\frac{4}{N}\delta\left(K-2\right)\\&+\frac{2\left(H-2\right)+2\left(W-2\right)}{N}\delta\left(K-3\right)\\&+\frac{\left(W-2\right)\left(H-2\right)}{N}\delta\left(K-4\right),\end{aligned} \tag{19}$$

where $\delta\left(x\right)$ is the Kronecker delta. The four corner vertices each have degree 2, those on the outermost edges (not including the corners) have degree 3, while all other vertices have degree 4. In contrast the periodic rectangular lattice's normalized degree distribution, $\rho\left(k\right)=\delta\left(K-4\right)$, has a single peak at $k=4$ as all vertices have degree 4. From inspection of the graph it is evident that the lack of triangles means the clustering coefficient $C=0$ for both periodic and non-periodic versions of the graph.

1.1.5 *Circular Lattice*

Like the rectangular lattice the circular lattice is a regular graph. While the former consists of repeated square units the latter is made up of repeated tri-

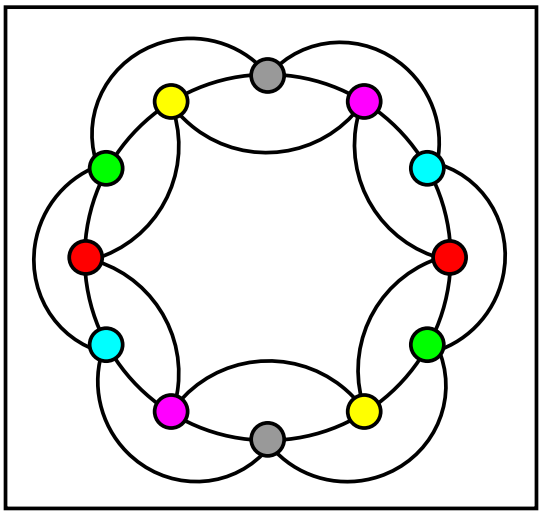


Figure 7.: A circular lattice with $N = 12$ and $2K = 4$. Vertices with the same colour are diametrically opposite one another. Thus each similarly coloured vertex is the other's furthest vertex.

angular units. As a consequence the clustering coefficient of the circular lattice is non-zero and dependent on the number of nearest neighbours. In its basic form this graph makes for a poor model of a social network. However as will be discussed shortly its properties make it ideal for creating small-world networks.

At its most basic the circular lattice is a set of vertices arranged in a circle with edges to the $2K$ nearest neighbours. As long as the number of nearest neighbours is much smaller than the number of vertices in the graph far from each other should not be able to influence each other's opinion dynamics. In counterpoint to that the triangular nature of structure means that vertices near each other share neighbours. This means opinion dynamics of vertices near each other will be influenced by the same neighbours resulting in similar opinions. It is a small effect which is much greater within communities.

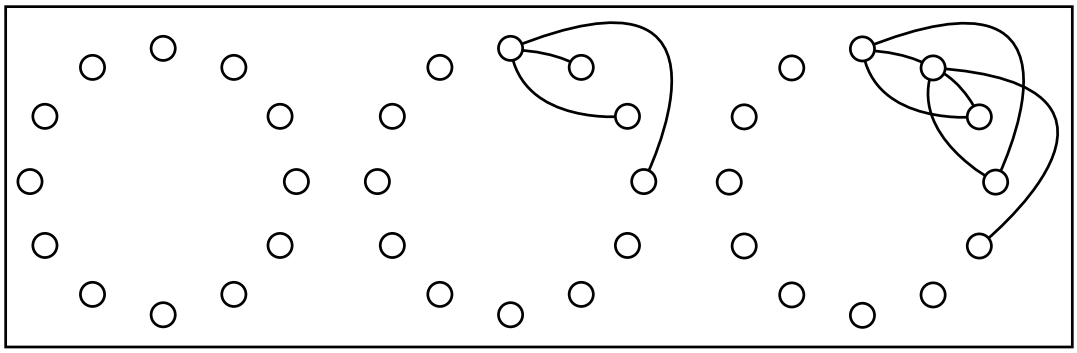


Figure 8.: A circular lattice being generated with parameters $N = 12$ and $2K = 6$. Left: vertices are arranged in a circle. Middle: the edges between the first vertex and it K nearest neighbours in the clockwise direction are created. Right: the edge creation process is repeated for the next vertex. This continues until all vertices create edges.

We can find the diameter of the circular lattice by noting the furthest any two vertices can be on a ring is diametrically opposite one another, see figure 7. For lattices with $K > 1$ the diameter of a circular lattice [26] is

$$D\left(N,K\right) = \mathcal{O}\left(\frac{D\left(N,1\right)}{K}\right) = \mathcal{O}\left(\frac{N}{2K}\right). \tag{20}$$

The circular lattice consists of one component. Similarly its degree distribution $\rho\left(k\right) = \delta\left(2K\right)$ contains a single feature: a sharp peak at $2K$.

The clustering coefficient can be obtained by considering a single vertex i and its nearest neighbours, see figure 9. First we count the number of triangles which are formed by vertices are nearest each other ($h = 1$), then we count those that are formed by vertices second nearest ($h = 2$) and so on. We find that the total number of triangles the central vertex is a part of is

$$\begin{aligned} \theta &= \sum_{h=1}^{K} 2K - h - 1 \\ &= \frac{3K\left(2K-2\right)}{4}. \end{aligned} \tag{21}$$

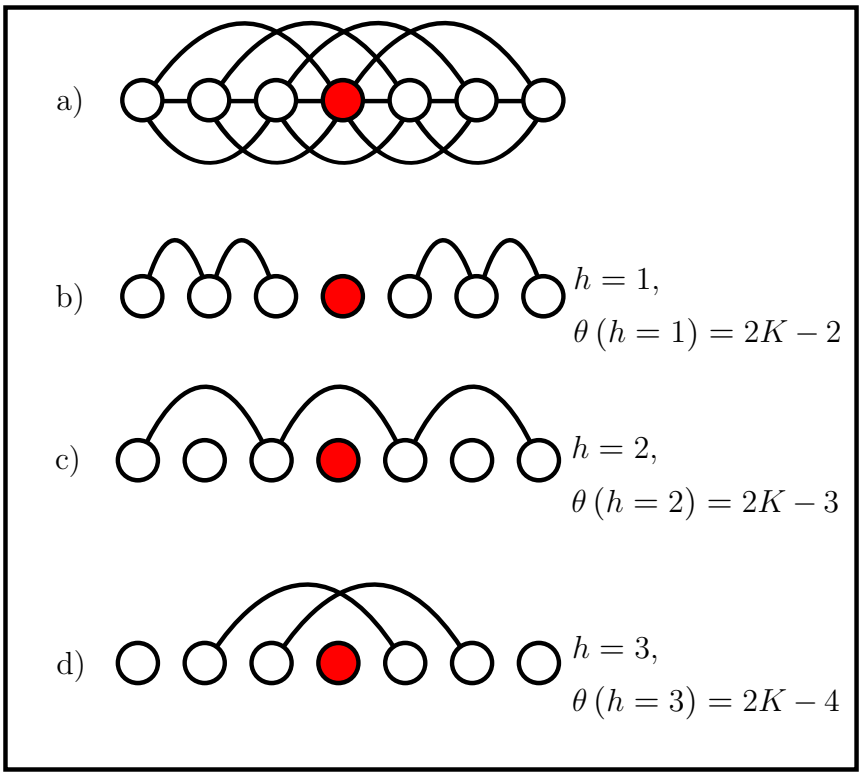


Figure 9.: The nearest neighbours of a single node in the circular lattice. a) All the edges that form a triangle with the vertex at the centre. b-d) Shows edges that are in the triangles that contain the centre vertex but are not connected to the centre vertex itself, where $h - 1$ is the number of vertices between those shown as connected.

Thus we then have the clustering coefficient[28]

$$\begin{aligned} C(K) &= \frac{3K(2K-2)}{4} \cdot \frac{2!\,(2K-2)!}{(2K)!} \\ &= \frac{3(2K-2)}{4(2K-1)}. \end{aligned} \tag{22}$$

The assumption that the ring is infinitely large ($N \to \infty$) has been made in equation 22 thus it only holds true if $2K \ll N$. When the degree is very large on a finite sized circular lattice, $2K = \mathcal{O}(N)$, the graph is approaching a *complete* graph and the clustering coefficient becomes linearly proportional to the degree, $C(2K = \mathcal{O}(N)) = \mathcal{O}\left(\frac{2K}{N}\right)$, see figure 10.

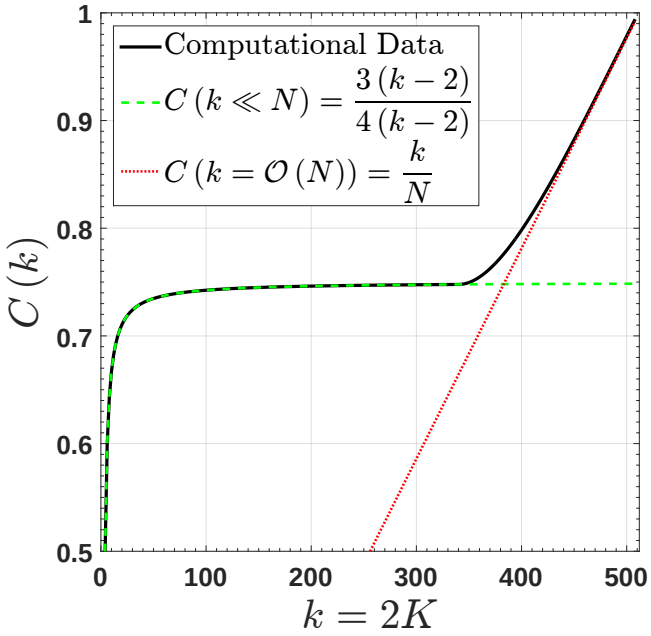


Figure 10.: Clustering coefficient of a circular lattice graphs with different degrees, where $N = 512$ for all graphs. The computational data (thick black line) shows that the relationship changes from equation 22 (green dashed line) to become proportional to the degree (red dotted line).

Consequently we introduce a new term into the clustering coefficient, equation 22 to get

$$C(K) = \frac{3(2K-2)}{4(2K-1)} + \mathcal{O}\left(\frac{2K}{N}\right). \tag{23}$$

1.1.6 *Erdős-Rényi Graphs*

The term random graph is used to describe a graph generated by a random process. The standard used is the Erdős-Rényi graph [24, 29, 30]. These graphs are not good models of social networks as they do not account for the fact that neighbours of a vertex are more likely to be neighbours with each other. However the structures of these graphs are irregular and thus complex. In

general it is unlikely for Erdős-Rényi graphs to contain any special structural features such as communities or very short average path lengths. Furthermore when generating Watts-Strogatz graphs its structure will be similar to that of a circular lattice with low amounts of rewiring and similar to the Erdős-Rényi graphs with large amounts of rewiring, this is discussed in Section 1.1.7. Consequently we will be required to analyse the results of the Spin Model simulations on Erdős-Rényi graphs to be able to tell when the structure of the Watts-Strogatz graphs is more random than small-world.

There are two different approaches to generating Erdős-Rényi graphs. Edgar Gilber describes the first of the two models in *Random Graphs* [31], where one samples a graph $G(N, m)$ from a set of graphs $\Gamma(N, m)$. Each graph in $\Gamma(N, m)$ has N vertices and m number of edges. The number of graphs in the set is

$$|\Gamma(N, m)| = \binom{\binom{m}{2}}{N} \tag{24}$$

and each of these have an equal probability of being picked. The set of all possible graphs for small graph, for example of 500 vertices and 70 edges, becomes computationally intractable to produce and thus sample from. This makes it useful only when wanting to sample a small graph at random.

The second method for generating random graph considers every possible edge $\{v, w\} \forall v \neq w \in V$ and creates it with a probability p_w [32]. This model is referred to as $G(N, p_w)$ as it begins with N vertices and each edge has a probability p_w of existing. In this case there is an ensemble of graphs that can

be produced where the probability of a vertex i having a particular degree is $P(K_i = k) = p^k (1-p)^{\frac{N(N-1)}{2-k}}$ [24, 29].

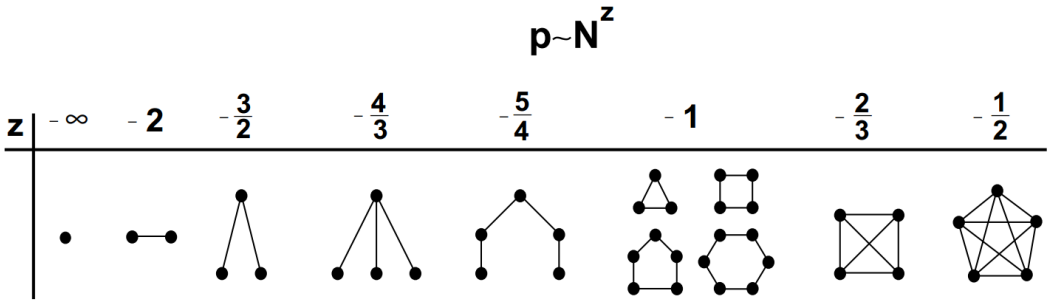


Figure 11.: The features that appear in Erdős-Rényi graph as the scale invariant wiring parameter Z is increases. Reproduced from [24].

A major property of the $G(N, p)$ graphs is that their structure changes wildly for different values of p. The connectedness of the subgraphs increases with the wiring probability. The subgraphs observed are independent of the size of the graph if the wiring probability changes according to $p \sim N^z$, where the control parameter is z, Fig. 11 [24]. When $z \to -\infty$ the wiring probability $p \to 0$ which results in N components, i.e. all the nodes are disconnected from each other. As z increases graphs with edges start being generated thus components consist of more than 1 vertex. When $z >= -1$ the generated graphs contain cycles. Eventually more and more triangles exist in the graphs and the graph tends towards a clique. At some critical wiring probability p_c the graph structure undergoes a major change, above p_c a giant component which containing the majority of the vertices forms.

The critical wiring probability $p_c \sim \frac{\ln N}{N}$ above which a giant component forms can be obtained through the use of percolation theory [24]. We shall use this to generate random graphs which contain giant components.

The graphs produced by the generative algorithm have the following characteristics. For an Erdős-Rényi graph the average path length is given by

$$l \sim \frac{\ln N}{\ln \langle k \rangle} \tag{25}$$

where $\langle k \rangle = pN$ is the expected degree of a vertex in the graph. The degree distribution of an undirected graph is Poisson,

$$P(k) \approx \frac{\langle k \rangle^k}{k!} e^{-\langle k \rangle} \tag{26}$$

The clustering coefficient has a simple result [24, 28–30, 33–36]. If the expected number of triplets a vertex has is given by,

$$\text{Number of unique Triplets} = \frac{\langle k \rangle!}{2!\left(\langle k \rangle! - 2\right)!}, \tag{27}$$

and the expected number of triangles a vertex has is,

$$\text{Number of unique Triangles} = \frac{\langle k \rangle!}{2!\left(\langle k \rangle! - 2\right)!} p, \tag{28}$$

as each pair of vertices has probability p of being connected. When we use these to calculate the clustering coefficient we are left with

$$C_{ER}(p_w) = \frac{\langle k \rangle}{N} = p_w. \tag{29}$$

In essence the clustering coefficient is inversely proportional to the graph's size. Consequently Erdős-Rényi graphs of different sizes are not directly comparable if they have the same wiring probability p_w.

1.1.7 *Watts-Strogatz Graphs*

[37] published an article in Psychology Today on what he called 'The Small World Problem', in it he details what has been popularly dubbed as 'Six Degrees of Separation'. It is the concept that the graphs describing social connections is structured such that two complete strangers are connected to each other by a very short chain of friends of friends. A couple of years later Milgram et al. published an experimental study investigating the small-world properties of an acquaintance graph. People in Nebraska and Boston, picked at random, were asked to send file to a target person in Massachusetts. The participants were limited to sending the file to an acquaintance they are on a first name basis with. Each person would write their name and the date in the file before sending it on. This allowed them to track how many people the file had to pass through before reaching the target and the time it took. Their data showed that the average number of people the file passed through was 6, hence the term 'Six Degrees of Separation'.

The distinguishing properties of the small world graph structure can be distilled to very short path length and high clustering coefficient. In terms of opinion dynamics a short average path length might allow the influence of each

vertex to reach more vertices. While the high clustering coefficient means that many vertices will be forming opinions based on information from the same neighbours. The implication of these two effects of the network structure is that we should expect strong consensus of opinion in some regions of small-world graphs.

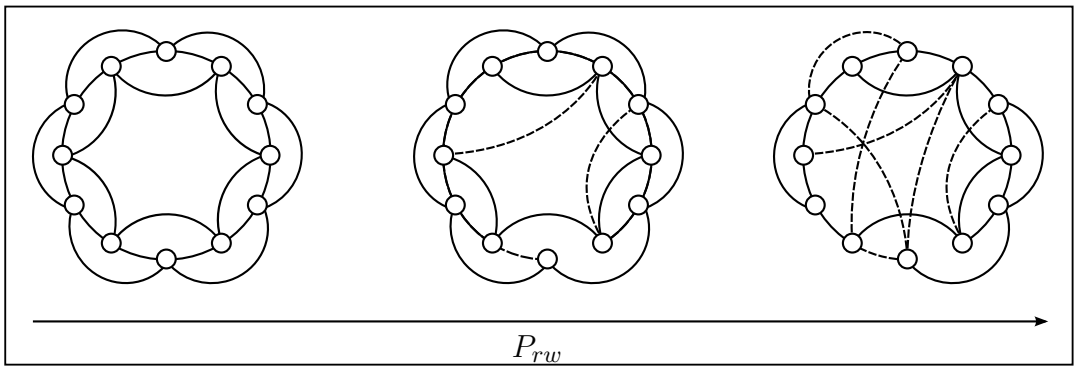


Figure 12.: This image illustrates the introduction of shortcuts into a circular lattices as edges are rewired. As the rewiring probability p_{rw} increases the number of shortcuts increases and the graph becomes less regular. Rewired edges have been highlighted using dashed lines.

Duncan Watts and Steven Strogatz in a letter to Nature, [33], introduce their model for generating small-world graphs. In their model they start with a regular lattice and rewire each edge once with probability p_{rw}, Fig. 12. Below we have the generation for the Watts-Strogatz Graphs in algorithm 4. Unlike previous graphs which start of with N disconnected vertices this one begins with a pre-built ring lattice each with degree $2K$ and then rewires edges at random.

The effect of the rewiring is that short-cuts are introduced into the graph decreasing the average path length L of the graph without increasing the average degree. Figure 13 shows the dependence of the shortest path length $L\left(p_{rw}\right)$ and

clustering coefficient $C(p_{rw})$ to the rewiring probability in an intuitive manner. Watts and Strogatz provide a new definition of the clustering coefficient: for some vertex n in the graph $C_n = \frac{K_n}{k_n(k_n-1)/2}$. k_n is the degree of vertex n, thus the denominator is the maximum number of edges possible between the neighbours of vertex n. Whereas K_n is the number of actual edges between the neighbours of vertex n. As $C_n \to 1$ the neighbourhood of vertex n becomes maximally connected, this is also called a clique. It is in the region of p_{rw} where $L(p_{rw})$ is smaller than that of a regular lattice and $C(p_{rw})$ is near 1 that a graph is considered to have small-world properties.

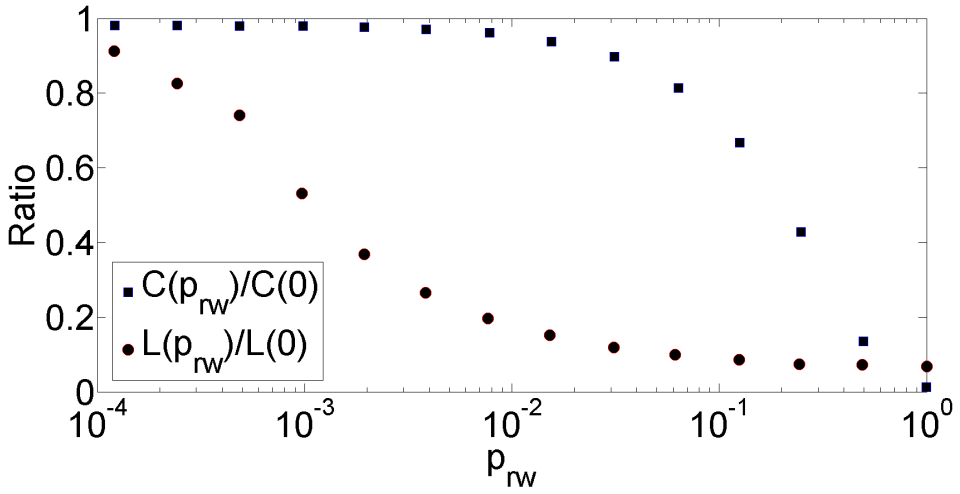


Figure 13.: A reproduction of the plot found in [33], it shows the relationship between the rewiring probability p_{rw} (horizontal axis) and the normalized average path length $\frac{L(p_{rw})}{L(0)}$ (vertical axis) as well as with the normalized clustering coefficient $\frac{C(p_{rw})}{C(0)}$ (vertical axis). [33]

Rigorous analytical solutions for the average path length, clustering coefficient and the probability distribution of the degree were produced by [28]. However they eschew from using the definition of the clustering coefficient in-

troduced by [33] and instead use the ratio of triangles to triplets instead as we have defined in equation 13.

They first consider what the coefficient would be for a graph with $p_{rw} = 0$, see equation 23 in Section 1.1.5, then introduce disorder to that system (increase p_{rw}). They found that the probability of there being a triangle reduces by $(1 - p_{rw})^3$ up to the order of $\frac{1}{N}$, the final result is

$$C_{WS}(p_{rw}) = \frac{3(2K-2)}{4(2K-1)}(1-p_{rw})^3 + \mathcal{O}\left(\frac{2K}{N}\right) = C(0)(1-p_{rw})^3 + \mathcal{O}\left(\frac{2K}{N}\right) \tag{30}$$

In the limit $p_{rw} \to 1$ the clustering coefficient acts like $\frac{2K}{N}$, in other words similarly to an Erdős-Rényi graph.

The procedure for working out the degree distribution is simple, [24]. For a circular lattice where each vertex starts with degree $2K$, half are considered for rewiring and k_1 of those are not rewired. k_2 is the number of edges gained due to the rewiring process. The total number of edges a vertex has after the rewiring is finished is $k = K + k_1 + k_2$. The probability that k_1 edges are not rewired is

$$P_1(k_1) = \binom{k_1}{K/2}(1-p_{rw})^{k_1} p_{rw}^{K/2-k_1} \tag{31}$$

The probability that k_2 edges are gained due to the rewiring process is

$$P_2(k_2) = \binom{k_2}{NKp_{rw}/2}\left(\frac{1}{N}\right)^{k_2}\left(1-\frac{1}{N}\right)^{NKp_{rw}/2-k_2} \approx \frac{(Kp_{rw}/2)^{k_2}}{k_2!}e^{-Kp_{rw}/2} \tag{32}$$

then the probability of a vertex having degree k after the rewiring process is complete is given by

$$P(k) = \sum_{n=0}^{(min)(k,K)} \binom{K/2}{n} (1-p)^n p^{K/2-n} \frac{(pK/2)^{k-K/2-n}}{(k-K/2-n)!} e^{-pK/2} \tag{33}$$

Which is a Poisson distribution just as the Erdős-Rényi graphs were.

1.2 SPIN MODELS OF VOTING BEHAVIOUR

In this section we will present a few spin models that are of interest. These models were chosen for their simplicity and their potential for interesting emergent behaviour when paired with the structure of the complex graphs. What is interesting is that the basic mechanisms used to model magnetism can be used to model the voting behaviour of people. A small amount of knowledge of magnetism and its origins is beneficial for understanding Spin Models and thus how they may pertain to models of voting.[10, 16, 38–44]

Crystalline materials, such as metals, consist of atoms in a regular lattice. Each atom has an intrinsic property called *spin* which can be -1, 0 or 1. When the spin is non-zero the atom has a *magnetic dipole*. If the magnetic dipoles of the atoms are randomly aligned then the magnetic fields of the atoms cancel out and the material overall has no magnetic field. However if the magnetic dipoles are aligned the material produces a magnetic field. The orientation of a dipole is affected by the temperature. At low temperatures the orientation rarely

change but at high temperatures it can take essentially any value. Consequently materials above a critical temperature do not exhibit magnetism.

There are three types of magnetism. All materials are intrinsically *diamagnetic* where the magnetic dipoles of atoms in a material align anti-parallel to an externally induced magnetic field. In *paramagnetic* materials the magnetic moments align parallel to the external field and thus enhance the strength of the external field. However once the external field is removed they become randomly aligned and lose their magnetic field. The third type are *ferromagnetic* materials, they have the same properties as paramagnets but the atoms also try to align themselves parallel to their neighbours. Consequently in the absence of an external field ferromagnets maintain their magnetism. These are simple descriptions as the true mechanics are outside of the purview of this thesis.

Spin models of ferromagnetism have been long studied and the Ising Spin model is one such very simple model. In this model particles can be either be in the -1 or $+1$ state. Each particle changes state to match the majority of its neighbours. As alluded to earlier this simple model can be used in multiple fields of research and the specific nomenclature varies with them. In physics the particles may be seen referred to as 'lattice points', 'vertices', 'molecules', 'atoms' or 'particles' whereas in computer science and sociology we might see 'agents' or 'cellular automata'. In mathematics any of these terms may be found depending on the specific application of the work, in this thesis we shall use 'vertices'.

1.2.1 *Ising Spin Model*

The Ising Spin model we shall be using is a discrete time Markov process where the spin configuration of a system at time $t+1$ depends only on its configuration at time t. The systems we shall consider consist of N vertices each of which can be in only 1 of 2 spin states (-1 or $+1$) during each time step. To make it clear we are discussing the configuration states of a Markov system we define the ordered set,

Definition 14. $\Sigma = \left\{\sigma^0, \sigma^1, \ldots, \sigma^t, \sigma^{t+1}, \ldots \sigma^T\right\}$ *is the ordered set of spin configuration states of a system in the period of time* $[0, T]$*, where* σ^t *is the spin configuration at time* t*. For all* $\sigma^t : t > 0$ *are the results of a Markov process and thus depend only on the configuration state of* σ^{t-1}*.*

The spin of a single vertex i at time t will be written as σ_i^t. In this section we will shall define the Ising Spin model in terms of its Hamiltonian function and discuss the resulting behaviour of such a system as a whole and its indiviudal vertices.

As a physical model each configuration σ has an *energy* which is given by the Hamiltonian function [10, 16, 38–44],

$$H(\sigma) = -\frac{1}{2}\sum_{i=1}^{N}\sum_{j=1}^{N} \boldsymbol{A}_{ij}\boldsymbol{J}_{ij}^{\text{int}}\sigma_i\sigma_j - \mu\sum_{i=1}^{N} J_i^{\text{ext}}\sigma_i \tag{34}$$

where the $\boldsymbol{J}_{N\times N}^{\text{int}}$ is a matrix of the interaction strength between vertices, J_i^{ext} is the interaction strength of vertex i with an external magnetic field and μ

is the magnetic moment. The function consists of contributions to the energy from internal and external interactions. The double sum in the function is the energy due to the internal interactions between each vertex and its nearest neighbours. Whether $\boldsymbol{J}_{ij}^{\text{int}}$ is positive or negative decides whether the material being modelled is ferromagnetic or anti-ferromagnetic while it is zero when modelling diamagnetic materials. Consequently a positive $\boldsymbol{J}_{ij}^{\text{int}}$ means the system has a lower energy if neighbouring vertices have the same spin and vice versa for $\boldsymbol{J}_{ij}^{\text{int}} < 0$.

In our work we focused on systems where there are no external fields and where the interactions between neighbours will be of the same strength and sign, i.e. we set $\mu = 0$ and $\boldsymbol{J}_{ij}^{\text{int}} = J \; \forall \; i, j \in [1, N]$. Thus we can write equation 34 in a simpler form [10, 16, 38–44],

$$H\left(\sigma\right) = -\frac{J}{2} \sum_{i=1}^{N} \sum_{j=1}^{N} \boldsymbol{A}_{ij} \sigma_i \sigma_j. \tag{35}$$

Given N vertices there are 2^N unique configurations therefore there is a $\frac{1}{2^N}$ of a system being in any particular configuration. However different configurations can have the same energy and the probability of the system having a particular energy E is given by the Boltzmann distribution [10, 16, 38–44],

$$P\left(E\right) = \frac{e^{-E/k_B T}}{Z}, \tag{36}$$

where $k_B \approx 1.3806 \times 10^{-23}\text{m}^2\text{kgs}^{-2}\text{K}^{-1}$ is the Boltzmann constant and,

$$Z = \sum_{\forall i} e^{-E_i/k_B T}, \tag{37}$$

is the partition function [10, 16, 38–44]. When $k_B T \gg E$ the system having a configuration with low, mid or high energies are equally likely. Should $k_B T \leq 1$ the system is unlikely to have a configuration that has low or high energies and when $k_B T \ll 1$ the system is most likely to have a configuration with a low energy.

We can apply equation 36 to calculate the probability of a system going from σ^a to σ^b. Let us first define the change in energy $\Delta H\left(\sigma^b, \sigma^a\right) = H\left(\sigma^b\right) - H\left(\sigma^a\right)$ then,

$$P\left(\sigma^b, \sigma^a\right) = \frac{e^{-\Delta H\left(\sigma^b, \sigma^a\right)/k_b T}}{\sum\limits_{\forall x,y} e^{-\Delta H(\sigma^y, \sigma^x)/k_b T}}, \tag{38}$$

is the probability of a system with spin configuration σ^a changing to σ^b.

We can also use the Hamiltonian function on single vertices to calculate the probability of a vertex changing spin state. The partition function Z has only to account for a vertex's spin staying the same or changing. If the vertex keeps the same spin its change in energy is $\Delta H\left(\sigma_i^{t+1} = \sigma_i^t, \sigma_i^t\right) = 0$ whereas if it does change its spin then $\Delta H\left(\sigma_i^{t+1} = -\sigma_i^t, \sigma_i^t\right) = -2H\left(\sigma_i^t\right)$. Thus the partition function is $1 + e^{2H\left(\sigma_i^t\right)/k_B T}$, the probability a vertex i does not change spin is,

$$P\left(\sigma_i^{t+1} = \sigma_i^t, \sigma_i^t\right) = \frac{1}{1 + e^{2\beta H\left(\sigma_i^t\right)}}, \tag{39}$$

and the probability of the changing spin is,

$$P\left(\sigma_i^{t+1} = -\sigma_i^t, \sigma_i^t\right) = \frac{e^{2\beta H\left(\sigma_i^t\right)}}{1 + e^{2\beta H\left(\sigma_i^t\right)}}, \tag{40}$$

where $\beta = 1/k_B T$.

Equation 40 can be rewritten in terms of the number of nearest neighbours that have the same spin as a vertex i. Let S_i^t be the number of neighbours of vertex i that are in the same spin state at time t,

$$S_i^t = \sum_{j=1}^{N} \boldsymbol{A}_{ij} \delta\left(\sigma_i^t, \sigma_j^t\right). \tag{41}$$

Then we can now define $H\left(\sigma_i^t\right) = -J\left(2S_i^t - k_i\right)$ where k_i is the degree (number of nearest neighbours) of vertex i. Thus

$$P\left(\sigma_i^{t+1} = -\sigma_i^t, \sigma_i^t\right) = \frac{e^{-2\beta J\left(2S_i^t - k_i\right)}}{1 + e^{-2\beta J\left(2S_i^t - k_i\right)}}. \tag{42}$$

If $2S_i^t - k_i > 0$ vertex i has a low probability of changing spin, if $2S_i^t - k_i < 0$ it has a high probability of changing spin. However should $S_i^t = k_i$ then the probability of changing is a $1/2$. The figure 14 below plots equation 42 for different $\beta = 1/k_b T$. It shows how the probability tends towards the Heaviside function for large values of β and a constant half when it is very small.

The pseudo-code and description of the algorithm used to implement the Ising model can be found in the appendix D. Implementations of the code in C++ can be found at https://github.com/karthiksowdirb.

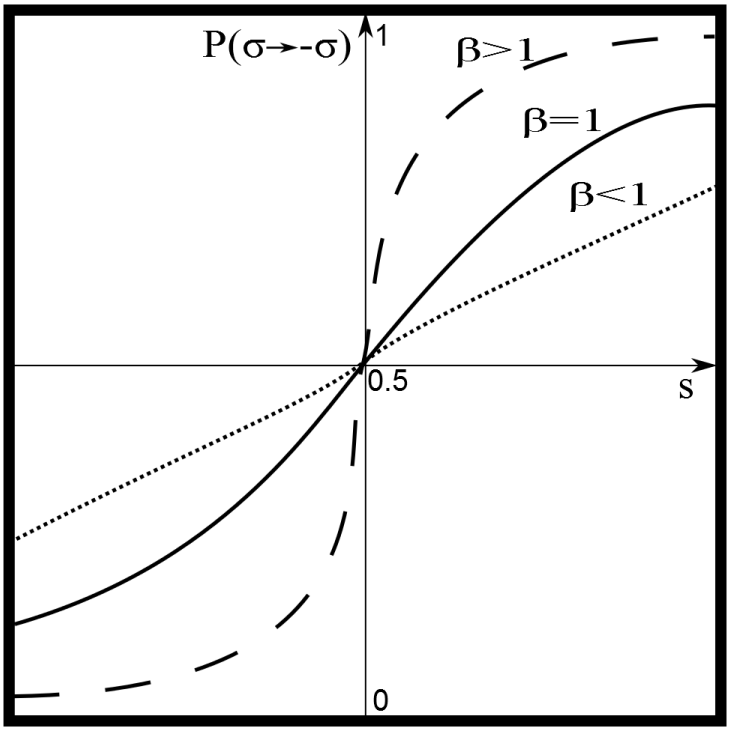


Figure 14.: The probability that an vertex will change spin $P\left(\sigma_i^{t+1} = -\sigma_i^t, \sigma_i^t\right)$ as a function of the number of neighbours with spin σ_i^t. As $\beta = 1/k_B T$ when the temperature T is high $\beta << 1$ the probability tends towards a $1/2$s. However as the temperature becomes low T the probability tends towards the Heaviside step function, $\lim_{T\to 0} P\left(\sigma_i^{t+1} = -\sigma_i^t, \sigma_i^t\right) = \mathcal{H}(0)$.

1.2.2 *Potts Model*

The Potts Spin model is a generalisation of the Ising Spin model [43]. Vertices are no longer limited to 2 possible spins but can choose one of l spin states to be in. Although the Potts model is not the main focus of study we shall be discussing a spin model with many spins in Section 1.3 and it may be useful to understand how changes to the Hamiltonian can effect the behaviour.

The change in the Hamiltonian function has little effect on the basic mechanics. If we quickly repeat the steps taken in the previous section we can once

again obtain the probability distribution function for a single vertex's change in spin state.

Let us say that an vertex i at time t may have one of l spin states, $\sigma_i^t \in \{1, 2, ..., l\}$. We also require that the energy of the system decreases if and only if neighbouring vertices are in the same spin state. It is important to note that despite the labelling scheme each spin state is orthogonal to every other in the sense that the Kronecker delta of any two different spin states is always zero, $\delta(\sigma_i, \sigma_j) = 0 \forall \sigma_i \neq \sigma_j$, and one when they are the same, $\delta(\sigma_i, \sigma_j) = 1 \forall \sigma_i = \sigma_j$. Thus equation 34 can be written as

$$H\left(\sigma^t\right) = -\frac{1}{2}\sum_{i=1}^{N}\sum_{j=1}^{N}\boldsymbol{A}_{ij}\boldsymbol{J}_{ij}^{\text{int}}\delta\left(\sigma_i^t, \sigma_j^t\right) - \mu\sum_{i=1}^{N}J_i^{\text{ext}}\sigma_i^t \tag{43}$$

where once again $\boldsymbol{J}_{ij}^{\text{int}}$ is a matrix of the interaction strength between vertices i and j, $\boldsymbol{J}_i^{\text{ext}}$ is the interaction strength of an vertex i with an external magnetic field, μ is the magnetic moment and now $\delta(\sigma_i, \sigma_j)$ is the Kronecker delta function [43]. The equivalent simple version is then

$$H(\sigma) = -\frac{J}{2}\sum_{i=1}^{N}\sum_{j=1}^{N}\boldsymbol{A}_{ij}\delta\left(\sigma_i^t, \sigma_j^t\right) \tag{44}$$

and for a singular vertex:

$$H\left(\sigma_i^t\right) = -J\sum_{j=1}^{N}\boldsymbol{A}_{ij}\delta\left(\sigma_i^t, \sigma_j^t\right). \tag{45}$$

In the previous section we defined S_i^t, equation 41, as the number of neighbours in the same spin state as vertex i at time t. That definition only accounted for the existence of 2 possible spin states now we redefine it to include an arbitrary number of spin states. We now define $S_i^t(\psi)$ as the number of neighbours of i that are in state ψ at time t and define it mathematically as,

$$S_i^t(\psi) = \sum_{j=1}^{N} \boldsymbol{A}_{ij}\delta\left(\psi, \sigma_j^t\right). \tag{46}$$

The change in energy is $\Delta H\left(\sigma_i^{t+1} = \psi, \sigma_i^t\right) = J\left\{S_i^t(\sigma_i^t) - S_i^t(\psi)\right\}$ it follows then that the probability of change is given by,

$$P\left(\sigma_i^{t+1} = \psi, \sigma_i^t\right) = \frac{e^{-\beta J\left\{S_i^t\left(\sigma_i^t\right) - S_i^t(\psi)\right\}}}{Z_i^t} \tag{47}$$

where $\beta = 1/k_B T$ and the denominator Z_i^t is the partition function,

$$Z_i^t = \sum_{\psi=1}^{l} e^{-\beta J\left\{S_i^t\left(\sigma_i^t\right) - S_i^t(\psi)\right\}}. \tag{48}$$

Once again the value of β, and thus temperature T, controls the shape of the distribution. When T is high and β is small every spin state is equally as likely to be chosen, while if T is small the spin states with largest population are significantly more probable for an vertex to change its spin to.

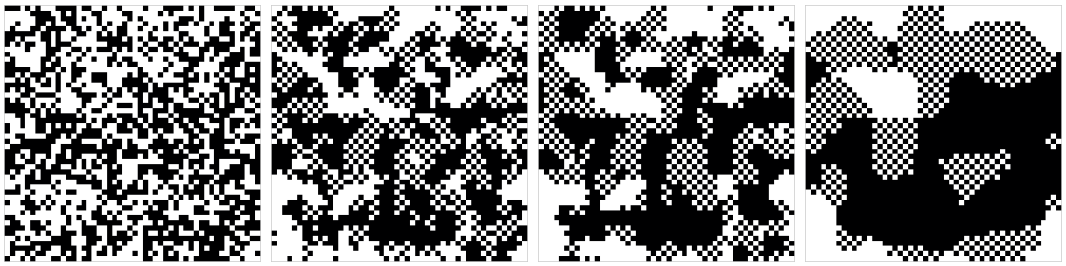


Figure 15.: The configuration states of a rectangular 50x50 spin lattice immediately after quenching. As time t progresses the regions either evaporate or condense. Overall the lattice appears to coarsen. The colours black and white corresponds to the spin of a lattice point.

1.2.3 *Consensus Formation*

Spin models like those so far discussed are sometimes referred to as *coarsening* models. This is due to the growth of regions with similar spin as a control variable such as the temperature T is lowered or *quenched*. Initially the system contains many small regions but as T is lowered some regions shrink and others grow. Eventually the system consists of a few large regions where every vertex in the same region has the same spin. Figure 15 shows the configuration states after quenching of a rectangular lattice where each square represents the spin of a vertex in the lattice. The vertices have chosen their spins according to the Ising Spin model and can thus have 1 of 2 spin states represented by the colours black and white. The square at (x, y) in the images are the spin states of vertex $v = 50y + x$ at times $t = 0$, 5, 10, and 50 time steps after quenching. Displaying the configurations in this way means that squares immediately above, below, right and left of a square (x, y) naturally represent the spins of the nearest

neighbours of a vertex v. Consequently the images are a intuitive representation of the configuration states.

By visual inspection the configuration state for $t = 0$ shows lots of small thin strands of white and black regions throughout the system, i.e. fine structure. After only 5 time steps the configuration has changed significantly as there are slightly larger regions of white and black and there are also regions with a checker board pattern. At $t = 5$ there is less fine structure and it has become coarser and this continues to lose fine structure with time. At $t = 10$ the regions are large and almost all of the fine structure and jumping forward to $t = 50$ the system is dominated by a large black region and several checker board regions and some slightly smaller white regions. This coarsening behaviour is of interest to both physicist and sociologists, to the former it is a model describing the appearance of magnetism in materials and to the latter it models how groups of humans form a consensus of opinion.

The process of coarsening on complex graphs can lead to one opinion (spin) having an overwhelming majority which is called a *consensus*. The density of vertices in either state needed to form a consensus is slightly arbitrary, it can require anything from 65% to 95% of all vertices on a graph to have the same spin state. A variable threshold allows for the existence and classification of weak and strong consensuses. Consensus formation is a repeatable result and is as much due to the graph structure as well as the initial spin state configuration. In figure 16 shows how quickly different types of graph form a consensus. Complete and to a lesser extent scale-free graphs satisfy the

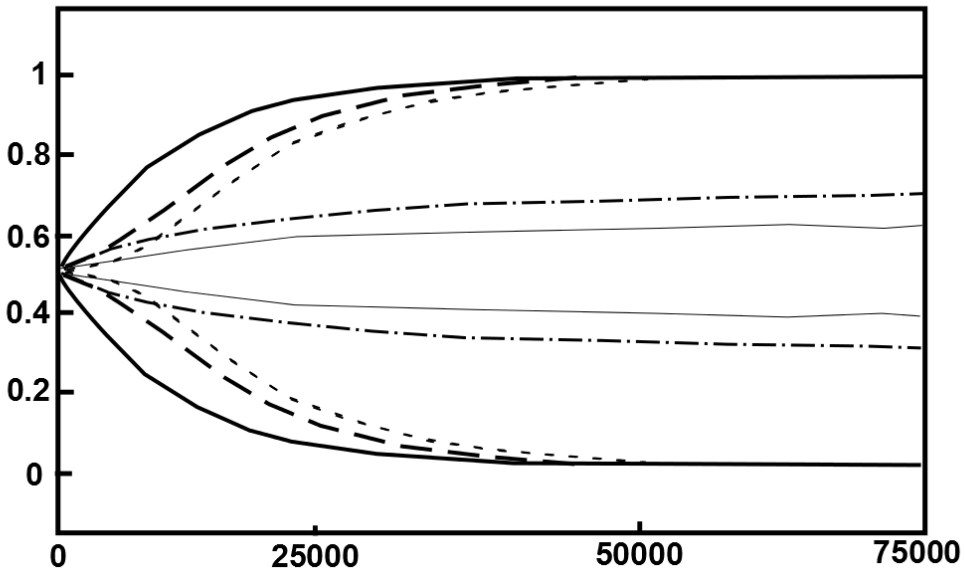


Figure 16.: Evolution in time of the density of vertices in spin state +1 for the Ising Spin model. Several graphs have been used ($N = 10^4$): complete graph (thick solid line), circular lattice with $K = 6$ (thin solid line), scale-free with $\gamma = 2.5$ (thin-dashed line), scale-free with $\gamma = 3$ (thick-dashed line), and Watts-Strogatz with $p = 0.05$ and $K = 6$ (dot-dashed line). Consensus forms quickly for graphs which fulfil the homogeneity condition. Reproduced from [45].

homogeneity condition. To fulfil the condition the number of neighbours an vertex i has in state +1 must be on average $\langle k_i \rangle \rho(t)$ given that $\rho(t) = N_{+1}/N$, where N_{+1} is the number of vertices in state +1 and N is the total number of vertices [45]. We can see from the plot in figure 16 that Watts-Strogatz do not form strong consensuses. This is due to their high clustering coefficient and characteristic community structure. Communities have weak links between each other an so have little influence over each other thus communities can come different consensuses resulting in no consensus for the whole graph. We shall describe communities in more detail in Section 1.3.

When it comes to consensus formation or magnetism which opinion or spin forms majority does not matter. We shall use magnetism as defined here as a measure of consensus,

$$M\left(\sigma^t\right) = \frac{1}{N}\left|\sum_{i=1}^{N}\sigma_i^t\right|, \tag{49}$$

where $N = \left|\sigma^t\right|$ is the number of vertices in the graph, σ_i^t is the spin state of vertex i at time t. Then $\langle M\rangle_T$ denotes the time average taken over the non-transient period and $\langle\langle M\rangle_T\rangle_C$ is for configurational averages, [46].

1.3 COMMUNITY STRUCTURE IN COMPLEX GRAPHS

Communities in the real world are groups of people that have some sort of social connection. For example consider a religious community they share the same beliefs and visit the same place of worship regularly consequently they are more strongly linked socially than those who are not of the same religion. Graphs are used to represent such relationships and it is no surprise that communities appear in graphs as well. In terms of graphs a community is a group of vertices that are more connected to each other than they are to vertices not in the group. This is a vague definition and there are many interpretations and thus approaches to identifying communities in a graph. We shall discuss *devisive*, *agglomerative* and *statistical mechanics* approaches.

All the algorithms will be *partitioning* the graph into groups of vertices each of which is a community. To determine whether any particular partition is a good one or not we use a *modularity* measure. Community partitions with

larger modularity are better partitions than those with low modularity. Below we provide definition of modularity used by Girvan and Newman [47],

Definition 15. *Modularity is a measure of how separate the connected subgraphs in a partition are from each other. Given that a graph has been partitioned into k communities we can define a matrix* $\boldsymbol{\mathcal{E}}$ *such that its element* $\boldsymbol{\mathcal{E}}_{ij}$ *is the fraction of all edges that link a community i to community j. We also define where* $a_i = \sum_j \boldsymbol{\mathcal{E}}_{ij}$ *which is the fraction of all edges that connect to vertices in community i [47]. Then the modularity of the partition is,*

$$Q = \sum_i \left(\boldsymbol{\mathcal{E}}_{ii} - a_i^2 \right). \tag{50}$$

The divisive algorithms start with the graph as a whole and removes edges based on some criteria. As edges are removed at some point the graph split into two components, the removal of edges continues eventually one of the components will also be split in two as well. The splitting continues until the graph consists of disconnected vertices.

One of the standard divisive algorithms is the Girvan-Newman algorithm [47], where edges removed have the largest *edge-betweenness*. The definition of edge-betweenness is,

Definition 16. *Given a graph* $G(V, E)$ *the edge-betweenness of an edge* $e = \{v, w\}$ *is the fraction of all the shortest paths on the graph which use e.*

$$B_e = \sum_{i \neq j} \frac{g_{iej}}{g_{ij}}, \tag{51}$$

where $g_{ij} = |\{\rho^*(i,j) \mid i,j \in G\}|$ *the size of the set of all paths between vertices* i *and* j *and* $g_{iej} = |\{\rho^*(i,j) \mid i,j \in G \wedge \exists v_x, v_{x+1} \in \rho i,j : v_x \in e, v_{x+1} \in e \backslash v_x\}|$ *is the size of the set of all paths between* i *and* j *that uses the edge* $e = \{v,w\}$ *[47, 48].*

Consider that vertices send messages to all other vertices using only the shortest paths connecting them. Within a community there are lots of edges and therefore many routes a message can use to traverse the graph, consequently each edge in the community tends to be used the same amount. When messages are sent between vertices in different communities the number of routes between them is less, as a consequence the small number of edges connecting communities have a lot of message traffic. Edge-betweenness can be a thought of as a measure of this traffic, by removing the edges with high edge-betweenness (message traffic) a graph can be partitioned into its communities.

Agglomerative algorithms could be considered the opposite of divisive ones as they start with the vertices and merge them into connected subgraphs based on some criteria. There are several methods that are efficient at detecting communities using by maximising modularity using greedy methods such as in the EAGLE [49] and the CNM algorithm [50]. These algorithms also produce a dendrogram at its top it has as many roots as there are vertices in the graph, branches merge such that the modularity of the resulting partition is greater than the one before it. Eventually at the bottom of the dendrogram a partition of communities with the largest modularity is left.

The statistical mechanics approach is very different to the other two. A simulation of a stochastic process is applied on the graph such that each vertex is assigned some value. The partitioning the graph according to these values results in connected subgraphs which are communities. An example of such a method is modelling the graph as spin glass and use simulated annealing to find configuration of spin states with the minimum energy. The model allows each vertex to be in 1 of q spin states, vertices which are in the same spin state are in the same community. The Hamiltonian is different to that discussed in Section 1.2.2 and is given as,

$$\mathcal{H}(\sigma) = -\sum_{i,j \in E} \delta(\sigma_i, \sigma_j) + \frac{\gamma}{4M} \sum_{s}^{q} K_s^2, \tag{52}$$

where δ is the Kronecker delta function, M is the total number of edges in the graph, and K_s is the sum of the degrees of vertices in spin state s. The parameter γ controls the weight of the internal edges of a community: when γ is small the number of existing internal edges will not matter, when γ the number of internal edges becomes important.

The procedure for these algorithms are discussed in appendix C and the software used to extract the community structure is the open source igraph library [51]. Implementations of the code in C++ can be found at https://github.com/karthiksowdirb.

2

FURTHER DEFINITIONS AND VALIDATION OF SIMULATION

2.1 INTRODUCTION

In the literature review we described how graphs are a way of modelling relationships and spin models as a way of modelling opinion forming processes. In Section 1.2.3 an example was given of how these two models can be used together to model how groups of people come to hold a common opinion. There is clear evidence that graphs with different structures facilitate consensus formation in different ways. Then in Section 1.3 we discussed how spin dynamics can be used to obtain structural properties of graphs - namely identifying communities.

In this chapter we define a mesoscopic feature of spin-dynamics and how their properties may be of interest to us. As the spin-dynamics are affected by the structure of a graph we shall provide details on the properties of the graphs we

investigated and validate our implementation of the Ising Model by comparing our observed values for the critical temperatures against theoretical values.

Implementations of the code used to generate the graphs, extract community structures, simulate the Ising Spin dynamics, and analyse the data can be found at https://github.com/karthiksowdirb.

2.2 CROWDS

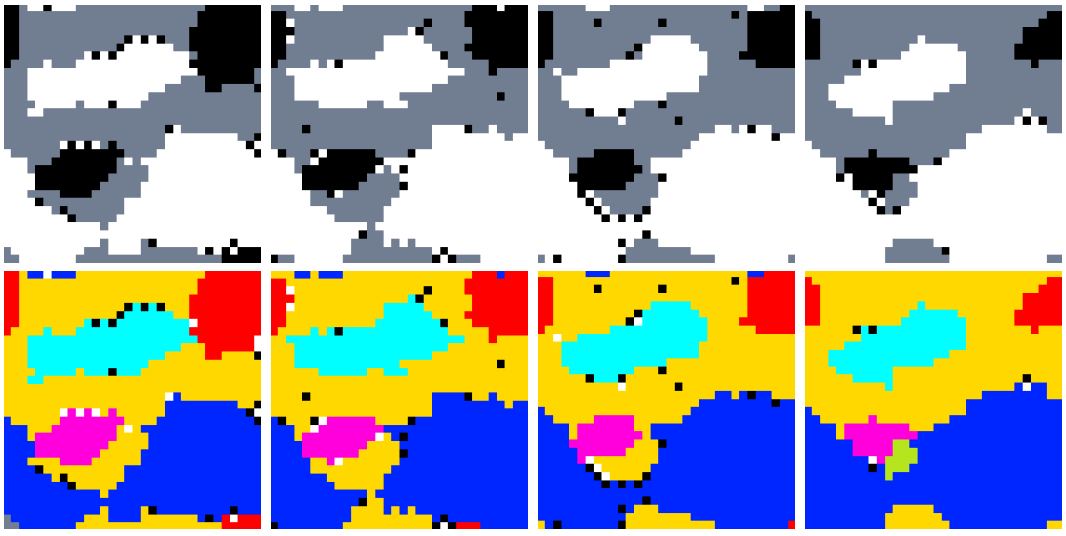


Figure 17.: The images depicts the states of vertices in a rectangular graph, G_{RL}, during the time steps $t = 50$, 60, 70 and 80 after quenching, the images the ij-th square represents a vertex $v = 32i + j$ in the graph, i.e. $v \in G_{RL}$. In the top row colour of the square represents the spin states of each vertex where black, grey and white are -1, 0 and $+1$ respectively. While in the bottom row each of the different colours represents a different crowd, all vertices coloured yellow are in the same crowd. Crowds persist over time, the yellow crowd at $t = 50$ is the same as the yellow crowd at $t = 60$ however the constituent vertices in each crowd during the different time steps can change.

In our system we are applying a spin model on top of a graph, where each vertex i at time step t has a spin state $\sigma_i^t \in \{-1, +1\}$. We can say that two vertices i and j are *aligned* if they both have the same spin state at the same time, with the Kronecker delta of the two spin states is $\delta\left(\sigma_i^t, \sigma_j^t\right) = 1$. It is also possible to determine the alignment of an entire graph G, we call this measure 'magnetisation' (Section 1.2.3),

$$M = \frac{1}{N}\left|\sum_{i=1}^{N} \sigma_i^t\right|. \tag{53}$$

Alignment, $\delta\left(\sigma_i^t, \sigma_j^t\right)$, is microscopic measure and the magnetisation macroscopic measure of alignment, we can also determine alignments at the mesoscopic scale such as by calculating the magnetisations subgraphs. This can be useful to see if the alignments of the communities in a graph are independent of each other.

An alternative method is to use alignment to define regions of the graph; the number of regions, their sizes and lifetimes can be used to learn about what is occurring in more detail at mesoscopic scales. At intermediate scales regions of the graph form clusters of aligned spin. This is illustrated in the top row of figure 17 which shows the spin configuration of a rectangular lattice during different time steps. The colour of each pixel indicates the spin state of a vertex where -1 is black, 0 is grey, and $+1$ is white - vertices with the same colour are aligned. Notice that multiple spin-clusters can have the same alignment but are separated from each other by spin-clusters which have a different spin-states.

The bottom row of images shows the spin-clusters during different time steps, vertices with the same colour are in the same spin-cluster. We obtain the spin-clusters at each time step t by trimming the edges of the graph $G \equiv G(V, E, \Sigma)$ between vertices with different spin states, i.e. the edge $\{i, j\}$ is removed if $\delta\left(\sigma_i^t, \sigma_j^t\right) = 0$. The resultant graph is $G^t \equiv G^t(V, E^t)$ where $E^t = \left\{\{i, j\} \mid \{i, j\} \in E \wedge \delta\left(\sigma_i^t, \sigma_j^t\right) = 1\right\}$ consists of 1 or more components, each of which is one of the spin-clusters shown in the figure.

One of the most important characteristics of the spin-clusters is that they are amorphous, they have no fixed shape. In the bottom row of figure 17 we indicate that two spin-clusters at different times are the same spin-cluster by using the same colour. To visual inspection this is easily noticeable as there only small changes between each time step. We have decided that two components, $K_1 \equiv K_1(V_1, E_1) \subseteq G^t$ and $K_2 \equiv K_2(V_2, E_2) \subseteq G^{t+1}$ represent the same spin-cluster during consecutive time steps if and only if more than 50% of $V_1 \cup V_2$ is in both components. We define the similarity of two components as,

$$\Phi(K_1, K_2) \frac{|K_1 \cap K_2|}{|K_1 \cup K_2|} \equiv \frac{|V_1 \cap V_2|}{|V_1 \cup V_2|}, \tag{54}$$

where $\Phi(K_1, K_2) > 0.7071$ means that K_1 and K_2 represent the same spin-cluster. We choose the threshold 0.7071 as it means that the number of vertices that K_1 and K_2 have in common is greater than 50%. This ensures that for all $K_1 \in G^t$ there does not exist 2 or more components in the next step which could be considered the same same spin-cluster as K_1, i.e. $\nexists, K_2, K_3 \in G^{t+1}$: $\Phi(K_1, K_2) > 0.7071 \wedge \Phi(K_1, K_3) > 0.7071 \forall K_1 \in G^t$. It follows naturally

then that the components K^x and K^y which exist at time steps x and $y > x$ respectively represent the same spin-cluster if and only if there exists a chain of spin-clusters, $K^x, K^{x+1}, \ldots, K^t, K^{t+1}, \ldots, K^t$, where each pair of adjacent spin-clusters share more than 50% of the same vertices, i.e. $\Phi\left(K^t, K^{t+1}\right) > 0.7071 \forall t \in [x, y)$.

Consider now a spin-cluster C that only exists for a finite time $\mathcal{L} = D - B + 1$, where B and D are the birth and death time steps of the spin-cluster, then we can say that the ordered set of subgraphs of a graph $G(V, E, \Sigma)$,

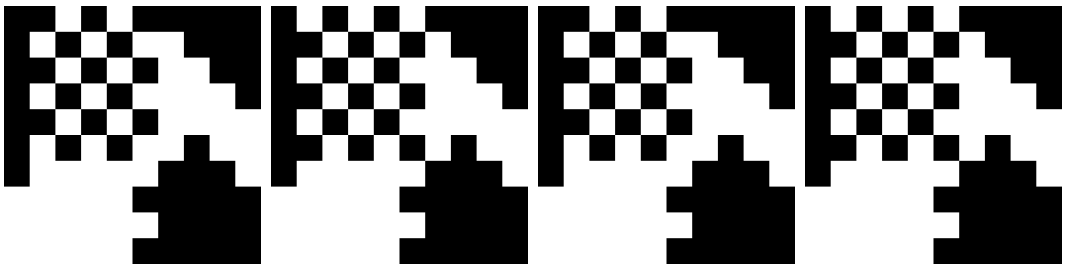
$$\begin{aligned} C = \Big\{ K^0, K^1, \ldots, K^\tau, \ldots, K^{\mathcal{L}-1} \mid & K^\tau \subseteq G^{B+\tau} \forall \tau \in [1, \mathcal{L}) \\ & \wedge \Phi\left(K^\tau, K^{\tau+1}\right) > 0.7071 \forall \tau \in [0, \mathcal{L}) \\ & \wedge \nexists K \subseteq G^{B-1} : \Phi\left(K, K^0\right) > 0.7071 \\ & \wedge \nexists K \subseteq G^{D+1} : \Phi\left(K^{\mathcal{L}-1}, K\right) > 0.7071 \Big\}, \end{aligned} \tag{55}$$

describes the spin-cluster in its entirety. The first condition of the set ($K^\tau \subseteq G^{B+\tau} \forall \tau \in [1, \mathcal{L})$) states that the τ-th component in C must be a component of the trimmed graph $G^{B+\tau}$ and implies that K^τ and $K^{\tau+1}$ must be components of trimmed graphs for consecutive time steps. The second the condition of the set is that the number of vertices they have in common must be greater than 50% of all their vertices together. The third condition $\Phi\left(K, K^0\right) \leq 0.7071 \forall K \subseteq G^{B-1}$ states that there exists no component at time $B - 1$ that could be considered as part of this spin-cluster. The fourth condition states the same thing for the components of time step $D + 1$.

From this point on in the thesis we shall use the term *crowd* to refer to spin-clusters. Our reasoning for this is foremost a matter of consistent terminology: whereas a spin-cluster is a physical concept a crowd is social one. We also feel that our choice in terminology is more descriptive as spin-clusters are amorphous, and they gain and lose vertices over time like a crowd which also has no defined shape as it gains and loses people. Furthermore by carefully selecting the spin dynamics the spin-clusters can be used to identify communities (see Section 1.3) which is similar to how people segregate into their communities at social functions under the correct circumstances.

Pseudo-code and a description of the algorithm used to identify and extract crowds from the spin-configuration can be found in appendix D.1.

2.2.1 *Pre-Processing Spin Data*



(a) $t = 0$ (b) $t = 1$ (c) $t = 2$ (d) $t = 3$

Figure 18.: A manufactured example of an indecisive region on a rectangular graph. The vertices in the top left hand corner flip opinions every time step. The reasons for doing so are a result of the Ising Spin model and it is clear that this region is different from the others.

As we are using the Ising Spin model, see Section 1.2.1, the vertices in a crowd we identify all are in either the -1 or $+1$ opinion state. This conjures a

picture of the configuration of the graph consisting only of uniform regions of spin however this is not entirely true. There are actually three stable states for the graph: all the vertices have the opinion -1, all vertices have the opinion $+1$, and half are -1 and the other half $+1$ arranged in a checker board pattern. The first two configuration states are global minimum energy states and thus are stable while the third is the global maximum and unstable. What is possible for the entire graph is also possible for regions of the graph. The vertices in the checker board regions tend to flip opinions frequently which characterises them as being *indecisive* and those in aligned regions as *decisive*, [52, 53].

Visually on a rectangular graph regions of mixed spin can form a checker board pattern the colours of which inverts every time step, see figure 18. The indecisive regions are created by the dynamics of the Ising Spin model and maintained by them as well. These dynamics allow them to grow and decay just like the aligned regions. Consequently we believe that vertices in these regions should be considered as a crowd together instead of individually as separate crowds. In this section we shall provide our procedure for pre-processing the spin configurations which have only one of two opinion states (-1 and $+1$) to new spin configurations where vertices can have one of three opinion states (-1, 0, and $+1$).

The results of our simulations is a matrix $\boldsymbol{Z}_{N\times T}$ where each column is the opinion configuration states of a graph of N vertices over the time period $[0, T)$. Thus the element $\boldsymbol{Z}_{vt}$ is the opinion state of vertex v during time step t. We

define a vertex as indecisive if it changes opinion states more than once every 2 time steps on average,

Definition 17. *Let $\boldsymbol{\mathcal{F}}_{N\times T}$ be a matrix where the elements are the proportion of flips in opinion a vertex makes during the time period $max\,(t-w,0) \leq t \leq min\,(t+w,T)$, where $w \in \mathbb{Z}^+$ is the maximum size of the time window to either side of t. Then we define the elements of $\boldsymbol{\mathcal{F}}$ as,*

$$\boldsymbol{\mathcal{F}}_{vt} = \frac{\sum_{\tau=max(t-w,0)}^{min(t+w,T)-1} \left[1-\delta\left(\boldsymbol{Z}_{v\tau}, \boldsymbol{Z}_{v,\tau+1}\right)\right]}{min\left(t+w,T\right) - max\left(t-w,0\right)}, \tag{56}$$

where $\boldsymbol{Z}$ is the matrix of opinion states. Then a vertex v during time step t is indecisive if $\boldsymbol{\mathcal{F}}_{vt} \geq 0.5$.

When $\boldsymbol{\mathcal{F}}_{vt}$ is in the interval $0 < \boldsymbol{\mathcal{F}}_{vt} < 0.5$ it is indicates that a vertex v has a decisive opinion but some flips still occur. Infrequent changes may be due to noise and we would also like to correct these noisy opinions during our pre-processing procedure. We define an opinion $\boldsymbol{Z}_{vt}$ as a result of noise if it has opposite sign to the moving average $\bar{\boldsymbol{Z}}_{vt}$. We define,

$$\bar{\boldsymbol{Z}}_{vt} = \frac{1}{2w+1} \sum_{\tau=\max(t-w,0)}^{\min(t+w,T)} \boldsymbol{Z}_{vt} \tag{57}$$

as the moving average opinion of vertex v during time step t where $w \in \mathbb{Z}^+$ is the maximum size of the time window to either side of t. When $\bar{\boldsymbol{Z}}_{vt} > \frac{1}{3}$ the expected spin state $\boldsymbol{E}\left(\boldsymbol{Z}_{vt}\right) = +1$ thus if the observed value of $\boldsymbol{Z}_{vt} = -1$ we can infer this is due to noise. Similarly if $\bar{\boldsymbol{Z}}_{vt} < -\frac{1}{3} \implies \boldsymbol{E}\left(\boldsymbol{Z}_{vt}\right) = -1$ thus if

the observed opinion state $\boldsymbol{Z}_{vt} = +1$ this is due to noise. On the other hand it is also possible for the moving average to be in the interval $-\frac{1}{3} \leq \bar{\boldsymbol{Z}}_{vt} \leq \frac{1}{3}$ then it can not be determined whether the opinion of a vertex is a result of noise or not. If we can determine if the opinion state of a vertex is due to noise then we should correct it otherwise it mistakenly be identified as a crowd. If we can not determine whether an opinion is the result of noise we leave its opinion state as is.

Once the elements of $\boldsymbol{\mathcal{F}}$ and $\bar{\boldsymbol{Z}}$ have been computed we can use them to compute the matrix $\hat{\boldsymbol{Z}}_{N\times T}$ the elements of which are,

$$\hat{\boldsymbol{Z}}_{vt} = \begin{cases} 0 & \text{if } \boldsymbol{\mathcal{F}}_{vt} \geq 0.5, \\ -1 & \text{if } \boldsymbol{\mathcal{F}}_{vt} < 0.5 \text{ and } \bar{\boldsymbol{Z}}_{vt} < -\frac{1}{3}, \\ +1 & \text{if } \boldsymbol{\mathcal{F}}_{vt} < 0.5 \text{ and } \bar{\boldsymbol{Z}}_{vt} > \frac{1}{3}, \\ \boldsymbol{Z}_{vt} & \textit{otherwise.} \end{cases} \tag{58}$$

This pre-processing is applied on the matrix of opinion states before crowds are identified. It removes noise that would otherwise be identified as crowds of a single size. The time window we use for counting the number of flips (equation 56) and the average opinion state (equation 57) is $w = 10$.

2.2.2 *Models of Crowd Population Dynamics*

In the spin models vertices change opinion and thus switch between crowds over time, this causes the population of a crowd to change over time. In this section we shall explore how the population size changes of a crowd can be modelled by a random walk. This is helpful as it simplifies crowd population dynamics to a process which can be thought of as largely independent of crowd-crowd interactions.

Let us consider a crowd C, its elements are subgraphs of a graph $G \equiv G(V, E, \Sigma)$. We provide this definition for crowd population,

Definition 18. *The population of a crowd C at τ time steps after forming is the number of vertices that form the subgraph $C^\tau \in C$,*

$$\mathcal{P}(C, \tau) = |C^\tau|. \tag{59}$$

In the interval $1 \leq \tau < \mathcal{L}(C)$ the population size changes by a random integer X_τ with each time step. Thus we can say that the population of a crowd $\tau < \mathcal{L}(C)$ steps after it is formed is given by,

$$\mathcal{P}(C, \tau) = \mathcal{P}(C, 0) + X_1 + \cdots + X_i + \cdots + X_\tau,$$

with $\mathcal{P}(C, \tau = 0) = \mathcal{P}(C, 0)$ and each X_i are random integers whose distributions are not necessarily identical or independent of each other. The mathe-

matics described here is analogous to that of a discrete random walk in a single dimension, [54, 55],

Borrowing insight from random walks an important indicator of the dynamics is the root mean square of the displacement. First we define the population change during time step t as,

$$\begin{aligned} \Delta\mathcal{P}\left(C,\tau\right) &= \mathcal{P}\left(C,\tau\right) - \mathcal{P}\left(C,0\right), \\ &= X_1 + \cdots + X_i + \cdots + X_\tau, \end{aligned} \tag{60}$$

then the root mean square is

$$\begin{aligned} \left[\Delta\mathcal{P}\left(C,\tau\right)\right]_{\text{rms}} &= \sqrt{\left\langle \Delta\mathcal{P}\left(C,\tau\right)^2 \right\rangle}, \\ &= \sqrt{\left\langle \left(\sum_{i=1}^{t} X_i \right)^2 \right\rangle} \\ &= \sqrt{\sum_{i=1}^{t-1} \left\langle X_i^2 \right\rangle + \sum_{i \neq j \in [1,\tau)} \left\langle X_i \cdot X_j \right\rangle} \end{aligned} \tag{61}$$

We do not know what the distributions for each X_i is but if the population size changes are analogous to Brownian motion then we would expect to observe this relationship in our results,

$$\left[\Delta\mathcal{P}\left(C,\tau\right)\right]_{\text{rms}} = \sigma\sqrt{\tau} \tag{62}$$

where σ^2 is the variance of X_i and τ is the number of time steps after a crowd was born.

If crowd population dynamics are a normal diffusive process then the population of a crowd changes by small amounts at regular intervals of time [27], our results in Chapter 3 shows this is not the case. When this is not the case, such as when the population size changes by large amounts or changes rarely the diffusive dynamics are said to be *anomalous* [54, 55].

In the case that it is unknown whether the distributions of $X_1, \ldots, X_i, X_\tau$ are all identically distributed and independent of each other we can write equation 61 as,

$$\left[\Delta\mathcal{P}\left(C, \tau\right)\right]_{\text{rms}} = D\tau^{\alpha/2}, \tag{63}$$

where D is the *diffusion coefficient* and α is the *anomalous diffusion exponent*. The dynamics of the population change is *ballistic* if the exponent $\alpha = 2$ and it is a *super-diffusion* process if $1 < \alpha < 2$, the population can sometimes change by large amounts in short periods of time. If $\alpha = 1$ then the dynamics are a *normal diffusion* process, which are regular amounts of change in regular periods of time. It is also possible for the anomalous diffusion exponent to be in the interval $0 \leq \alpha < 1$ which indicates that the dynamics are a *sub-diffusion* process [54, 55]. When the population dynamics are sub-diffusive the population size changes by small amounts over long periods of time compared to normal diffusion.

In the rest of this section we shall provide some mathematical models of anomalous diffusion. We do not use these models for analysis in later chapters however some knowledge of them may provide the reader with a deeper understanding of the results presented in Chapter 3 and onward.

Super-diffusion and sub-diffusion can be introduced into the random walk formalism by relaxing the requirement for changes in population size to be small and occur over short periods of time [54, 55]. By using the Continuous Time Random Walk (CTRW) with the population size change distributions (X_i) be defined by a symmetric Levy distribution in Fourier space [55] as,

$$\tilde{q}^{L,\eta}(k) = \exp(-a|k|^{\eta}), \tag{64}$$

Varying the exponent η in the interval $0 < \eta \leq 2$ allows the control of the population change distribution. When $\eta = 2$ we recover the traditional Brownian motion Gaussian distribution, where the mean and variance are finite consequently populations change diffusively. For $\eta < 2$ the variance is infinite which means that large changes in population size are possible resulting in super-diffusive population dynamics. When $\eta \leq 1$ the mean of the distributions becomes infinite as well which causes population sizes to change ballistically.

So far we have obtained a way of modelling super-diffusive population dynamics, by similarly making the time between changes in population size variable we can obtain sub-diffusive dynamics. Let $T = T_1, \ldots, T_i, \ldots, T_\tau$ where T_i is the amount of time it takes for a change in population size X_i to occur. If the size of T_i follows a one-sided Levy distribution, for example defined in the Laplace space as [55],

$$\tilde{q}^{L1,\omega}(s) = \exp\{-\langle t \rangle s^{\omega}\}, \tag{65}$$

where $b \geq 0$. Now we can vary ω in the interval $0 < \omega \leq 1$ to control the sub-diffusiveness of the population size changes. When $\omega = 1$ the mean is finite, i.e. $T_i = \langle t \rangle \, \forall i$ and every change in population takes the same amount of time whether they are large or small. If $\omega < 1$ the mean is not finite and changes in population size can take different amounts of time.

With both Equations 64 and 65 the anomalous diffusion equation (Equation 63) can be written in the Fourier and Laplace space as,

$$[\Delta \mathcal{P}\,(C, s)]^2_{\text{rms}} = -\frac{2a^2\eta^2|k|^{2\eta-2}}{bs^{2\omega+1}} + \frac{a\eta\,(\eta-1)\,|k|^{\eta-2}}{bs^{\omega+1}}. \tag{66}$$

The values of η and ω decide whether population size changes are sub-diffusion, normal diffusion, or super-diffusion. An analogous result can be obtained when using a fractional calculus approach to diffusive processes [54, 55].

2.3 PROPERTIES OF THE GRAPHS STUDIED BY SIMULATION

The graphs we chose to investigate are the Rectangular Lattice (RL), Circular Lattice (CL), Erdős-Rényi (ER), and Watts-Strogatz (WS). We chose the RL graph as it has simple regular structure and is commonly used graph in the field allowing us to compare our results with those found in the literature for validation of our implementation of our models. The CL allows us to vary the clustering coefficients of a graph which will allow us to analyse what effect clustering in the graph structure has on opinion dynamics of the vertices. Fur-

ther the CL graph is used to generate WS graphs and has similar structure to WS graphs with low rewiring probabilities $p_{rw} \ll 1$. We choose to study the ER graphs as the WS graphs have similar structure to them when the wiring probability becomes large enough, $p_{rw} \to 1$. ER graphs are also have complex structure but no clustering coefficient thus we can use them to analyse the importance of vertex degree to the opinion dynamics. Finally the structure of WS graphs is a mix of regularity and randomness which allows the formation of communities. WS graphs can be used to model the complex social structure between people which may result in unique emergent behaviour in how opinions form. The graphs and their properties are defined detailed in Section 1.1.3. In this section we provide the numeric quantities of the properties for graphs we used in our simulations.

The Monte Carlo Method

We use the Monte Carlo method to produce data this allows us to prevent rare structures in the graphs or initial spin-configurations from having undue influence on the results. In general the Monte Carlo method is given as [56],

1. Define the model, its inputs, and parameters.

2. Select the inputs at random using the appropriate probability distribution.

3. Run the simulation using the sampled inputs.

4. Aggregate the results for analysis.

In our case the model is the Ising Spin dynamics on graphs and which has two inputs. The first of the inputs are the graphs, we are required to generate a large sample of ER and WS graphs to be used in the simulations. The second input is the initial spin-configurations which we sample by running the simulation with the inverse temperature at $\beta_s = 0$ for a 1000 time steps before quenching to the desired inverse temperature β_q.

We aggregate together results of simulations which have the same inverse quenching temperature β_q and were performed on graphs generated with the same parameters. For example consider the crowds extracted from the results of all the realisations on an ER graph with $p_w = 0.12$ and $\beta_1 = 0.33$, they are a sample of the distribution of the crowds we would expect to see on any ER graph with that wiring probability at that inverse temperature.

Acceptance-rejection algorithms such as the Metropolis-Hastings algorithm attempt to prefer new spin-configurations such that the energy change of the system is small [56]. While this is a great choice when attempting to find minimum energy states of a system however such methods reduce the noisy behaviour of the vertices which drive much of the dynamics we will be studying and as such will not be used.

Rectangular Lattice

The RL graph used was a 32×32 grid with periodic boundary conditions. This type of graph was chosen as it has a regular homogeneous structure and no clustering. We performed 200 realisations for each value of β.

Circular Lattice

The CL and ER graphs on the other hand were chosen due to their relationship with the WS graph. As the rewiring probability of the WS graph gets very small, $p_{rw} \to 0$, its structure becomes closer and closer to that of a CL graph. Similarly as $p_{rw} \to 1$ the WS graph becomes an ER graph, see Section 1.1.7. By studying each of these types of graphs separately we can determine the effect of clustering and small-world links on crowd behaviour and properties.

$\boldsymbol{N}$	256	384	512	640	789	896	1024
$\boldsymbol{k}$	4	6	8	10	12	14	16
$\boldsymbol{C\,(k)}$	0.500	0.600	0.643	0.667	0.681	0.692	0.700
$\boldsymbol{\langle l \rangle}$	32	32	32	32	32	32	32

Table 1.: The number of vertices (N), degree (k), clustering coefficient $C\,(k)$, and average path length ($\langle l \rangle$) of the Circular Lattice graphs studied.

For the CL graphs we chose to vary the clustering in the graphs while keeping the average path length constant. The graph size, degree and their associated clustering coefficients are given in table 1. We ran around 800 realisations of

the Ising Spin model for each of the graphs at each various values of β. The values of β have been chosen such that there are smaller steps in β near β_c.

Erdős-Rényi

z	0.85	0.80	0.76	0.73	0.70	0.64
p_w	0.0041	0.0057	0.0074	0.0089	0.0109	0.0160
$\langle k \rangle$	2.64	3.64	4.72	5.72	6.95	10.24

Table 2.: The number of vertices (N), wiring exponent z, wiring probability p_w, and average degree ($\langle k \rangle$) of the Erdős-Rényi graphs studied.

The wiring probability p_w controls the properties of the ER graphs as discussed in Section 1.1.6. By using a scaling parameter z such that $p_w = N^{-Z}$ we can create graphs with properties independently of the graph size. Our main concern with ER graphs is that below a particular wiring exponent z_c the generated graphs are unlikely to be connected. If the ER graphs are formed of many components it will effect the crowds dynamics by limiting their growth and interactions. Thus we have chosen to study ER graphs which have giant components which consist of at least 90% of the vertices in the graph. Table 2 shows the number of vertices, wiring exponent, wiring probability and average degree of the ER graphs we ran simulations on. As the generation of ER graphs is stochastic we generated 200 different graphs for each value of z and performed 20 realisations of the Ising Spin model on each. Thus for each value the wiring probability there are 4000 realisations.

Watts-Strogatz

$\boldsymbol{p_{rw}}$	0.0045	0.007	0.01	0.025	0.045	0.1	0.2
$\langle \boldsymbol{C}\left(\boldsymbol{k}, \boldsymbol{p_{rw}}\right)\rangle$	0.5839	0.5750	0.5640	0.5105	0.4474	0.3120	0.1502
$\langle \boldsymbol{l} \rangle$	15.903	12.550	10.608	7.1413	5.8719	4.7815	4.1743

Table 3.: The rewiring probabilities (p_{rw}), average clustering coefficients ($\langle \boldsymbol{C}\left(\boldsymbol{k}, \boldsymbol{p_{rw}}\right)\rangle$), and average path lengths ($\langle \boldsymbol{l} \rangle$) of the Watts-Strogatz graphs studied.

The final type of graph studied is the Watts-Strogatz graph, its main characteristics are high clustering and short path lengths which are controlled by the rewiring probability p_{rw}. Table 3 contains the rewiring probabilities and the clustering coefficients and average path lengths calculated from the graphs generated.

2.4 VALIDATION OF ISING MODEL IMPLEMENTATION

In this section we validate our implementation of the Ising Model by comparing our computationally derived values of the inverse critical temperatures $\beta_c = 1/k_B T_c$ for each of the graphs against those in the literature. β_c was obtained by plotting the maximum magnetisation against β and identifying the mid-point of the slope indicating a phase transition,

$$\left.\frac{\mathrm{d}\left[\langle M\rangle_T\right]^{\max}}{\mathrm{d}\beta}\right|_{\beta=\beta_c} = \left[\frac{\mathrm{d}\left[\langle M\rangle_T\right]^{\max}}{\mathrm{d}\beta}\right]^{\max}. \tag{67}$$

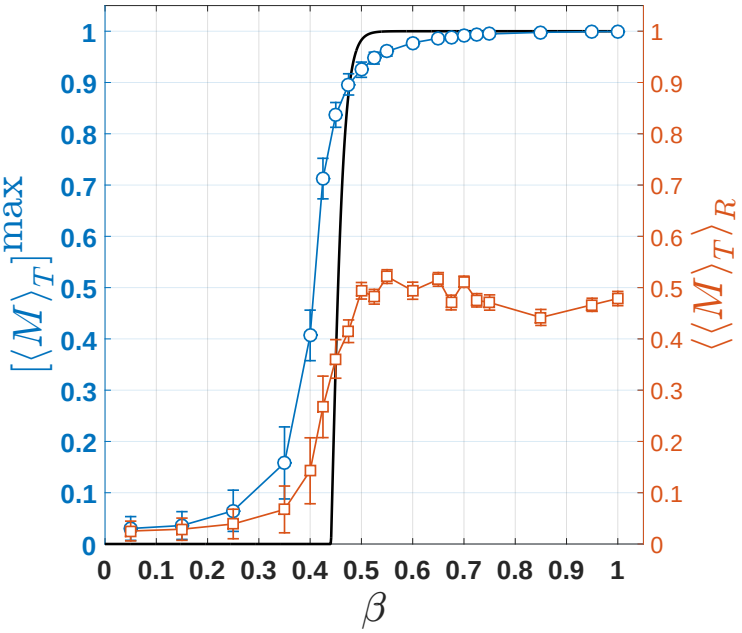
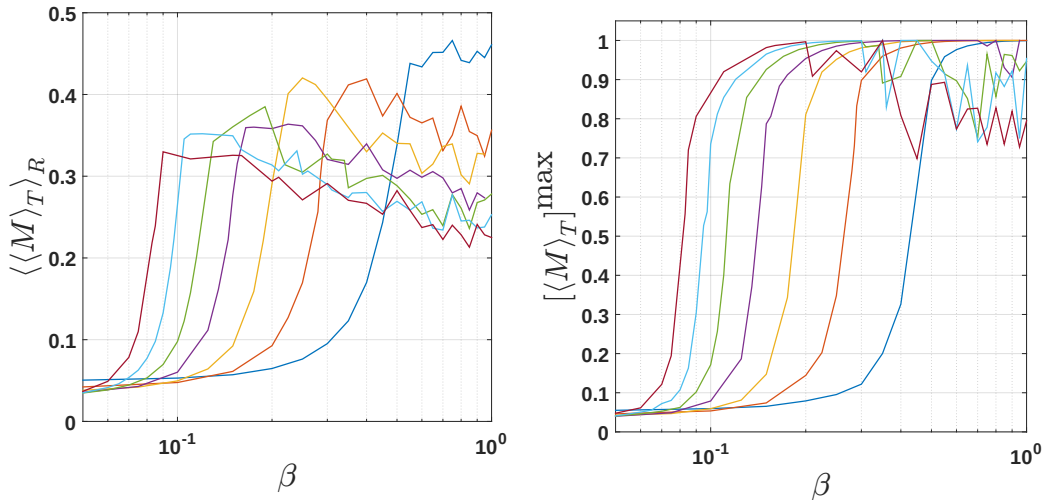


Figure 19.: At low inverse temperatures, $\beta < \beta_c$, the vertex spin states are being chosen at random without influence of neighbouring opinions, this leads to a roughly equal mix of spin states and low magnetisation. At high $\beta > \beta_c$ the influence of neighbours becomes important resulting in large amounts of aligned spin states which results in a high magnetisation. The switch over from low to high magnetisation is a phase transition which means there is a sharp change at $\beta = \beta_c$. There is a notable difference between the maximum magnetisation (blue circles) and the mean magnetisation (red squares). This indicates that while it is possible for the rectangular graph to form a strong consensus it is not often unanimous. The error bars indicate the standard deviation of the values used to calculate the averages plotted. The thick black line is a depiction of the expected behaviour of $\langle\langle M\rangle_T\rangle_R$ [41], it shows a phase transition occurring at $\beta_c \approx 0.46$. The difference between the analytical result and our computational results is due to our system not being infinitely large.

According to Baxter [41] we should expect to see a sharp phase transition in the magnetisation $\langle\langle M\rangle_T\rangle_R$ at $\beta_c \approx 0.46$ on Rectangular Lattice graphs. Our results, figure 19, show that the magnetisation increases from 0 to 0.5 but is not strictly indicative a phase transition. The fact that the maximum magnetisations observed at each β show the expected response indicates that the phase transition does occur. The disparity between the average and maximum

magnetisations is due to a large variance in the magnetisation over different realisations. A sharp quenching produces lots of small regions with different opinions which then grow larger over time, when $\beta \geq \beta_c$ a single opinion eventually dominates, [9]. This differs from an annealing process which encourages a system to find the lowest energy state. Consequently a phase transition can occur as expected during the annealing process but it is not a definite result in a quenched system .



(a) (b)

Figure 20.: From right to left on both plots are the results for Circular Lattices with sizes $N = 256, 384, 512, 640, 789, 896, 1024$ plotted against β, each graph has the clustering coefficients $C(k) = 0.500, 0.600, 0.643, 0.667, 0.682, 0.692, 0.700$ respectively. As the clustering coefficient increases the critical value of β decreases. Markers and error bars have been omitted for presentation purposes.

For a 1D lattice with degree $k = 2$ the analytical result [28] suggests there should be no phase transition at a finite temperature. However our graphs have degrees $k > 2$ for which phase transitions do exist. The average and maximum magnetisations (figure 20a) for the CL graphs portray a similar story as for the

RL graphs. On average the CL graphs do not form a consensus but they do occur as indicated by the sharp phase transitions in figure 20b.

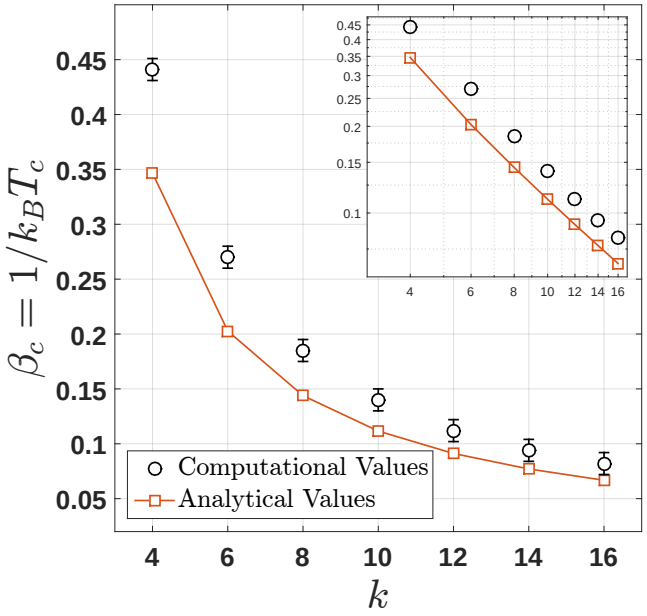


Figure 21.: The inverse critical temperatures β_c plotted against degree k for the circular lattice graphs. Our computational values (circles) have error-bars indicating the standard error due to method in obtaining the values. The analytical results (squares) are the values calculated using Equation 69, where $\beta_c(k) == \frac{1}{2}\ln\left(\frac{k}{k-2}\right) \sim \frac{1}{k}$, the lines are a guide for the eye. Inset is the same plot on log-log scale.

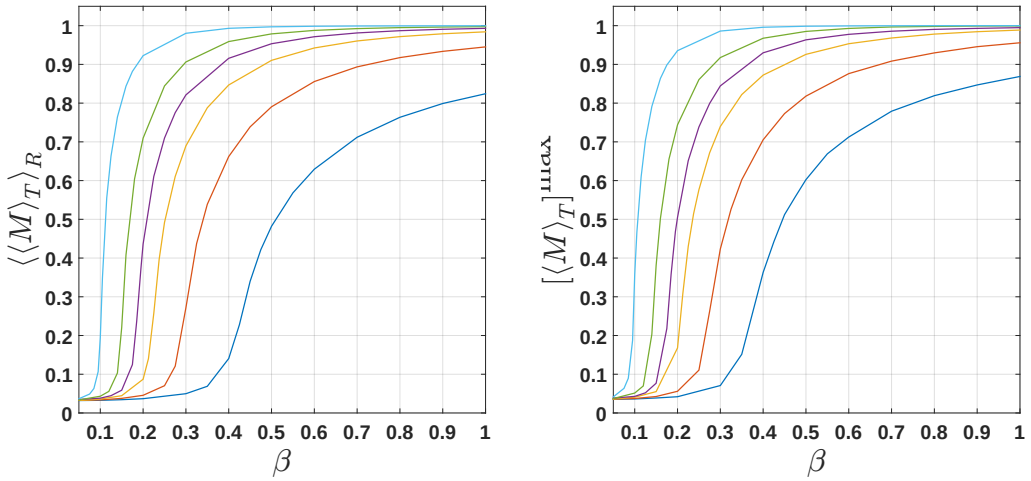
Our next step is to check that the inverse critical temperatures $\beta_c = 1/k_B T_C$ match the theoretical values, where k_B is the Boltzmann constant. [16] show that for a Cayley tree the critical value of β is given by,

$$\beta_c = \frac{1}{2}\ln\left(\frac{\langle k^2\rangle}{\langle k^2\rangle - 2\langle k\rangle}\right). \tag{68}$$

This can be used for many graphs with arbitrary degree distributions. A regular graph such as a circular lattice has $\left\langle k^2 \right\rangle \equiv \langle k \rangle^2 = k^2$, thus by substituting this into Equation 68 we can say that

$$\beta_c(k) = \frac{1}{2}\ln\left(\frac{k}{k-2}\right) \sim \frac{1}{k}. \tag{69}$$

Our computational results plotted in figure 21 are asymptotic to the analytical results. The discrepancy arises as the degree k is proportional to the graph size N, at low k the graph is smaller and the analytical results are for infinitely large graphs.



(a) (b)

Figure 22.: From right to left the wiring probabilities of the ER graphs are $p_w = 0.0041$, 0.0057, 0.0074, 0.0089, 0.0109, and 0.0160. The graphs with higher wiring probabilities undergo a phase transition at higher temperatures. Markers and error bars have been omitted for presentation purposes.

The magnetisation of the Erdős-Rényi graphs (figure 22a) shows that as the wiring probability increases not only does β_c decrease but the phase transition becomes sharper too. Therefore the more connections a graph has means that

it can form a consensus even at high temperatures when there is a lot of noise. Unlike the average and maximum magnetisations for the CL graph the results for ER graphs are indistinguishable by eye. This indicates that there is only a small variance in the magnetisations in the steady state for graphs with the same wiring probabilities.

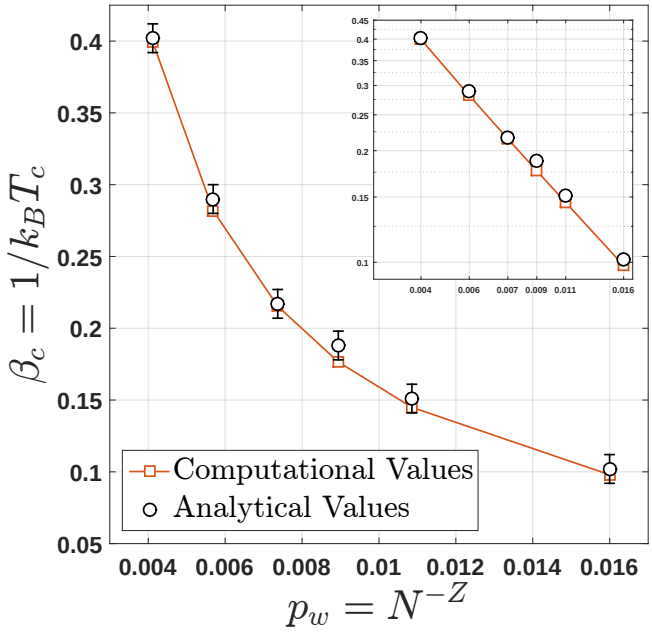


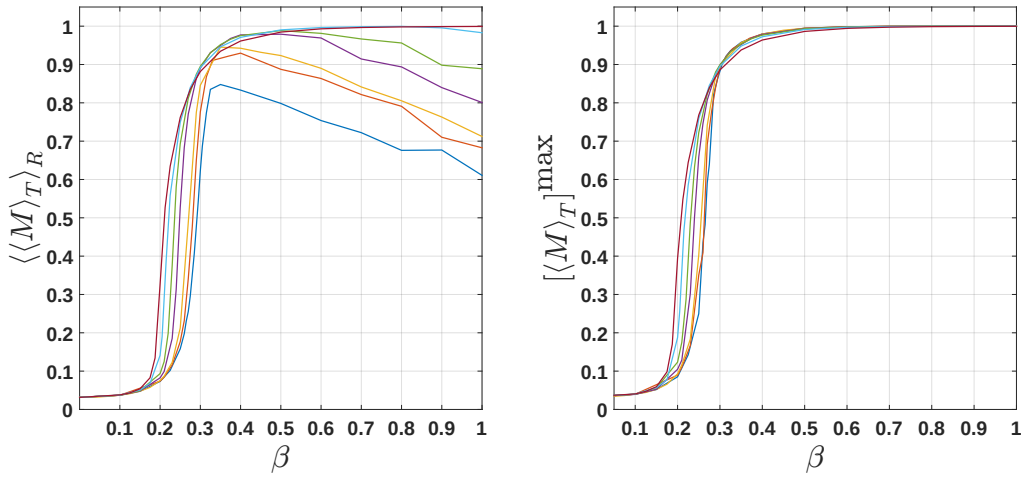
Figure 23.: The observed inverse critical temperatures (circles) are plotted with the theoretical estimates (squares) for various Erdős-Rényi graphs. The analytical values were obtained using equation **??**. The error-bars indicate the standard error in observed β_c.

While there is no exact analytical solution for the Ising model on Erdős-Rényi graphs the critical temperatures can be estimated very well by using the results for comparable tree like graphs, i.e. we can use equation 68 again, [16]. As the degree distribution of an ER graph is Poisson we can use the

Gaussian approximation and say that $\left\langle k^2 \right\rangle = 2\langle k \rangle$, then we substitute these into equation 68 and get,

$$\beta_c = \frac{1}{2}\ln\left(\frac{\langle k \rangle + 1}{\langle k \rangle - 1}\right). \tag{70}$$

We plot these analytical results with those obtained from our simulations in figure 23. The values of the empirical results match those of the theoretical values well, thus we are sufficiently assured our implementation works as intended.



(a) (b)

Figure 24.: From right to left are the plots for $p_{rw} = 0.0045$, 0.007, 0.01, 0.025, 0.045, 0.1, and 0.2. Greater rewiring probabilities result in the phase transition occurring at higher temperatures. Also the average magnetisations becomes more like the maximum magnetisation as p_{rw} increases.

The average and maximum magnetisations for the Watts-Strogatz graphs (figure 24) show features observed in the results for both the CL and ER graphs. At low p_{rw} the average magnetisation behave similarly to the circular lattice, it decreases with β for $\beta > \beta_c$. However as $p_{rw} \gg 0$ we find that the average and maximum magnetisations become the same. Therefore when the disorder in a

graph is high this results in less variance in the magnetisation during different realisations.

For the WS graphs equation 68 does not provide correct estimates for the inverse critical temperatures as it has a mixture of regular and random structure. Instead we use an empirically derived relationship for the critical inverse temperatures [57],

$$\beta_c \sim p_{rw}^{-\alpha}, \tag{71}$$

the symbol $\sim$ being used to indicate a rough equivalence given that the equation has not been proven analytically and does not indicate an asymptotic relationship.

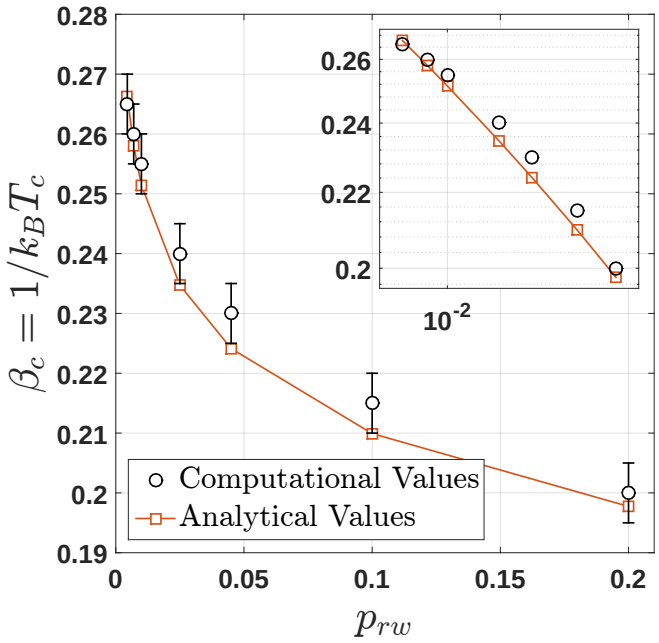


Figure 25.: The inverse critical temperatures β_c obtained by simulation (circles) are plotted with theoretical estimates (squares) for various Watts-Strogatz graphs. The analytical values calculated using equation 71 with $\alpha = 0.017 \approxeq 0.02$.

The inverse critical temperatures that we obtained from our simulations match well with the theoretical estimates for the RL, ER and WS graphs. On

the other hand the values obtained for the CL graphs do not agree with the theoretical values for small k but do conform at larger k. The CL graph with $k = 4$ has only $N = 256$ vertices and the theoretical values are for graphs with $N \to \infty$ therefore we do not find it surprising that there is large difference. Over all these results validate our implementation of the Ising Model on a wide range of graphs.

3

DYNAMICS OF CROWD POPULATIONS

3.1 INTRODUCTION

As defined in the previous chapter crowds are magnetised clusters of vertices, over time some vertices switch opinion due to noise and the voting behaviour. The switching of opinions is a stochastic process and thus so are the changes in population size. We analysed the relationship between the root mean square (R.M.S.) change in crowd population size $[\Delta\mathcal{P}]_{\text{rms}}$ and the their lifetimes $\mathcal{L}$ to determine the dynamics of crowd populations and present the results in this chapter.

We shall discuss the results for each graph individually and then compare them at the end. The results consist of $[\Delta\mathcal{P}]_{\text{rms}}$ plotted against $\mathcal{L}$ for low, mid and high temperatures. This will provide a picture of how the behaviour

changes with the temperature. Many of the results follow a power law such as the one presented in the chapter, where $[\Delta\mathcal{P}]_{\text{rms}} = \sqrt{D}\mathcal{L}^{\alpha/2}$. The exponent,

$$\alpha = 2\frac{\ln\left([\Delta\mathcal{P}]_{\text{rms}}/\sqrt{D}\right)}{\ln\left(\mathcal{L}\right)}, \tag{72}$$

is known as the diffusion exponent and can be computed by determining the slope of the line of best fit $[\Delta\mathcal{P}]_{\text{rms}}$ plotted as a function of $\sqrt{\mathcal{L}}$ on a log-log axes. We also plot α as a function of the inverse temperature β to determine whether the population dynamics are non-diffusive, sub-diffusive, normally diffusive or super-diffusive at different temperatures.

3.2 RECTANGULAR LATTICE

Figure 26 is for a low temperature system, each plotted point is the r.m.s. change in population size of a crowd that had a lifetime of $\mathcal{L}$ time steps. The points are scattered over an order of magnitude along the vertical axis and 3 orders of magnitude along the horizontal making the power law fit (red line) for this particular data a poor one. While the fit is not truly apt for these results they are for $\beta < 0.95$ where we found the scattering to be significantly less, as illustrated in Figure 27a. Further the fit does highlight that $[\Delta\mathcal{P}]_{\text{rms}}$ increases with respect to $\mathcal{L}$ which suggests some of the crowds are growing/decaying similarly to an anomalous diffusion process. On the other hand the scattering does indicate that there are a significant number that are not.

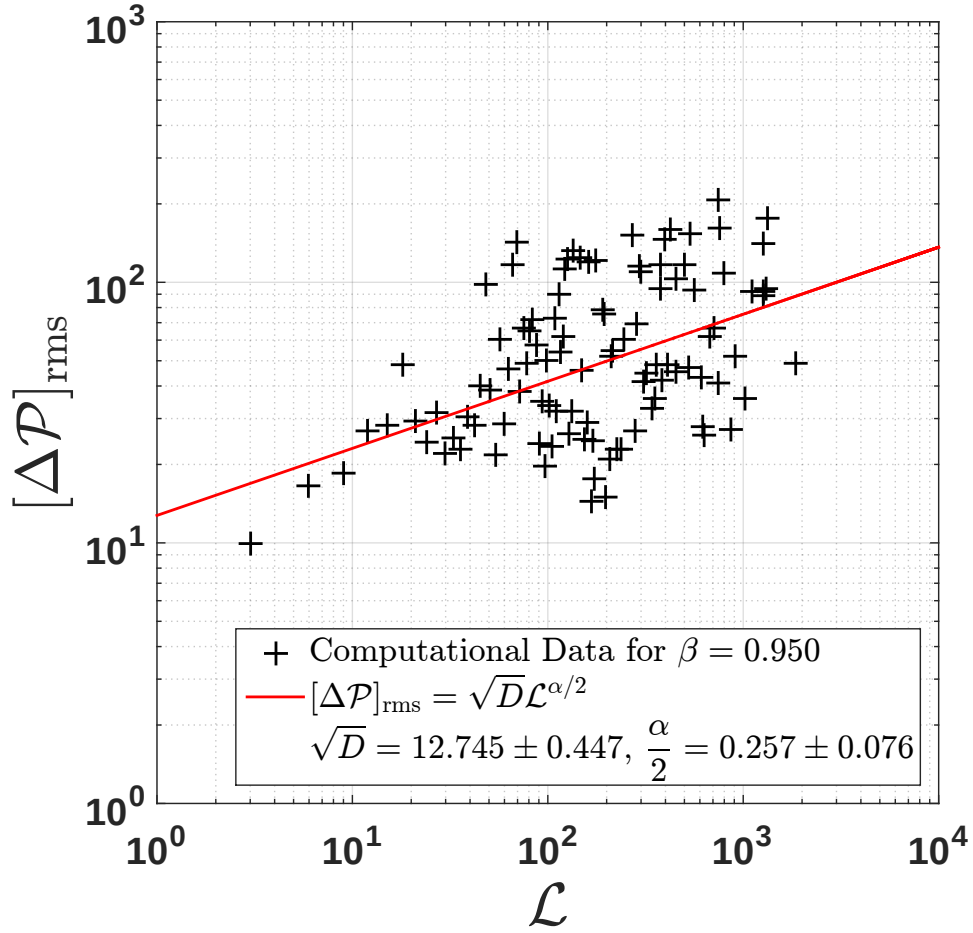


Figure 26.: The Root Mean Square Change in Population plotted against crowd lifetime for $\beta = 0.95$ (top). The red line is a power law fit of the data, where D and α are the diffusion coefficient and exponent respectively. The scatter of the data makes the fit poor at this inverse temperature.

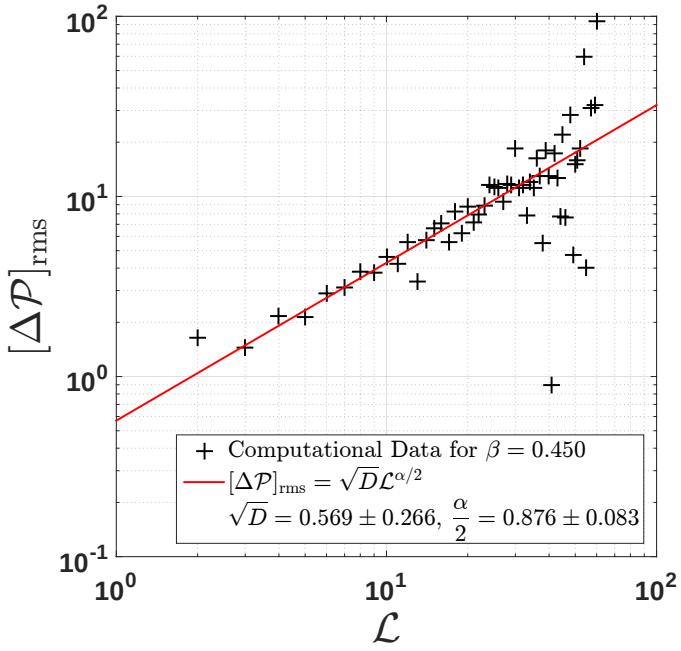
Results for $\beta < 0.95$ show less scattering and are a better basis for a power law fit and produce similar values for the diffusion exponent. We believe, because of this, that there is still some merit for using the diffusion exponent obtained from this data to draw some conclusions.

Notice that $\alpha = 0.51 \pm 0.15$, this suggests that the population dynamics for some crowds has the characteristics of a sub-diffusive process. The amount of

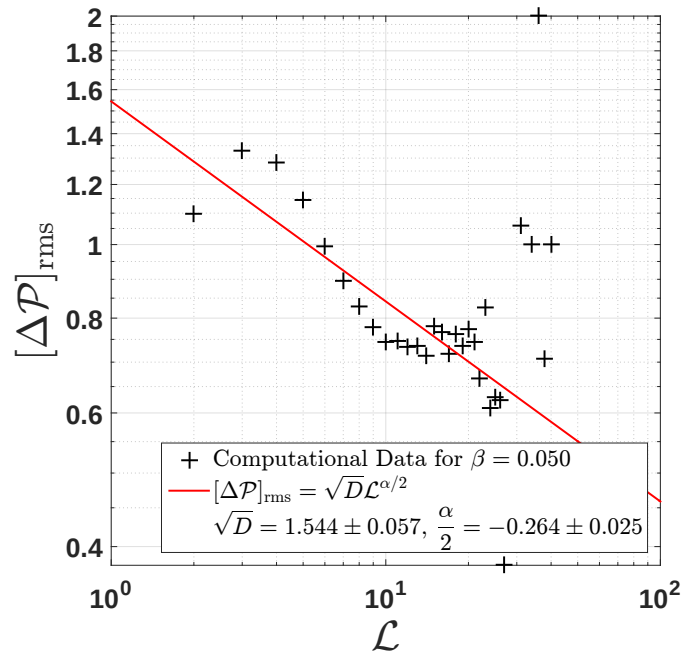
change in the population size over time tends to be small and less than what would be expected from a normal diffusion process.

From the lack of large changes in population size and the existence of crowds with very long lifetimes we can infer that crowds do not change much. This is due to the low temperature of the system which causes vertices to agree more often with its neighbourhood opinion than disagree. If a vertex does flip and disagree it is 'pressured' to flip back to the surrounding consensus opinion quickly. Overall this means that crowds rarely lose internal vertices due to noisy behaviour. It follows then that most of the population changes occur at boundaries with other crowds where vertices can be stolen by or converted from a neighbouring crowd. Noisy behaviour in this context can weaken a border region as it increases the number of vertices with the opposite spin which then influence more and more vertices to flip opinions and eventually join a neighbouring crowd. Thus noisy behaviour provides can equally provide an advantage to a crowd while disadvantaging another. However the mechanics behind noisy behaviour do not favour any particular crowd and consequently advantages and disadvantages are temporary. The effects of short period of noisy behaviour at a border may not be temporary as it may weaken a crowd too much to remain cohesive while it might bolster a crowd such that it becomes almost impossible to break apart. At low temperatures such behaviour is rare and boundaries can form an unstable equilibrium where neither crowd gains or loses vertices. The results presented in Figure 26 suggest this is the case

as population changes are small compared with the time-scale over which they occur.



(a) $\beta = 0.450$



(b) $\beta = 0.050$

Figure 27.: The Root Mean Square Change in Population plotted against crowd lifetime. The red line is a power law fit of the data, where D and α are the diffusion coefficient and exponent respectively.

Figure 27a shows the results for a system with a temperature near the critical value, $\beta = 0.45$. A couple of differences are immediately apparent when compared to the low temperature results. First of all the lifetimes are much shorter and secondly $[\Delta\mathcal{P}]_{\text{rms}}$ ranges over 2 orders of magnitude. This indicates that crowds live for less time but change in size a lot more than at low temperatures. The data is also less scattered and is even better fitted by a power law thus we can draw much stronger conclusion as to the behaviour the crowd population dynamics. We find that the changes in crowd size can be described as anomalous diffusion process. Note now that $\alpha = 1.75 \pm 0.17$ which informs us that the crowd population dynamics are super-diffusive. Crowds experience large changes in their population sizes over shorter periods of time for $\beta = 0.45$ than when $\beta = 0.95$. This paints a picture of continual change even after the transient period is over.

It is conceivable that the large changes in population sizes are a result of random flipping of opinions however if we check the probabilities of such occurrences happening it proves to be unlikely. Assume that a vertex i is in the middle of a crowd, i.e. all its neighbours have the same spin then the probability of it disagreeing with them is (see equation 42).

$$P\left(\sigma_i^{t+1} = -\sigma_i^t, \sigma_i^t\right) = \frac{e^{-0.45\cdot 4}}{1 + e^{-0.45\cdot 4}} \approx 0.1418 \tag{73}$$

which is approximately a 1 in 6 chance of a vertex disagreeing with its neighbours. Such a probability appears high however we are considering a group of n vertices flipping at the same time and the probability of that occurring is pro-

portional to 0.1418^n. Thus the larger the amount of change observed the less likely it is due to random flipping of opinions. We can however see that such a large probability of disagreement would lead to greater instability of crowds. Large crowds would find their borders changing frequently as noise destabilises them. Noise can also flip internal vertices which sometimes grow into larger crowds eventually replacing the crowd they started in.

The instability of crowds may also lead to the merging and branching of crowds which would explain the large changes in population size. In Section 2.2 the figure 17 showed a times series of configurations states of a rectangular lattice. In the last time step we see a section of the yellow crowd is cut off and a new green crowd is formed (branching), in this case the yellow crowd loses a large number of vertices. The reverse can also happen (merging) in which case the yellow crowd would have gained a large number of vertices. This would explain the large changes in population sizes over relatively short periods of time.

At very high temperatures, see figure 27b, the rectangular lattice is essentially jumping from one spin configuration to another with very little influence from the voting mechanics. Consequently it is not surprise that the results show that the population dynamics are not a diffusion type process. We observe a generally trend for longer lived crowds to exhibit less change in population size excepting those with the longest lifetimes. We know from the literature for coarsening models that high temperatures equate to small clusters of magnetism. Flipping of even a small number of vertices will destroy small crowds quickly

and so they live longer the less their vertices flip. The longest lived crowds do not fit into that explanation and is due to them being large enough to weather small changes.

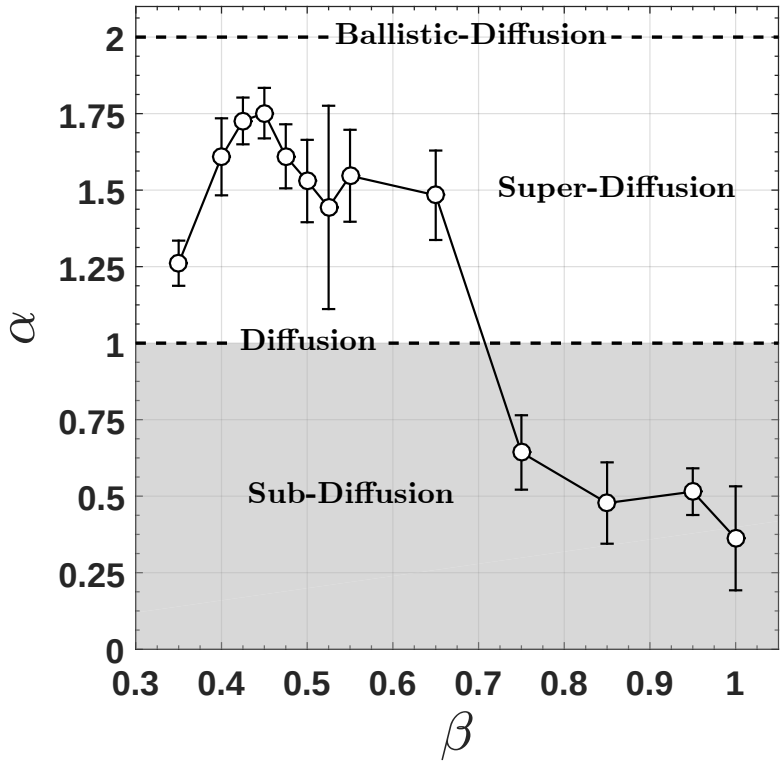


Figure 28.: The diffusion exponent α against the control parameter β. Systems with high levels of noise $\beta \lesssim 0.35$ are not diffusive and results are not included. When noise is at medium levels, $0.35 \lesssim \beta \lesssim 0.65$, crowds population changes super-diffusively. Unexpectedly we find that once noise is low enough, $\beta \gtrsim 0.75$, crowd populations change sub-diffusively.

Figure 28 shows the diffusion exponent α as a function of β. The error bars on the data points are the standard errors for the values of the exponents as given by the polyfit function in MatLab [58].

The plot, figure 28, shows that the population dynamics fall into 1 of 4 possible categories (sub-diffusion, normal diffusion, super diffusion and ballistic

diffusion) depending on the value of β. When applying the classical definitions to changes in population we are saying that sub-diffusion is changes in population size which are small or non-existent with long intervals of time between changes. Similarly super-diffusion is the case when both small and large changes in population size occur frequently. The special case of $\alpha = 1$ is normal diffusion process where population sizes change by small amounts nearly every time step. The other special case is $\alpha = 2$ which is ballistic-diffusion where large crowd population changes are very frequent. These definitions have analogues in terms of fractional diffusion and are discussed in Section 2.2.2.

At temperatures $\beta \lesssim 0.35$ the crowd population dynamics are non-diffusive processes. While at temperatures near the critical value $0.35 \lesssim \beta \lesssim 0.65$ the exponent α is greater than 1 which indicates a super-diffusive process. As the temperature is further reduced $\beta \gtrsim 0.75$ the population dynamics become sub-diffusive.

We know that the phase transition occurs at $\beta = 0.4407$ but we observe that the changes in crowd behaviour occur before that. It appears that two different types of diffusion processes allow the system to obtain spin configurations where a large majority of the vertices are aligned. Super-diffusive population change can allow for a crowd to grow very large very quickly eventually a large number of vertices will be part of that crowd and the system is strongly magnetised. Crowds can also grow slowly to the size of the graph by sub-diffusive processes.

One of the problems with this analysis is that we can only obtain information about some of the dynamics of the crowd populations. An estimate of the Hurst

exponent [60, 61] can provide us with more information, however it has some requirements that much of our data set does not meet. In Appendix A we cover how the estimate is calculated and some results for a reduced range of inverse temperatures for the RL graph.

3.3 CIRCULAR LATTICE

The low temperature results presented in figure 29a shows the r.m.s. change in population for 4 CL graphs with clustering coefficients $C(k=4) = 0.500$, $C(k=6) = 0.600$, $C(k=10) = 0.667$, and $C(k=16) = 0.700$. The data for each of the CL graphs is scattered for the longer lifetimes ($\mathcal{L} \gtrsim 20$) but show a strong power law distribution for $\mathcal{L} \lesssim 20$. From this we discern that the populations of crowds with lifetimes $\mathcal{L} \lesssim 25$ change diffusively but do not if they live for longer. This is due longer lived crowds have more chances of losing vertices to non-diffusive processes.

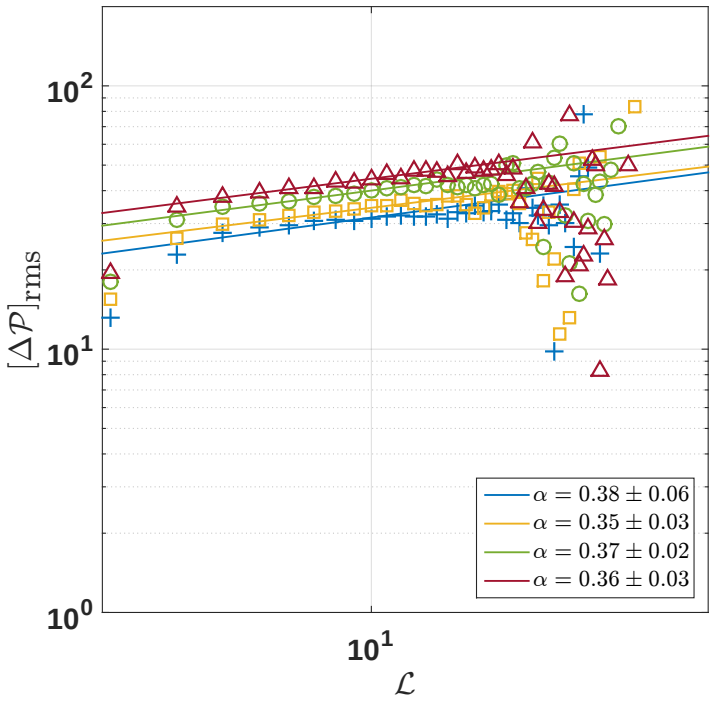
The crowd population dynamics has not been affected by the graph structure. The diffusion exponents are $\alpha \approx 0.4$ for all the graphs which tells us that the changes in population sizes are small relative to the lifetimes of the crowds. Crowds on circular lattices with greater degree show larger amounts of change for all lifetimes. This is as expected as crowds on a CL graph with more edges will have more neighbouring vertices to convert and more external vertices to lose and thus we observe overall larger changes in population size.

For all the graphs the lifetimes of the crowds are less than approximately 60 time steps. Which indicates that the CL structure does not allow crowds to be robust against noise and neighbour interactions. The longest lived crowds are outliers in that the amount of change observed for them is an order of magnitude less than others that live nearly as long.

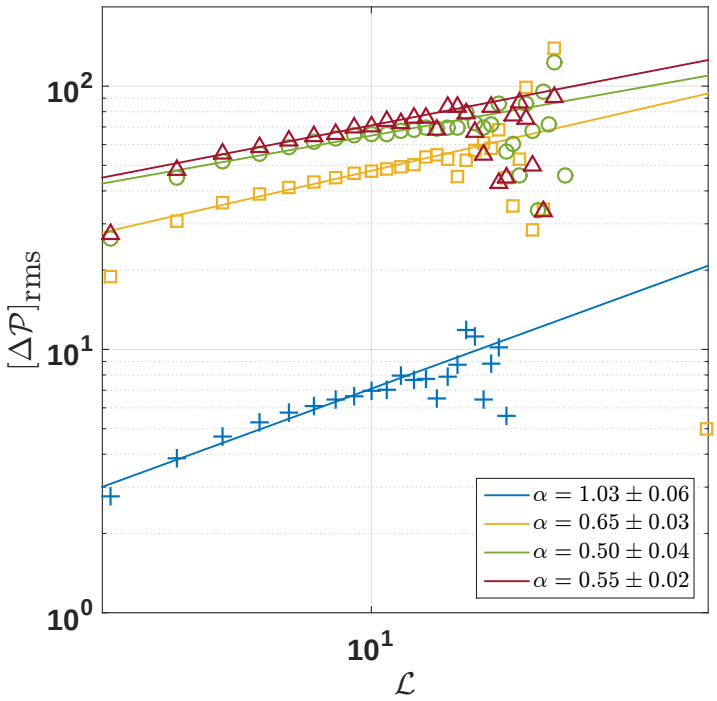
Figure 29b shows results near to the critical temperature. All the graphs have greater diffusion exponents and there are also differences in behaviour between the graphs. The most strongly affected is the CL with $C\left(k=4\right)=0.500$, the size of the changes has decreased by an order of magnitude but the crowd population dynamics is now a normal diffusion process as $\alpha = 1.03 \pm 0.06$. We also observe that the crowds do not live as long on this circular lattice. As there is less clustering in the graph vertices have fewer neighbours which means they are more susceptible to noise making it easier for flipped vertices to split a crowd.

The graph with $C\left(k=10\right)=0.667$ has also been affected by the higher temperature to a lesser extent. It too shows a decrease in the size of the changes and its diffusion exponent has increased - almost doubling its low temperature value. There is an outlier that shows very little change in population size and a very long lifetime - the observed longevity is likely due to its lack of change.

The crowd population dynamics on the graphs with $C\left(k=10\right)=0.667$, and $C\left(k=16\right)=0.700$ are roughly the same as indicated by the similar diffusion exponents. At this higher temperature the population dynamics of crowds on these graphs are still sub-diffusive. Comparing with the low temperature results



(a) $\beta = 0.95$



(b) $\beta = 0.30$

Figure 29.: Root Mean Square Change in Population plotted against crowd lifetime. Computational data for 4 different graphs with $C(k=4) = 0.500$ (blue crosses), $C(k=6) = 0.600$ (yellow squares), $C(k=10) = 0.667$ (green circles), and $C(k=16) = 0.700$ (red triangles). The lines are power law fits to the data.

the larger diffusion exponent ($\alpha \approx 0.5$) is a result of larger changes in crowd size over shorter lifetimes. This tells us that decreased robustness is essential for larger size changes to occur.

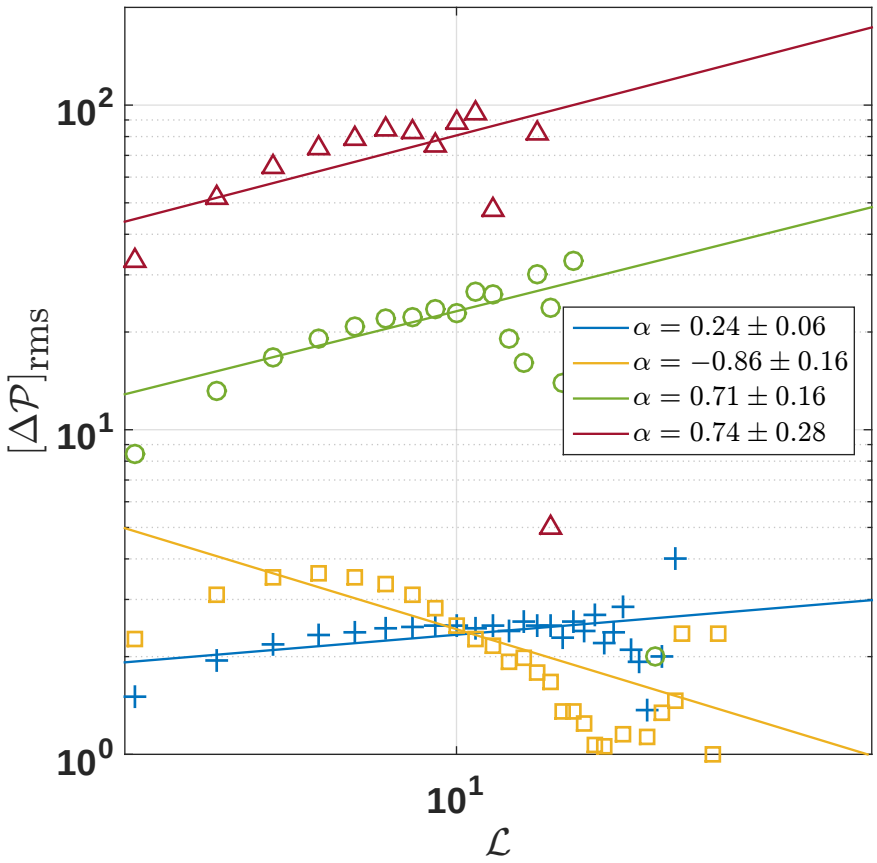


Figure 30.: Root Mean Square Change in Population plotted against crowd lifetime for $\beta = 0.05$. Computational data for 4 different graphs with $C(k = 4) = 0.500$ (blue crosses), $C(k = 6) = 0.600$ (yellow squares), $C(k = 10) = 0.667$ (green circles), and $C(k = 16) = 0.700$ (red triangles). The lines are power law fits to the data.

At very high temperatures we find that the results for each of the graphs has separated based on the amount of clustering in their structure. The crowd population dynamics of the CL graph with $C(k = 10) = 0.667$, and $C(k = 16) = 0.700$ are still similar as their diffusion exponents are $\alpha \approx 0.73$. However there is now a difference in the magnitude of the changes in population sizes, the

crowds on the CL graph with $C\,(k=10)=0.667$ shows smaller changes in size for all lifetimes compared to the CL graph with $C\,(k=16)=0.700$.

We observe that the results for $C\,(k=6)=0.600$ do not show diffusive behaviour as indicated by the negative diffusion exponent. These results are clearly anomalous when compared with the others and thus will not be used when plotting the diffusion exponent against the inverse temperature.

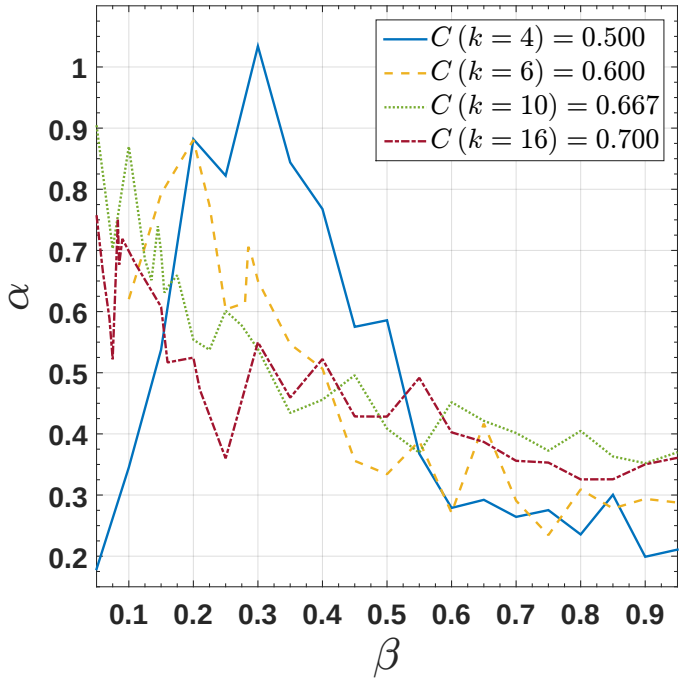


Figure 31.: We plot the diffusion exponent α against the control parameter β to show how the population dynamics of the crowds changes with the temperature. Each line represents the results for a different graph, $C\,(k=4)=0.500$ (solid blue line), $C\,(k=6)=0.600$ (dashed yellow line), $C\,(k=10)=0.667$ (dotted green line), and $C\,(k=16)=0.700$ (dot-dash red line). Markers and error bars have been omitted for clarity.

Figure 31 shows the diffusion exponent as a function of β for the 4 CL graphs. The diffusion exponent for the $C\,(k=4)=0.5$ graph is small at high temperatures and increase dramatically as $\beta \to \beta_c$ and then decreases as $\beta \to 1$. While

the diffusion exponent for the other graphs respond differently to changes in temperature. The other 3 CL graphs show a steady decline in the diffusion coefficient with temperature culminating in a similar value $0.3 \lesssim \alpha \lesssim 0.4$.

Vertices in circular lattices with fewer edges means that the crowds on them have fewer neighbouring vertices. At high temperatures this means they can only gain or lose a small number of vertices. As the temperature nears the critical value the voting mechanics start to become important and crowds are more stable allowing them to grow larger but it is still noisy enough that border are still unstable resulting in great amounts of change. There is also the contribution to changes in population due to the thin line like nature of the graph. It is highly probable for internal vertices to flip forming a new crowd which splits the original in two.

Vertices on circular lattices with large degrees have a large number of neighbours thus even if many neighbours are flipping due to noise it is likely that a vertex can remain connected to its crowd. This allows crowds to experience large changes in size without being broken apart by the noise. As the temperature decreases the crowds become more stable and are able to grow larger and most of the change in size occurs due to the dynamics at the borders. As this relies on voting mechanics changes in population size tend to be small and occur over longer time periods.

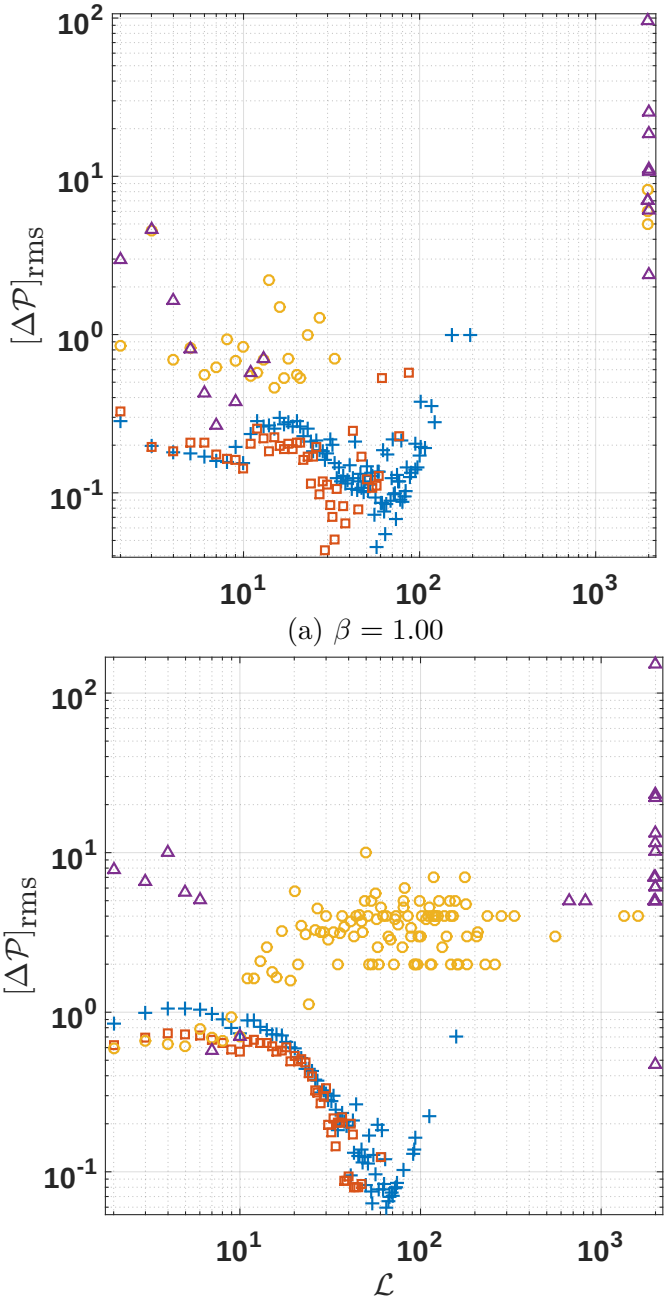
We find that the graph structure is indeed important to the crowd population dynamics. The 1-dimensional nature of the circular lattice means that the population dynamics is mostly driven by interactions at the borders of crowds

due to the clustering the graph structure. Even small amounts of clustering makes crowds extremely resistant to being broken up by noisy behaviour of their internal vertices and noisy vertices are heavily influenced by neighbours to revert to a matching opinion state. Consequently changes in opinion within a crowd are usually temporary while at borders changes can be longer lasting. Clustering causes crowds to be more robust to noisy behaviour at higher temperatures, however a certain amount susceptibility to change is required for crowds to exhibit normal and super diffusive behaviours which is why we do not observe them on circular lattices.

3.4 ERDŐS–RÉNYI GRAPHS

In this we discuss the behaviour of crowds on Erdős–Rényi graphs with $p_w = 0.0041$, 0.0057, 0.0089, and 0.016. Our main observation is that crowds do not exhibit diffusive behaviour at any temperature. The graph structure is either too weakly connected and thus there is no reinforcement of opinions within a crowd making them easily broken up or they ER graphs are too strongly connected and the forming of a singular large crowd is inevitable. However we can still make inferences as to how crowds are behaving based on these results.

Figure 32a) shows the results for the system at very low temperature, there are differences in behaviour that depend on the wiring probabilities. The graphs with lots of edges ($p_w = 0.0089$, and 0.016) have fewer data points which indicates that there are fewer crowds and that they all behave similarly. Crowds



(a) $\beta = 1.00$

(b) $\beta = 0.40$

Figure 32.: Root Mean Square change in population plotted against crowd lifetime for $\beta = 1.00$ (top) and $\beta = 0.300$ (bottom). The data for ER graphs with $p_w = 0.0041$ (blue crosses), $p_w = 0.0057$ (red squares), $p_w = 0.0089$ (yellow circles), and $p_w = 0.016$ (purple triangles) are plotted together.

on these graphs are more robust as there are many ways for the crowd to remain connected when a vertex flips due to noise. Thus they are not easily broken up by noise allowing them to stay whole for longer and grow larger which we see as

a large range of $[\Delta\mathcal{P}]_{\text{rms}}$ at long lifetimes. The greater number of edges means that the number of neighbouring vertices is larger allowing for greater increases or losses in size. On the other hand crowds which are born due to noise tend to be small and the voting mechanics will quickly revert their opinions to that of their neighbourhoods resulting short lifetimes and a small amounts of change.

Crowds on graphs with fewer edges ($p_w = 0.0041$, 0.0057) are less robust to noise as there are fewer ways for a crowd to remain connected when vertices flip opinions resulting in shorter lifetimes. Crowds also have fewer neighbouring vertices which means their border can reach an equilibrium and thus population sizes change little.

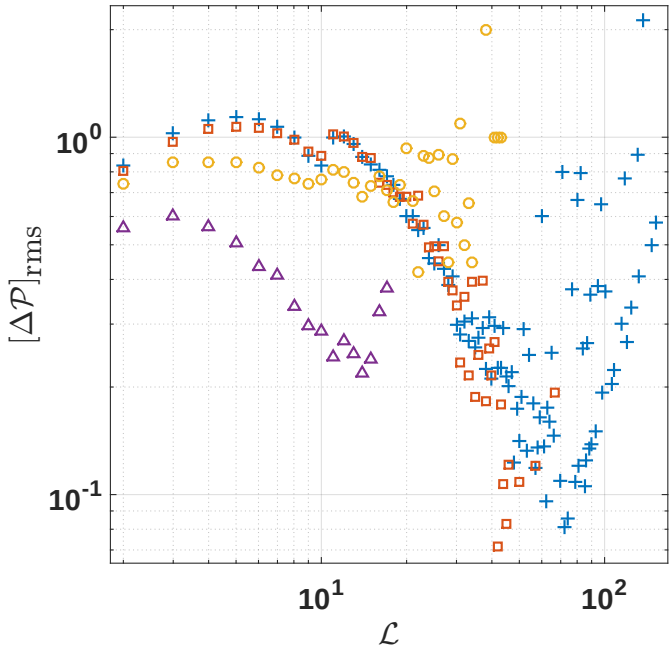


Figure 33.: Root Mean Square change in population plotted against crowd lifetime for $\beta = 0.00$. The data for ER graphs with $p_w = 0.0041$ (blue crosses), $p_w = 0.0057$ (red squares), $p_w = 0.0089$ (yellow circles), and $p_w = 0.016$ (purple triangles) are plotted together.

Results for the system at a higher temperature ($\beta = 0.30$) are presented in figure 32b. The results for the $p_w = 0.016$ graph have not changed by much,

however crowds on the $p_w = 0.0089$ graph behave significantly differently to before, they now have a large variety of lifetimes and the majority show changes in size of between 1 and 10 vertices. This indicates that there are more than 1 large crowd and many smaller ones that are not quickly destroyed by their more robust neighbours.

If we compare the distribution of $[\Delta\mathcal{P}]_{\text{rms}}$ for the $p_w = 0.0041$ and 0.0057 graphs in figure 32b ($\beta = 0.30$) and figure 33 ($\beta = 0.0$) we can see they are similar. Vertices at these temperatures are not choosing opinions based on the voting mechanics.

3.5 WATTS-STROGATZ GRAPHS

In this section we present the results for Watts-Strogatz graphs with $p_{rw} =$ 0.0045, 0.007, 0.01, and 0.025. The crowds on the graphs with $p_rw > 0.025$ show results similar to that of crowds on ER graphs and thus will not be discussed here.

Figure 34 shows the r.m.s. change in population at low temperature as a function of crowd lifetimes. The majority of crowds have lifetimes $lesssim$50 time steps, during that time their populations size changes by a approximately 100 vertices. This is true all the graphs. Crowds which live longer than 50 time steps were observed too infrequently to analyse and have been omitted from the plot. As crowds are mesoscopic feature of the Ising dynamics it is natural to think that they are influenced by mesoscopic features of the graph

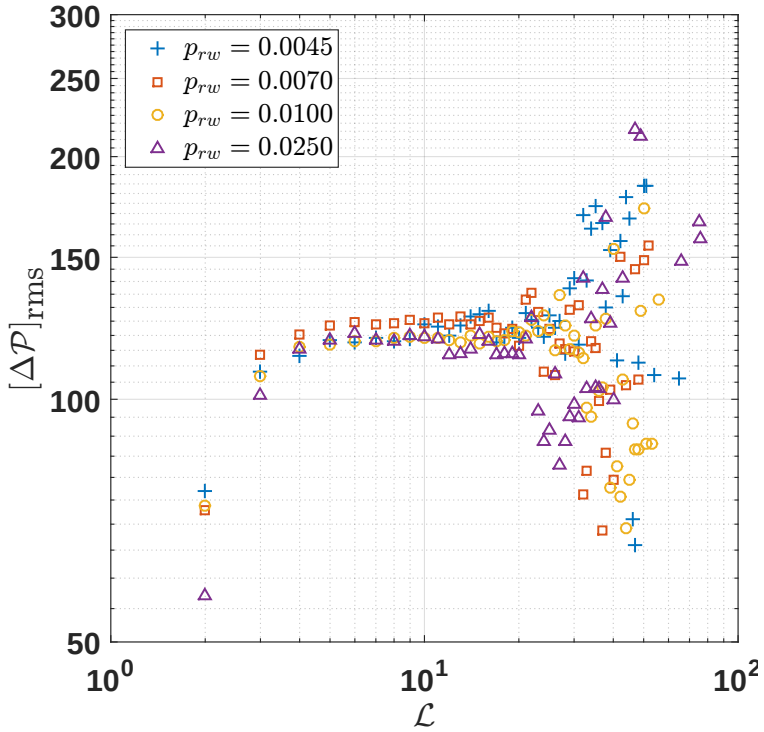


Figure 34.: Root Mean Square Change in Population Size plotted against Crowd Lifetimes at $\beta = 1.00$ for $p_{rw} = 0.0045$ (blue crosses), 0.007 (red squares), 0.01 (yellow circles), and 0.025 (purple triangles). We fit the data points in the interval $4 \leq \mathcal{L} \leq 30$ accounting for anomalous points. The diffusion exponents are $\alpha = 0.00 \pm 0.04$, 0.00 ± 0.04, 0.06 ± 0.02, 0.00 ± 0.03 respectively.

such as the community structure. At low temperatures the small-world links in the WS graph allow for it to become highly magnetised and thus a single crowd the size of the graph exists. However the structure of the graph is largely 1-dimensional and the regions with small-world links have less clustering. Consequently vertices flipping opinion break up the dominant crowd into several smaller crowds. Pressure from neighbours causes flipped vertices to revert but they do not all occur at the same time which allows the crowds to merge and form larger crowds. On average the amount of change the small crowds grow by is 100 vertices. There is corroborative evidence in Chapter 4 where we analyse the crowd population distribution. Crowds which live longer than 50 time steps

behave very differently. As whole they tend to change size less and do so in a non-diffusive manner.

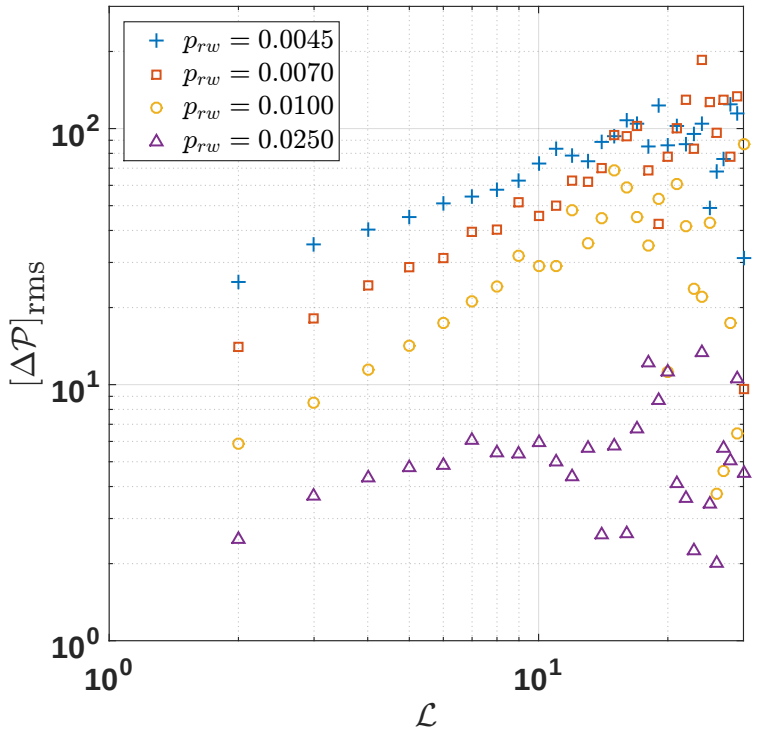


Figure 35.: Root Mean Square Change in Population Size plotted against Crowd Lifetimes at $\beta = 0.30$ for $p_{rw} = 0.0045$ (blue crosses), 0.007 (red squares), 0.01 (yellow circles), and 0.025 (purple triangles). The diffusion exponents are $\alpha = 1.3 \pm 0.1$, 1.6 ± 0.1, 2.0 ± 0.2, 1.0 ± 0.1 respectively. Data for crowds with lifetimes longer than 30 time steps have been omitted from the plot as they were too infrequently observed for analysis.

Figure 35 shows the results at a temperature near the critical value ($\beta = 0.30$). For lifetimes $\gtrsim 30$ the infrequency of observations resulted in large amounts of scattering in the interval $1 \lesssim [\Delta\mathcal{P}]_{\text{rms}} \lesssim 20$ and were not plotted. These results suggest that the crowd dynamics are not diffusive for the few long lived crowds, as the population size changes are very small it can be inferred that the crowds are robust against changes. The values of $[\Delta\mathcal{P}]_{\text{rms}}$ for crowds which live lifetimes $\lesssim 30$ are not scattered and are distributed according as a power

law. This suggests that short lived crowds change diffusively and long lived ones do not. he diffusion exponents for the short lived crowds are greater than 1 for the $p_{rw} = 0.0045$, 0.007 and 0.01 graphs indicating that changes are super-diffusive. The rewiring of edges has created lots of communities. Crowds are weakly contained by the communities and boundaries naturally occur at vertices with small-world links. Now a crowd does not need to convert all vertices of a neighbour before being able to merge just a portion that contains small-world links. Now that mergers are more likely we see that populations change super-diffusively.

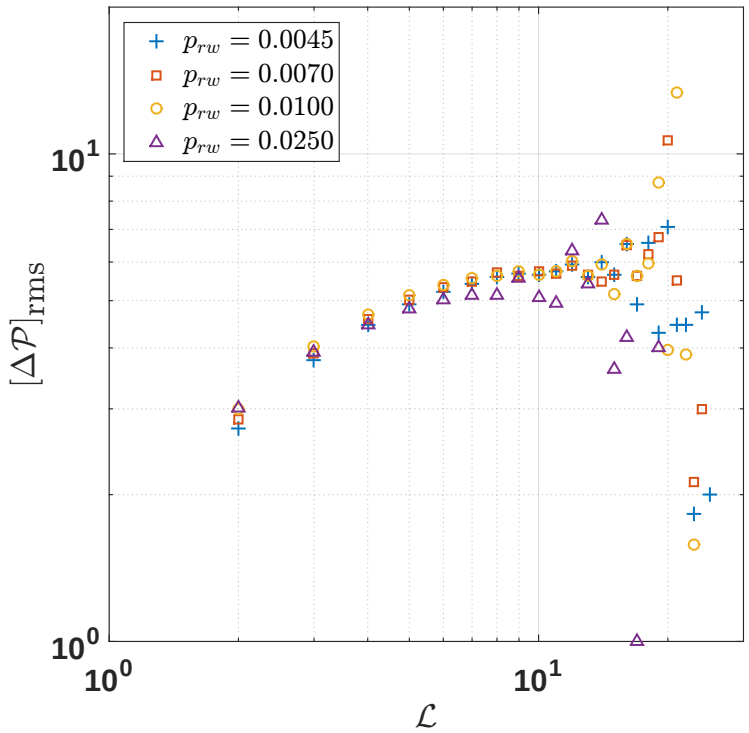


Figure 36.: Root Mean Square Change in Population Size plotted against Crowd Lifetimes at $\beta = 0.00$ for $p_{rw} = 0.0045$ (blue crosses), 0.007 (red squares), 0.01 (yellow circles), and 0.025 (purple triangles). The diffusion exponents are $\alpha = 0.32 \pm 0.05$, 0.00 ± 0.07, 0.24 ± 0.06, 0.0 ± 0.2 respectively.

The results for very high temperatures is shown in figure 36. Every vertex is flipping with a $\approx 50\%$ probability and there is no voting mechanics at play. Consequently crowd lifetimes are short and changes are small. While we do fit a power law to the data and obtain diffusion exponents the changes in population size are not diffusive.

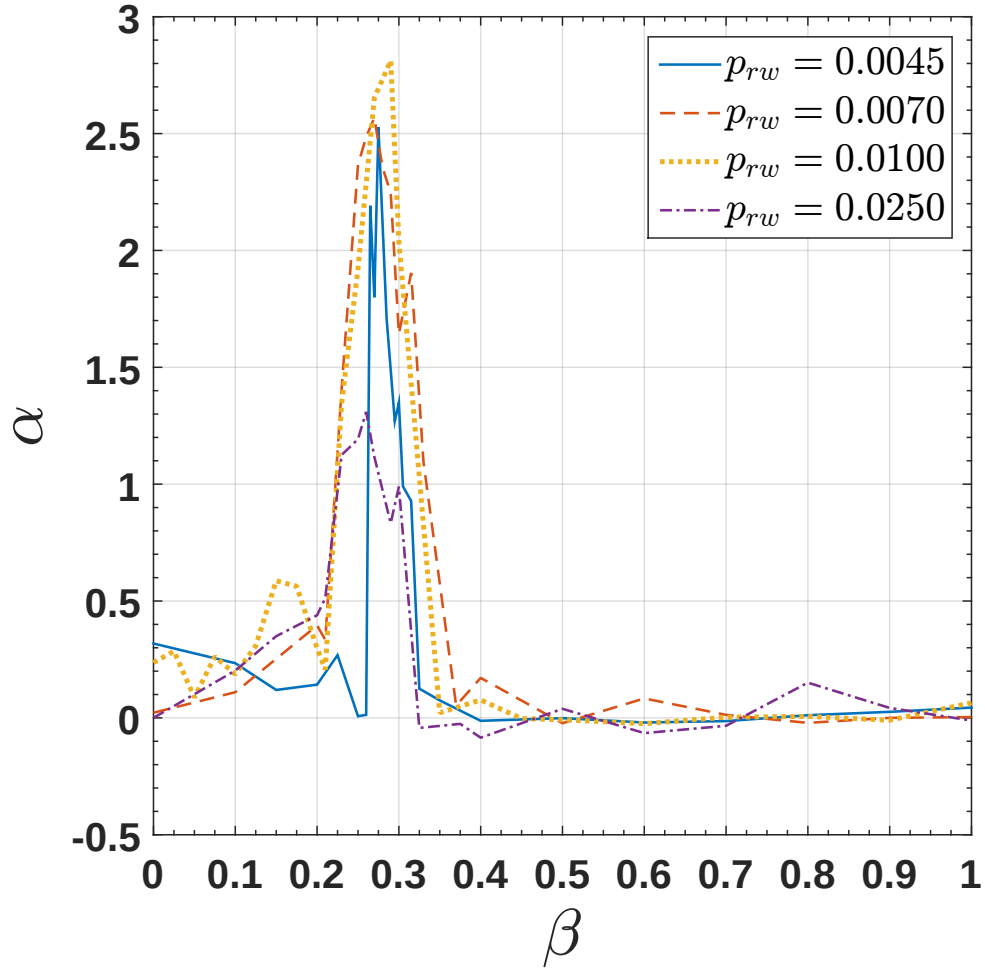


Figure 37.: Short Lifetimes

Figure 38.: Diffusion exponents of crowd population as a function of β for Watts-Strogatz graphs with $p_{rw} = 0.0045$, 0.007, 0.01, and 0.025.

Figure 38 shows the diffusion exponent as a function of the inverse temperature. At high temperatures crowds are either non-diffusive or extremely

sub-diffusive. Near the critical temperature the crowds become super-diffusive as the decrease in noise allows the formation of more robust crowds. As the temperature is decreased below the critical temperature the crowd population dynamics becomes non-diffusive.

The super diffusive region occurs in the interval $0.2 \lesssim \beta \lesssim 0.4$ for all the graphs. Crowds on the $p_{rw} = 0.0045$, 0.007, and 0.0250 graphs exhibit population changes which are greater than ballistic diffusion ($\alpha \leq 2$) indicating they grow extremely fast at those temperatures. However on the graph with $p_{rw} = 0.025$ the diffusion exponent in the super-diffusion regime are in the interval $1 \leq \alpha < 2$, thus indicates faster change than a normal diffusion process but not ballistic levels of change. A small amount of disorder in the graph structure encourages large changes in crowd size over short lifetimes but too much disorder hinders such changes.

3.6 DISCUSSION AND SUMMARY

In this chapter we analysed the behaviour of crowd populations using root mean square change in population distribution. We have found that behaviours exhibited depend on both the graph structure and the temperature of the system.

The 2-dimensional structure of the RL graph allowed crowds to remain cohesive for a large range of temperatures and allows crowds to form both robust and non-robust shapes. This meant we observe diffusive behaviour for $\beta \gtrsim 0.35$ and super-diffusive behaviour in the interval $0.35 \lesssim \beta \lesssim 0.65$. However for $\beta > 0.65$

the size changes become sub-diffusive. Thus being too robust hinders change and a certain amount of susceptibility to noise allows large amounts of change in short periods of time.

Circular Lattice graphs on the other hand are 1-dimensional, this forces the crowds into robust shapes and consequently we only observe sub-diffusive behaviour at all temperatures. We also note that crowds on CL graphs with large amounts of clustering in their structure are more sub-diffusive than those with less clustering. Thus we can say that clustering makes crowds more robust as well.

Crowds on ER graphs exhibit no diffusive behaviours at any temperature and is a result of the graph structure. When ER graph have low connectivity, $p_w \ll 1$, this results in a tree like structure with triangles or cycles of any kind being rare. The lack of cycles means that there is no reinforcement of opinions within a crowd making them extremely susceptible to being broken up by noisy behaviour at all temperatures. Crowds which are not robust have extremely short lifetimes which does not provide sufficient time for the interactions between crowds and are essential for them to exhibit diffusive changes in population size. On the other hand when the connectivity is high, $p_w \to 1$, there are lots of cycles in the graph structure resulting in crowds having a large amount of opinion reinforcement. As a consequence crowds are extremely robust, so much so that a single crowd rapidly grows to encompass the entire graph. This dominant crowd has no room to grow and is too robust to break

apart. The only cause of changes in population size is due to noisy behaviour of vertices flipping opinion at random.

Our results for the Watts-Strogatz graph shows how disrupting the 1-dimensional structure of a circular lattice can allow for super-diffusive behaviour. Small-world links allow crowds to merge without having to convert their way through an entire crowd separating them. On the other hand when $\beta \gtrsim 0.4$ the small-world links allow a single crowd to dominate the WS graphs. Consequently the population dynamics stop being diffusive.

The ability for crowds to merge is necessary for both normal and super-diffusive changes in size. To allow this to occur a graph's structure must allow crowds to have several different neighbours and to have varying weakness along its borders and internally. If crowds can not break through the one separating them they can not merge. Similarly if crowds are not susceptible to noise they will not shatter and allow new crowds to form. Sub-diffusive behaviour on the other hand requires only that crowds are resilient to large changes and noise.

4

POPULATION SIZE FREQUENCY DENSITIES

4.1 INTRODUCTION

In this chapter we present the frequency densities of the population sizes $f.d.(\mathcal{P})$. The form of the distribution can be used to ascertain how changes in temperature or graph structure can result in the formation of small, medium or large crowds on different graph types. These plots indicate how likely it is to observe crowds of a particular size and are also a measure of cohesiveness. Lots of small crowds would mean low cohesiveness and lots of large crowds would mean high cohesiveness.

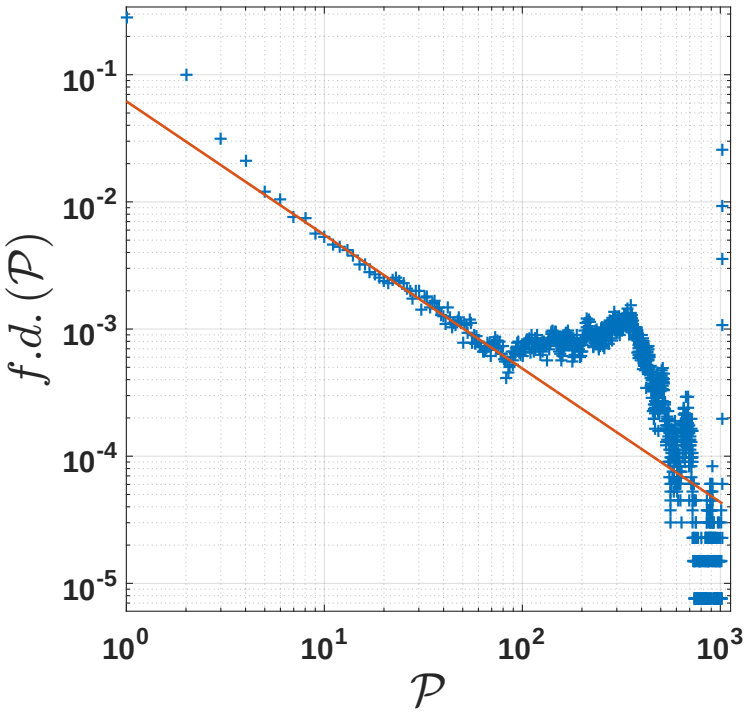
The sections in this chapter will consist of results at low, mid and high temperatures for each graph type. For many of the results we can fit them with an exponential or power law, in those case we also provide the exponents of those fits as a function of the inverse temperature β.

4.2 RECTANGULAR LATTICE

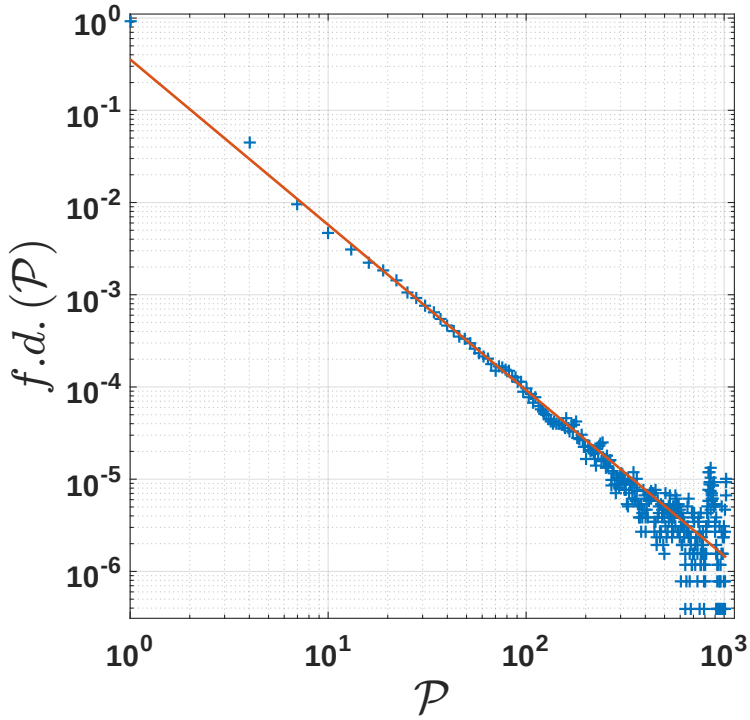
At low temperatures, shown in figure 39a, the crowd population size distribution is fitted with a power law (red line). The fit is very good in the interval $10 \lesssim \mathcal{P} \lesssim 100$ but the actual distribution has a much fatter tail than a power law. At such low temperatures the crowds are robust against noise and interactions with neighbours which allows many to grow to large sizes. However the finite size of the graph prevents crowds from growing larger than 1024 vertices thus crowds are forced to stop growing by more robust neighbours which leads to the deviation from the power law for population sizes between 100 and 700. We also observe a deviation from the power law for small population sizes, we shall discuss the cause of this later in this section.

Figure 39b shows the results at just above the critical temperature. At this higher temperature large crowds are less robust and consequently we do not observe a deviation from the power law for $\mathcal{P} \gtrsim 100$. There is once again a deviation for small crowds but it is noticeably smaller than at low temperatures.

The high temperature results are given in figure 26 and shows a power law fit for crowds with $\mathcal{P} \lesssim 17$ and an exponential distribution for $\mathcal{P} \gtrsim 17$. We attribute the difference to noisy behaviour dominating the voting mechanics, crowds are no longer robust against noise and so vertices which flip do not revert opinion swiftly. Large crowds form due to a purely random process, the probability of a crowd with n vertices forming is approximately proportional to 0.5^n, thus small crowds are significantly more likely to form than large ones.



(a) $\beta = 1.00$



(b) $\beta = 0.475$

Figure 39.: The frequency densities of the crowd sizes. The data (blue crosses) is the amalgamation from all the realisations at each temperature. The red line is a power law fit ($f.d.(\mathcal{P}) = \lambda \mathcal{P}^{-\gamma_{\mathcal{P}}}$).

Furthermore approximately 50% of a crowd's vertices will flip opinion during the next time step resulting in the crowds destruction. The crowds which form from the shattering of a large crowd are more probably small than large.

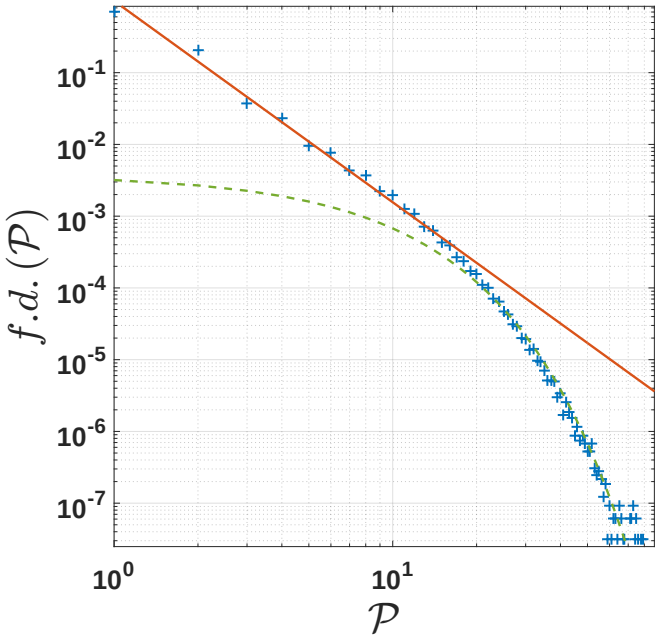


Figure 40.: The frequency densities of the crowd sizes for the inverse temperature $\beta = 0.050$. The data is the amalgamation from all the realisations at each temperature. The red solid line is a power law fit $f.d.(\mathcal{P}) = \lambda_1 \mathcal{P}^{-\gamma_{\mathcal{P}}}$, with $\gamma = 2.81 \pm 0.09$ and the green dashed line is an exponential decay fit $f.d.(\mathcal{P}) = \lambda_2 e^{-\theta \mathcal{P}}$, with $\theta_{\mathcal{P}} = 0.1724 \pm 0.0002$.

We mentioned earlier in this section that temperatures near the critical value an greater the population frequency distribution deviates from power law fit at very small sizes. A careful inspection of the results shows that the distribution for $\mathcal{P} \leq 10$ is roughly the same at all temperatures. Thus the processes which create the small crowds are unaffected by changes in the temperature and the distribution for $\mathcal{P} > 10$. From this we learn that the voting mechanics have little to no effect on the frequency of occurrence of very small crowds but are essential for larger crowds.

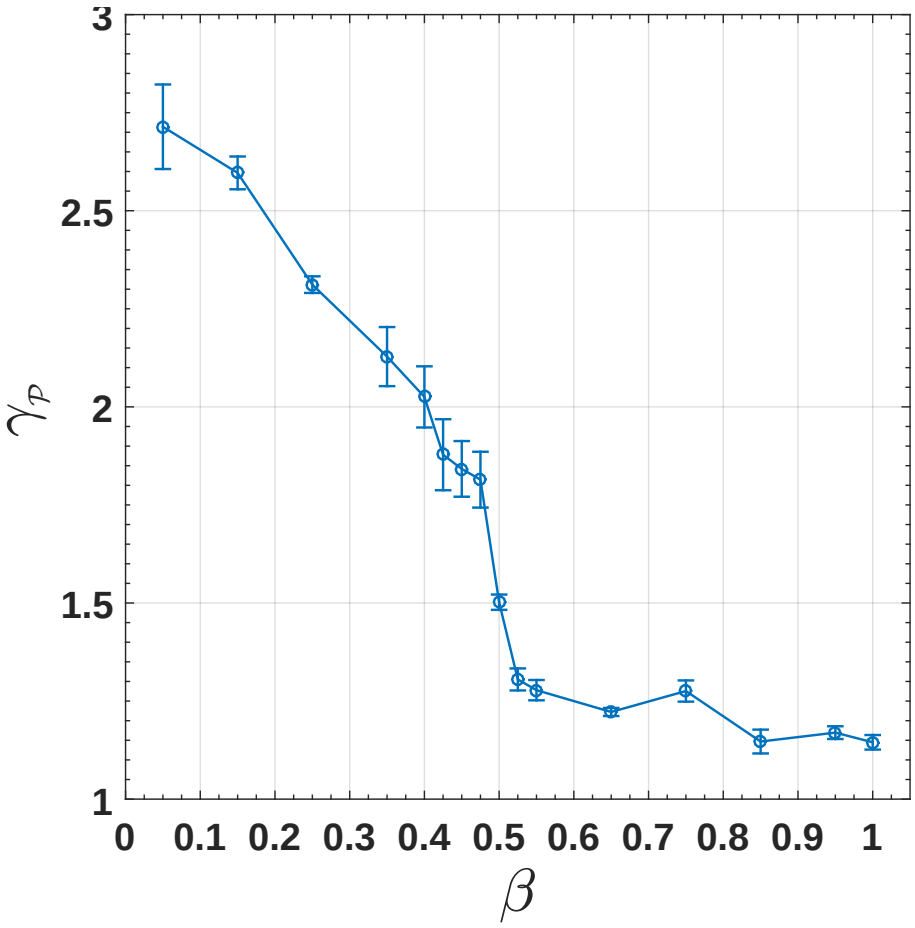


Figure 41.: The exponent of the power law fit, $\gamma_{\mathcal{P}}$ as a function of the inverse temperature β.

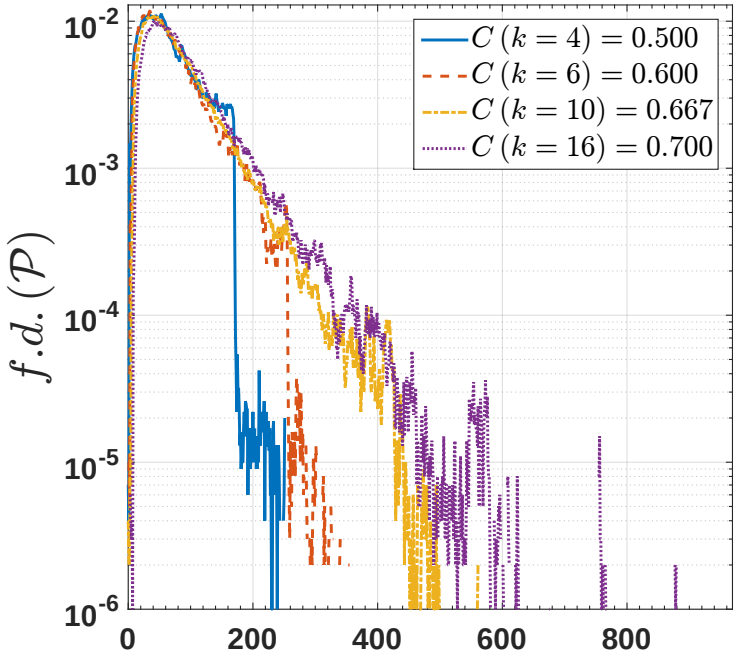
Figure 41 is a plot of the power law exponent as a function of the inverse temperature. A large $\gamma_{\mathcal{P}}$ indicates a thin tail and a small $\gamma_{\mathcal{P}}$ indicates a fat tail to the distribution. The exponent begins to decrease with temperature and becomes a trough just below the critical temperature. A much larger RL graph would allow us to find out if $\gamma_{\mathcal{P}}$ continues to decrease or if the population distribution truly levels out after β_c.

4.3 CIRCULAR LATTICE

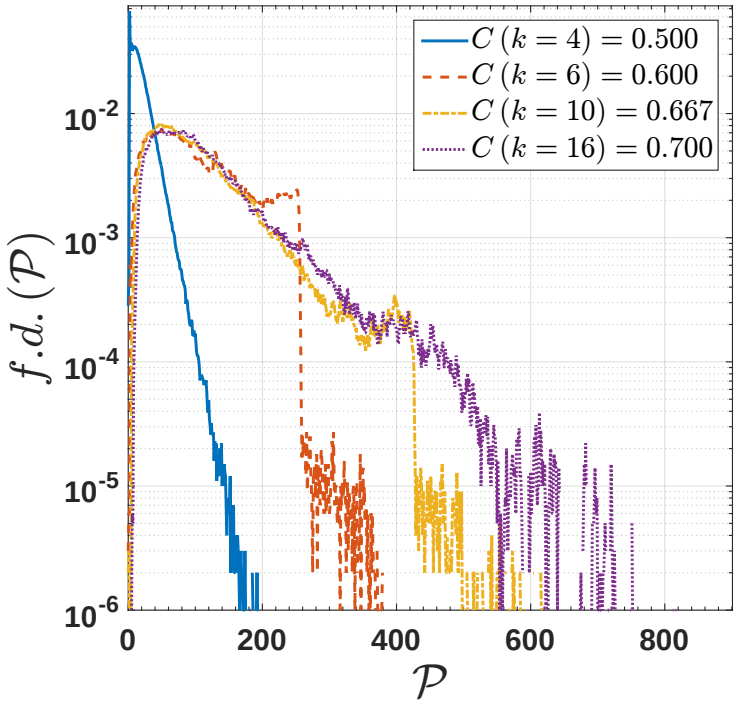
As in the previous chapter we provide the results for the $C(k = 4) = 0.500$, $C(k = 6) = 0.600$, $C(k = 10) = 0.667$, and $C(k = 16) = 0.700$ circular lattice graphs. Figure 42a shows the low temperature results on a semi-log scale plot. Barring finite size effects the distribution of observed population sizes is the same for all the graphs. The tail of the distribution decays exponentially, denoting that the majority of the crowds are small and large crowds are very rare. The similarity of the distributions means that clustering coefficient is not an important factor for crowd size.

At $\beta = 0.400$ the distributions start to show differences (see figure 42b). Crowds on the $C(k = 4) = 0.500$ circular lattice tend to be very small and crowds with sizes similar to that of the graph have a one in a million chance of occurring. Greater amounts of noisy behaviour due to the higher temperature creates lots of small crowds in the graph. This has a secondary effect of breaking up larger crowds and thus creating even more small crowds. On graphs with large clustering coefficients and higher degrees the crowds are more robust to noise, consequently their distributions have not changed much. In fact the higher amounts of noise has resulted in large crowds being more likely to form on the graphs. The effect is slight and the main body of the tails are relatively unchanged compared to the low temperature results.

At very high temperatures the crowd population distribution for the $C(k = 16) = 0.700$ remains unchanged. The large degree and clustering coefficient has re-



(a) $\beta = 0.950$



(b) $\beta = 0.400$

Figure 42.: The frequency densities of the crowd sizes for various CL graphs. Lines were used to plot the data to aid differentiation between results for different graphs: the data is discrete not continuous.

sulted in crowds which are extremely resistant to the effects of noise. Consequently the secondary creation of lots small crowds does not occur and thus

not affect the population distribution. On the other hand the distributions for both the $C\,(k=6)\,=\,0.600$ and $C\,(k=10)\,=\,0.6667$ graphs have narrowed significantly indicating that they are affected.

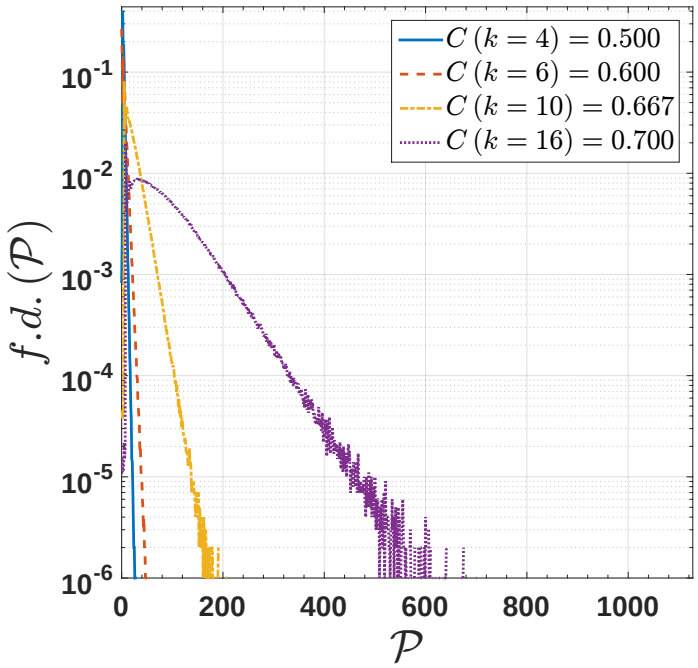
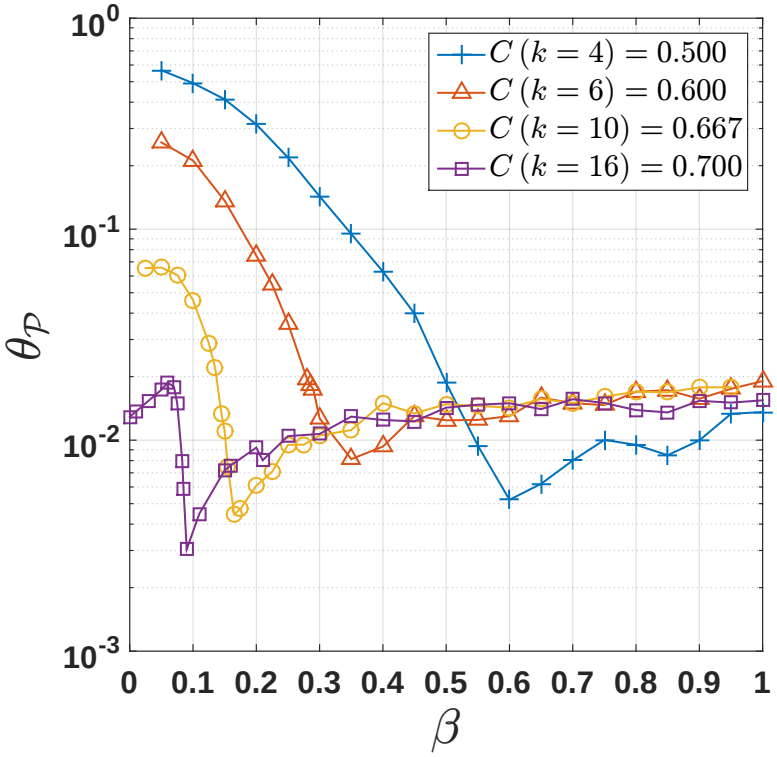
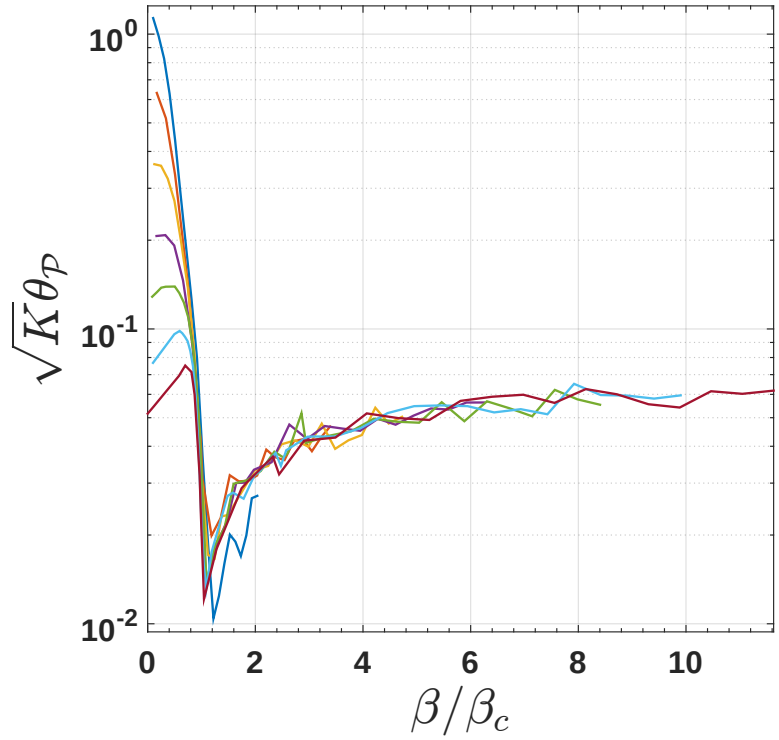


Figure 43.: The frequency densities of the crowd sizes for the inverse temperature $\beta = 0.050$.

Figure 44a plots the exponent of an exponential fit for the frequency density data for each of the 4 graphs. There are great similarities in how $\theta_{\mathcal{P}}$ changes with β for each graph. While we were unable to find a single analytical function which would fit the data we were able to perform a data collapse (see figure 44b). By multiplying $\theta_{\mathcal{P}}$ by $\sqrt{N}$ and dividing β by β_c we show that the population distributions respond in a similar manner. This means that the population sizes of crowds is dependent on the size of the graph and not dynamics of how crowd populations change.



(a)



(b)

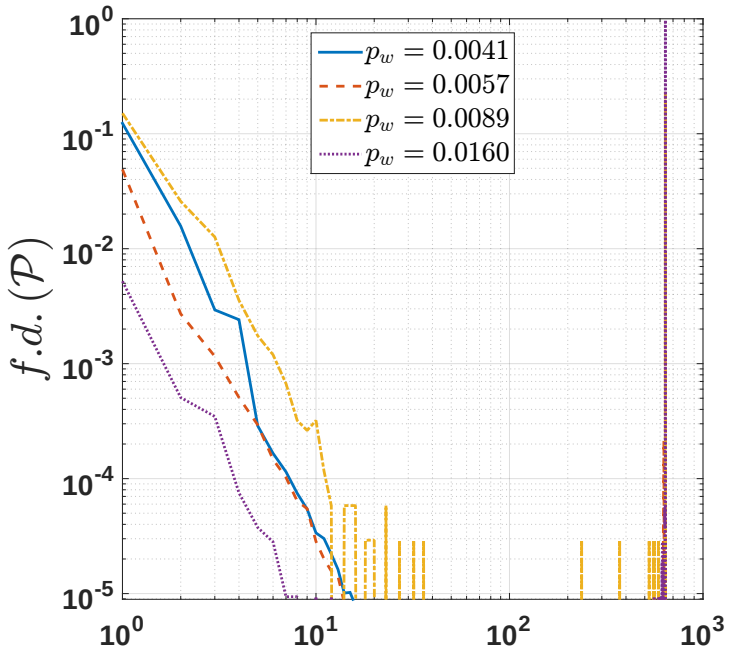
Figure 44.: In the top figure (44a) we plot, $\theta_{\mathcal{P}}$, the exponent of the exponential fit of the population frequency distributions as a function of β for 4 of the 7 graphs studied. Below we plot the results for all 7 graphs scaled to show that the population distributions change in the same way.

4.4 ERDŐS-RÉNYI GRAPHS

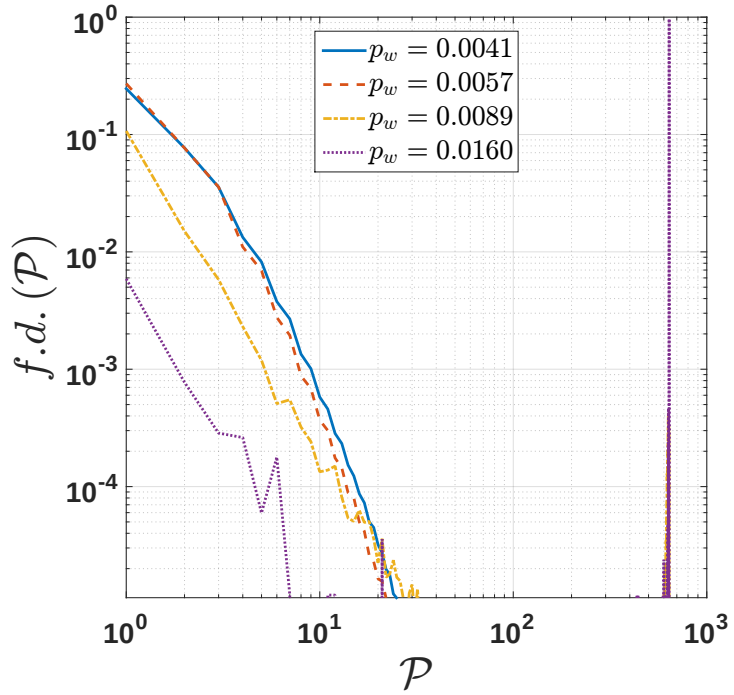
The population dynamics and magnetisation results for ER graphs hinted that a single crowd tends to dominate at low temperatures, figure 45a shows this to be true. The distribution of population sizes for all the wiring probabilities consists of two parts, a power law for $\mathcal{P} \lesssim 100$ and a delta function for $\mathcal{P} \approx N \equiv 640$. For $p_w = 0.0041$ (solid blue line) and 0.0057 (dashed red line) the frequency of crowds with only 1 vertex is ≈ 1, crowds of any other size are consequently extremely unlikely. While these graphs are connected they contain only a small number of edges therefore for the voting mechanics of the Ising model do not have any influence on the opinions of vertices. Also at such low temperatures noisy behaviour is rare, together the spin configuration of the $p_w = 0.0041$ and $p_w = 0.0057$ graphs becomes frozen when quenched. Thus any large crowds observed are due to chance.

The graphs for $p_w = 0.0089$ (dot-dashed yellow line) and 0.0160 (dotted purple line) have far more edges than the other two and the population size distribution is very different. The probability of observing a crowd with a size on the order of the graph's size is $P(\mathcal{P} \approx N) = 0.23$ and 0.97 respectively. Their increased connectedness allows the entire graph to form a unanimous consensus frequently. The occurrence of small crowds is due only to small amounts of noisy behaviour. However the $p_w = 0.0089$ graph is still not connected enough that the formation of the single dominating crowd is a given, in most realisations it

becomes frozen as lots of small crowds resulting in $P(\mathcal{P} \approx N) < 1$ instead of close to 1.



(a) $\beta = 1.00$



(b) $\beta = 0.200$

Figure 45.: The frequency densities of the crowd sizes have been plotted for several ER graphs. The distributions have power law tails and

Figure 45b shows the results for a higher temperature $\beta = 0.200$ near to the critical value. The population distributions for the $p_w = 0.0041$ and 0.0057 graphs have lost their Dirac delta function component and consist of a power law tail. Comparing with the low temperature results we find that this part of the distribution is almost unchanged. At these higher temperatures the spin-configuration does not become frozen when quenched instead the voting mechanics have absolutely no influence on the opinions at all. Hence we observe a similar distribution as the low temperature results.

The distribution for the $p_w = 0.0089$ still consists of the power law distribution and the Dirac delta function. However $P(\mathcal{P} \approx N) = 0.0004$ indicating that the formation of only a single crowd is extremely rare. Further the power law distribution has widened a little further and the probability $P(\mathcal{P} = 1) = 0.86$. The connectivity of this graph is high enough that even with the massive amounts of noise the voting mechanics still have enough influence for a single all encompassing crowd to form a significant fraction of the time.

There is no appreciable changes in the frequency distribution of crowd population on the $p_w = 0.0160$ graph. Even at these higher temperatures the connectivity of the graph is so high that a single dominant crowd forms, all other crowds are created due to noisy behaviour. Even though we would expect there to be more crowds created due to noisy flips we see only slight changes in the distribution for small population sizes. This lack of change is due to our

pre-processing step which removes some of the noise to make identifying crowds easier.

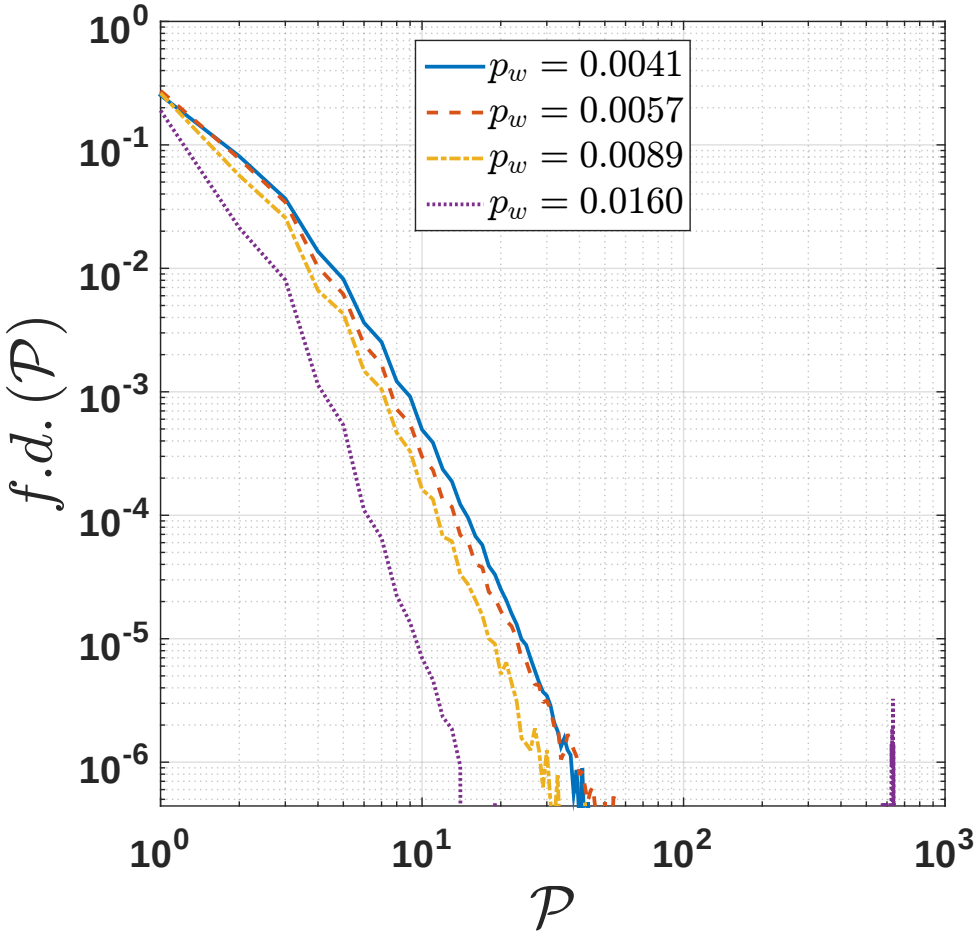


Figure 46.: The frequency densities of the crowd sizes for the inverse temperature $\beta = 0.000$.

Figure 46 shows the population frequency densities at very high temperatures $\beta = 0.000$. The results for the $p_w = 0.0041$, 0.0057 and 0.0089 graphs are roughly the same indicating noisy behaviour is the cause of the distributions. The distribution for the $p_w = 0.0160$ graph has a thinner tail than the others but amazingly still has a small peak at $\mathcal{P} \approx N \equiv 640$. In theory the voting part of the Ising Model should have no influence on opinion formation at these

temperatures and so the occurrences of a single all encompassing crowd are due to chance.

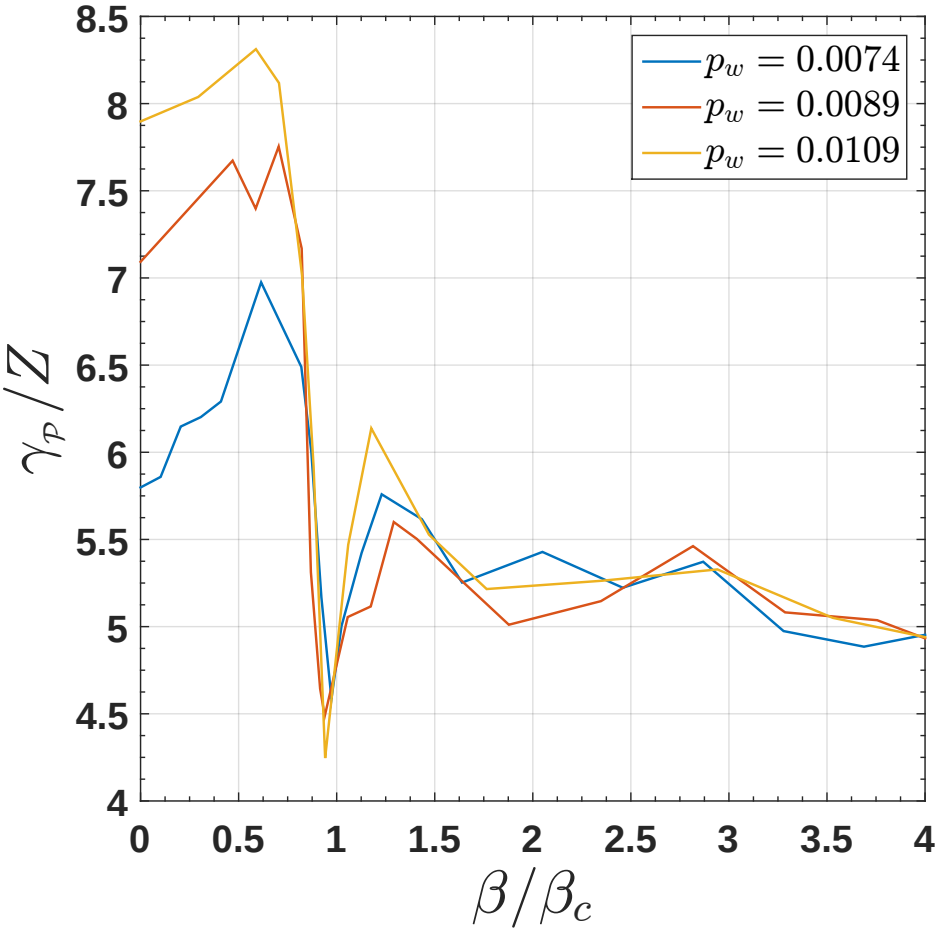


Figure 47.: The exponent of the power law fit as a function of the inverse temperature.

The exponents $\gamma_{\mathcal{P}}$ of power law fits of the data are shown as functions of the inverse temperature β in figure 47. The results show that the distributions for $p_w = 0.0041$ and 0.0057 become slightly wider as the temperature gets lower but does not change much. On the other hand the distributions of both $p_w = 0.0089$ and 0.0160 become wider suddenly as $\beta \to \beta_c$, then becomes narrower as β increases further. This is due to the emergence of the single all encompassing crowd which only happens for the two more connected graphs.

4.5 WATTS-STROGATZ GRAPHS

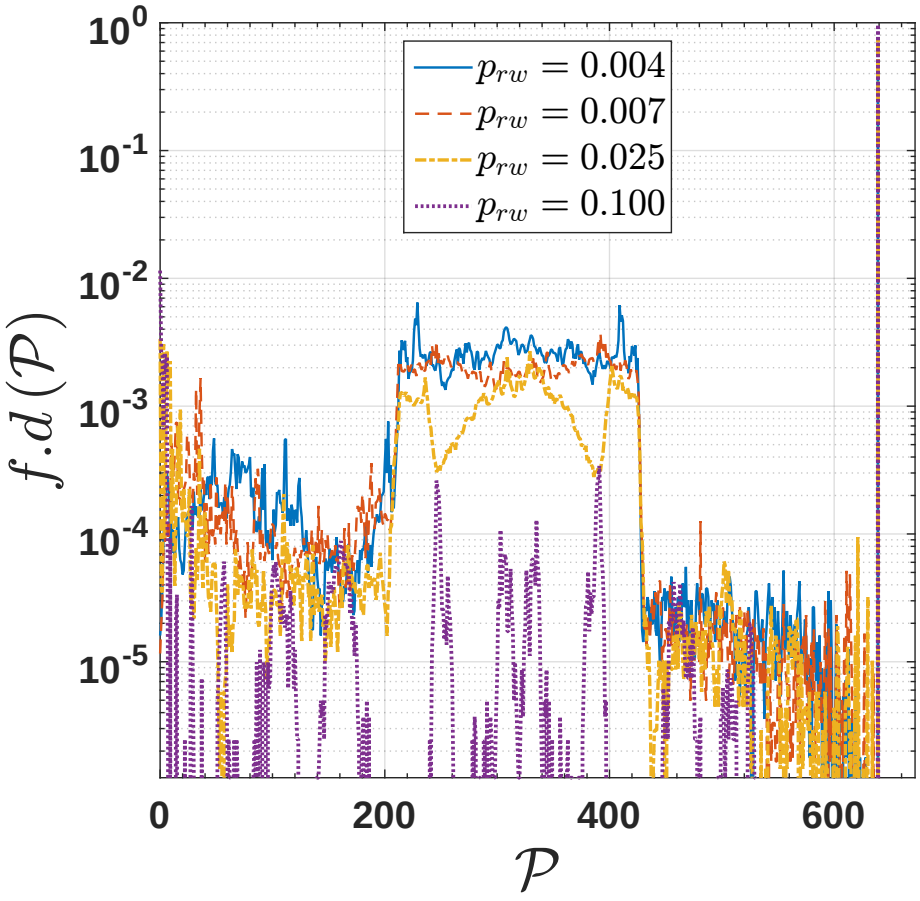


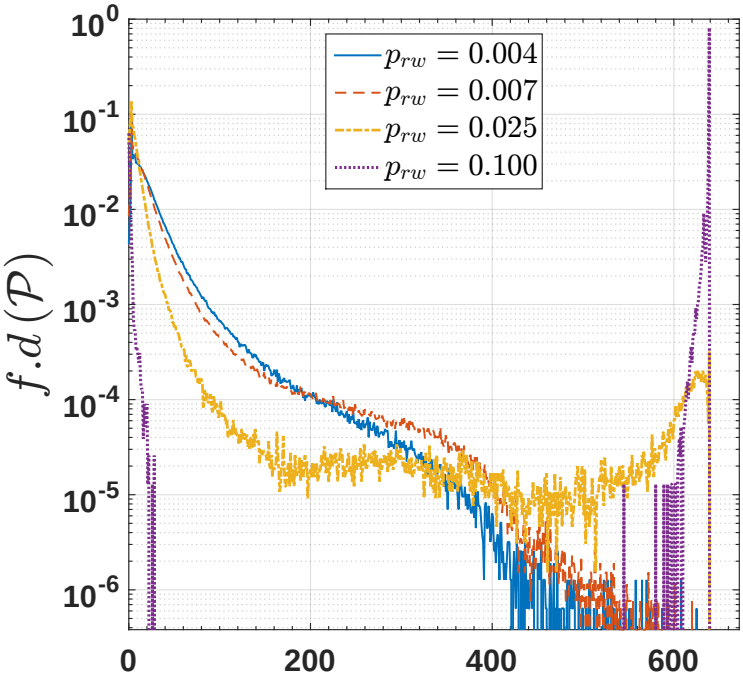
Figure 48.: The frequency densities of the crowd sizes for the inverse temperature $\beta = 1.000$ for several Watts-Strogatz graphs.

Figure 48 shows the population frequency densities for the $p_{rw} = 0.004$, 0.007, 0.025, and 0.100 Watts-Strogatz graphs of size $N = 640$. The probability of observing a single all encompassing crowd $P(\mathcal{P} \approx N) = 0.41$, 0.53, 0.74, and 0.97. Thus we can say that a greater amount of small-world links in the graph structure encourages the formation of a unanimous consensus - a single crowd the size of the graph.

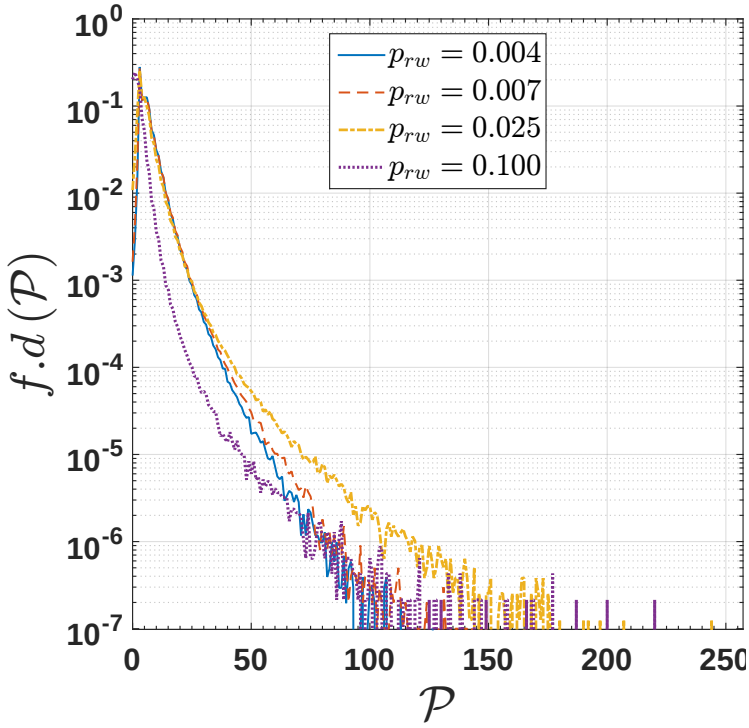
In Section 3.5 we stated that dynamics of the size changes was due to the community structure of the graphs and corroborative evidence would be provided in this chapter. The plateau in figure 48 is that evidence. At these low temperatures noisy behaviour occurs only occasionally, when it does due to the mainly 1-dimensional nature of the graph the large dominant crowd gets broken up into new smaller crowds. These crowds then merge when the opinions of noisy vertices are reverted.

An examination of symmetrical peaks and troughs in the plateau shows up that the populations of symmetrical pairs add up to 640. This indicates that most of the time the graph gets broken into 2 large pieces and the $[\Delta\mathcal{P}]_{\text{rms}}$ for these crowd is around 250. However the large crowd also breaks up into crowds of other sizes less frequently and the smaller crowds can be broken up, consequently the average change in size settles at approximately 100 vertices.

The frequency density of the symmetrical region decreases as p_{rw} increases. A small number of small-world links introduces a few weak points where noisy behaviour can have the greatest effect of breaking up a dominant crowd. However as p_{rw} increases the small-world links allow distant regions of the graph to remain connected and thus making it harder for noisy behaviour to split up a dominating crowd. The population distribution for the $p_{rw} = 0.1$ graph does not have a plateau; it does have distinct symmetrical peaks. Thus even on graphs with rewiring probabilities as high as 0.100 the dominant crowd is not so robust as to be unbreakable.



(a) $\beta = 0.25$



(b) $\beta = 0.00$

Figure 49.: The frequency densities of the crowd sizes for the inverse temperature $\beta = 1.000$ for several Watts-Strogatz graphs.

Figure 49a shows the population distributions when β is near β_c. At this temperature the crowd dynamics are super-diffusive on some of the graphs.

Parts of the distributions for $p_{rw} = 0.004$, 0.007, and 0.025 WS graphs decay according to a power law. However the tail ends for $p_{rw} = 0.004$ and 0.007 distributions show a sudden sharp cut off while the results for $p_{rw} = 0.025$ levels out and forms a sharp peak near $N \equiv 640$. The distribution for the $p_{rw} = 0.100$ graph is vastly different from the others. Its defining feature is the delta function peak at $\approx N$ and while the populations sizes for $\mathcal{P} \lesssim 20$ follows a power law. The population size f.d. for $p_{rw} = 0.1$ is similar to that of crowds on an ER graph.

At very high temperatures ($\beta = 0$) the tail of all the populations decay according to a power law, see figure 49b. Vertices are choosing an opinion at random with no bias, small crowds form very frequently and when destroyed are replaced by new small crowds. Large crowds on the other hand form very rarely and noisy behaviour causes them to break up into lots of small crowds. The small-world links however allow large crowds to remain connected for longer which results in the fatter tail.

4.6 DISCUSSION AND SUMMARY

The population frequency distribution for the RL graph had an exponential tail at high temperatures and the dynamics of the crowd populations were non-diffusive. We thus have further confirmation of the results obtained in Chapter 4. As the temperature decreased the population f.d. had a power law form and at these temperatures the dynamics of the crowds were super-diffusive. At very

low temperatures parts of the distribution follow a power law but the tail levels off before cutting off abruptly.

For circular lattices the crowd population f.d. were exponential distributions at all temperatures. We were able to show by performing a data collapse that the differences in the population distribution were due to graph size. The population dynamics of the crowds were sub-diffusive at all investigated temperatures but did not affect the population distribution.

The distribution for the ER graphs features of a power law for $\mathcal{P} \lesssim 100$ and delta function at $\mathcal{P} \approx N \equiv 640$. The existence delta function indicated that highly connected ER graphs tend form a single crowd that contains every vertex while those with fewer edges did not. All frequency distributions features a delta function at very low temperatures and lost them as the temperature increased.

Population frequency distributions on the Watts-Strogatz graphs changes the most as temperatures varied. At low temperatures the distribution consisted of a highly symmetrical region in the interval $200 \lesssim \mathcal{P} \lesssim 450$ and a delta function at $\mathcal{P} \approx N \equiv 640$. Once again the delta function indicated the existence of singe all encompassing crowd. At higher temperatures the two graphs with the least amount rewiring lost their delta function spike while other two retained them. The rest of the distribution for all the graphs followed a power law near at temperatures near to and greater than the critical value. The population dynamics were non-diffusive at low temperatures, became super-diffusive near the critical value and non-diffusive at high temperatures.

The population distributions of the Watts-Strogatz graphs have more in common with the rectangular lattices and Erdős-Rényi graphs than the circular lattices. At high temperatures the distributions for the ER and WS graphs are similar in form, i.e. both are power laws. While the RL and CL graphs have exponentially decaying tails. This suggest to us that random links connecting distant regions of a graph prevents large crowds to be broken up quickly by noisy behaviour. Then at $\beta \approx \beta_c$ the f.d. of the populations on WS graphs are still power laws which is similar to ER graphs. However there is also a significant increases in the maximum population sizes observed and is a result of the crowds populations changing super-diffusively like we observe for RL graphs.

5

LIFETIME FREQUENCY DENSITIES

5.1 INTRODUCTION

In Section 2.2 we defined a crowd as an amorphous cluster of consensus which changes with time due to Ising Spin dynamics. The ordered set of subgraphs $\mathcal{C} = \left\{K^b, \ldots, K^t, \ldots, K^d\right\}$ describes the constituents and relationships during the interval of time $[b, d]$ the crowd exists for. Each pair adjacent subgraphs $K^t, K^{t+1} \in \mathcal{C}$ are more than 50% similar, by which we mean

$$\Phi\left(K^t, K^{t+1}\right) = \frac{|V_t \cap V_{t+1}|}{|V_t \cup V_{t+1}|} > 0.7071, \tag{74}$$

where $K^t \equiv K^t\left(V_t, E_t\right)$ and $K^{t+1} \equiv K^{t+1}\left(V_{t+1}, E_{t+1}\right)$. A crowd dies when it changes so between a time step that it is not 50% similar,

$$\nexists K^{d+1} : \Phi\left(K^d, K^{d+1}\right) > 0.7071. \tag{75}$$

Thus we define the lifetime of the crowd $\mathcal{L} = |\mathcal{C}| = d - b + 1$ is defined as the number of elements in it. Thus the length of the interval of time a crowd existed for ($\mathcal{L}$) is a measure of how robust it was to large changes.

Crowds change by gaining or losing vertices as they switch opinion. The cause is either vertices behaving noisily or interactions between crowds at a boundary. The inverse temperature β controls the noisiness of the vertices, the probability of a vertex i flipping opinion is given by equation 42,

$$P\left(\sigma_i^{t+1} = -\sigma_i^t, \sigma_i^t\right) = \frac{e^{-2\beta\left(2S_i^t - k_i\right)}}{1 + e^{-2\beta\left(2S_i^t - k_i\right)}}.$$

where $S_i^t = \sum_{j=1}^{N} \boldsymbol{A}_{ij}\delta\left(\sigma_i^t, \sigma_j^t\right)$ is the number of neighbour of i that share its opinion. At high temperatures $\beta \to 0$ the probability of flipping is,

$$P\left(\sigma_i^{t+1} = -\sigma_i^t, \sigma_i^t\right) \approx 0.5, \tag{76}$$

when the temperature is low the probability of a vertex flipping becomes dependent on the opinions its neighbours. Thus graph structure is increasingly more important to the robustness of crowds at temperatures near the critical value and below. Having a large number of neighbours makes it less probable that vertex will flip opinion unless the neighbourhood opinion itself is unstable.

Vertices on their own do not have a memory of their past opinions however neighbours have a mutual influence over each other. This creates feedback loops between neighbours that reinforces an opinion, even if a vertex flips opinion its neighbours will influence it revert back. Such feedback loops can exist between

direct neighbours and through short paths through a graph. It stands to reason that crowds on a graph with lots of triangles should live longer and be more robust against noise. In this chapter we study the distribution of crowd lifetimes obtained by Monte Carlo simulations of the Ising Model on various graphs for a range of temperatures to determine how graph structure actually influences the robustness of crowds. We present the results for each graph type separately in the following sections and then discuss all the graphs together at the end of the chapter.

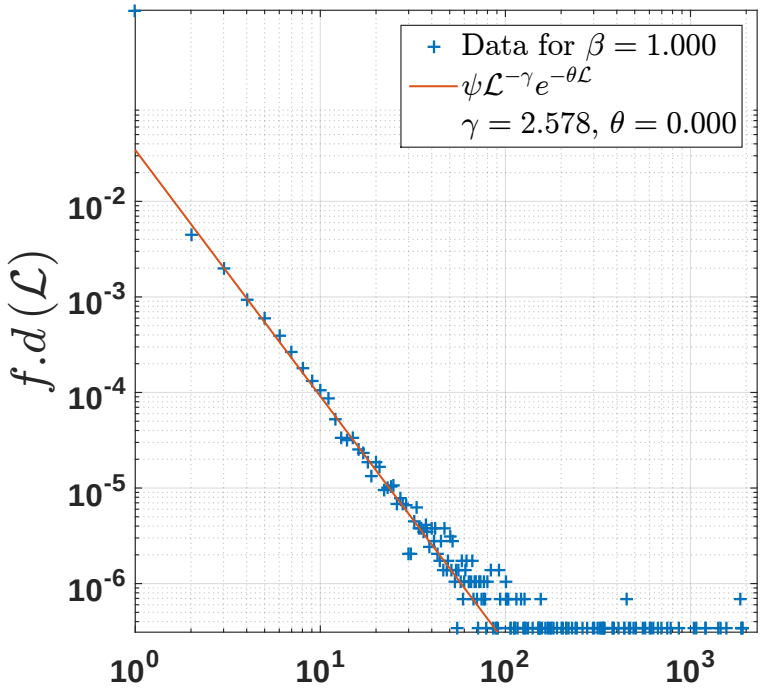
5.2 RECTANGULAR LATTICE

The rectangular lattice graph has no clustering but lots of 4-cycles (see Section 1.1.2), this allows vertices in a crowd to strongly reinforce each others opinions. At low temperatures this results in crowds with very long lifetimes.

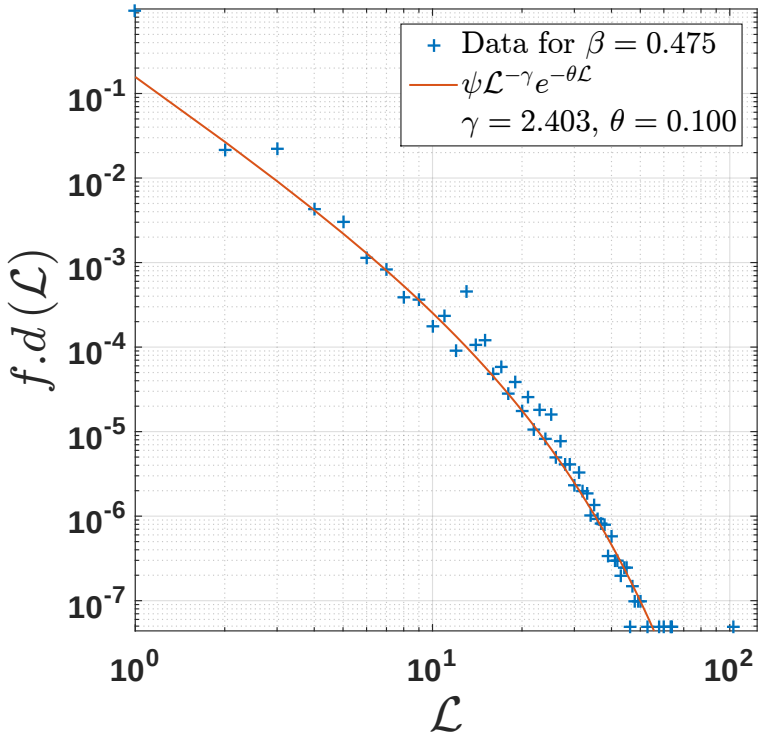
We found after noticing that the body of the lifetime frequency density distributions could be fitted by a power law, $\psi_1 \mathcal{L}^{-\gamma_\mathcal{L}}$, and the tail by an exponential decay, $\psi_2 e^{-\theta_\mathcal{L} \mathcal{L}}$ depending on the temperature. By using the ansatz that the distribution is product of both,

$$f.d.\left(\mathcal{L}\right) = \psi \mathcal{L}^{-\gamma_\mathcal{L}} e^{-\theta_\mathcal{L} \mathcal{L}}, \tag{77}$$

we found that it produced a good fit of the data over various temperatures. We rationalise after the fact that the exponential component represents the influ-



(a) $\beta = 1.00$



(b) $\beta = 0.475$

Figure 50.: The frequency densities of the lifetimes of crowds on RL graphs. Blue crosses are used for data obtained from simulations and the red lines are best fits for the equation $f.d.(\mathcal{L}) = \psi\mathcal{L}^{-\gamma_{\mathcal{L}}}e^{-\theta_{\mathcal{L}}\mathcal{L}}$.

ence of noisy behaviour on lifetimes as its contribution becomes more noticeable as the temperature increases.

Figure 50a shows the frequency density distribution of the crowd lifetimes at a low temperature ($\beta = 1.000$). The distribution has a power law tail, the exponential component of our fitting function has no influence on the form. A fat tail like this indicates that the long lifetimes are not caused by noisy behaviour and that they are a result of the voting mechanics of the Ising Model. Consequently the lifetimes of crowds are dependent on their interactions with their neighbours and the state of the system as a whole. Lifetimes of length 1 were observer far more often than our fitting function predicts. This indicates that flipping due to noisy behaviour occurs often but their neighbours pressure them to revert their opinions back quickly.

At temperatures near the critical value the tail of the distribution has both scale-free and exponential characteristics, figure 50b. We know that distributions at high temperatures when vertices are behaving noisily have an exponential form thus we say that the lifetimes of some crowds are being cut short due to noise. However most crowds are still sufficiently robust that their crowd-crowd interactions are still the deciding factor.

Figure 51 shows the results at a very high temperature $\beta = 0$. At these temperatures the lifetime of a crowd depends entirely on how quickly noisy behaviour of it constituent vertices cause it to shatter. In most cases it is almost immediately and longer lifetimes get exponentially less likely. However there is a small deviation at the longest lifetimes where they occur more frequently

than our fitting model predicts. The existence of deviations at both very short and very long lifetimes indicate that there is some process occurring for which our fitting model does not accounted for.

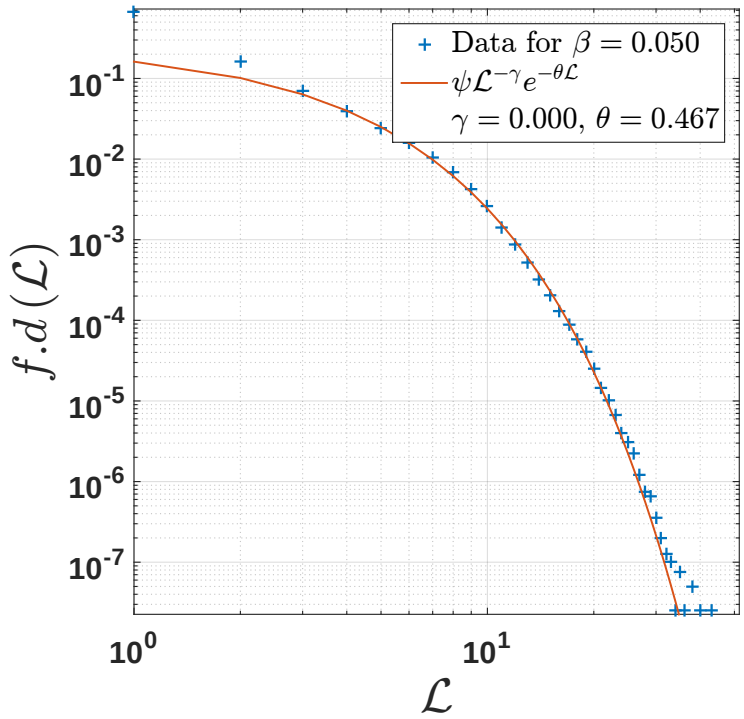


Figure 51.: The frequency density distribution of the lifetimes for $\beta = 0.050$. Blue crosses are used for data obtained from simulations and the red lines are best fits for the equation $f.d.(\mathcal{L}) = \psi\mathcal{L}^{-\gamma_{\mathcal{L}}}e^{-\theta_{\mathcal{L}}\mathcal{L}}$.

We fit the lifetime frequency distributions for each β with the function $f.d.(\mathcal{L}) = \psi\mathcal{L}^{-\gamma_{\mathcal{L}}}e^{-\theta_{\mathcal{L}}\mathcal{L}}$. The power law exponent γ and the exponential exponent θ are plotted as functions of β in figure 52. For $\beta \lesssim 0.25$ the power law component is not expressed at all, this is also the interval in which the crowd behaviour is non-diffusive. In the interval $0.25 \lesssim \beta \lesssim 0.65$ the exponential component becomes weaker and the power law stronger, the crowds populations are changing super-diffusively. For $\beta \gtrsim 0.65$ the exponential component is not expressed at all, and crowd populations change sub-diffusively. This sug-

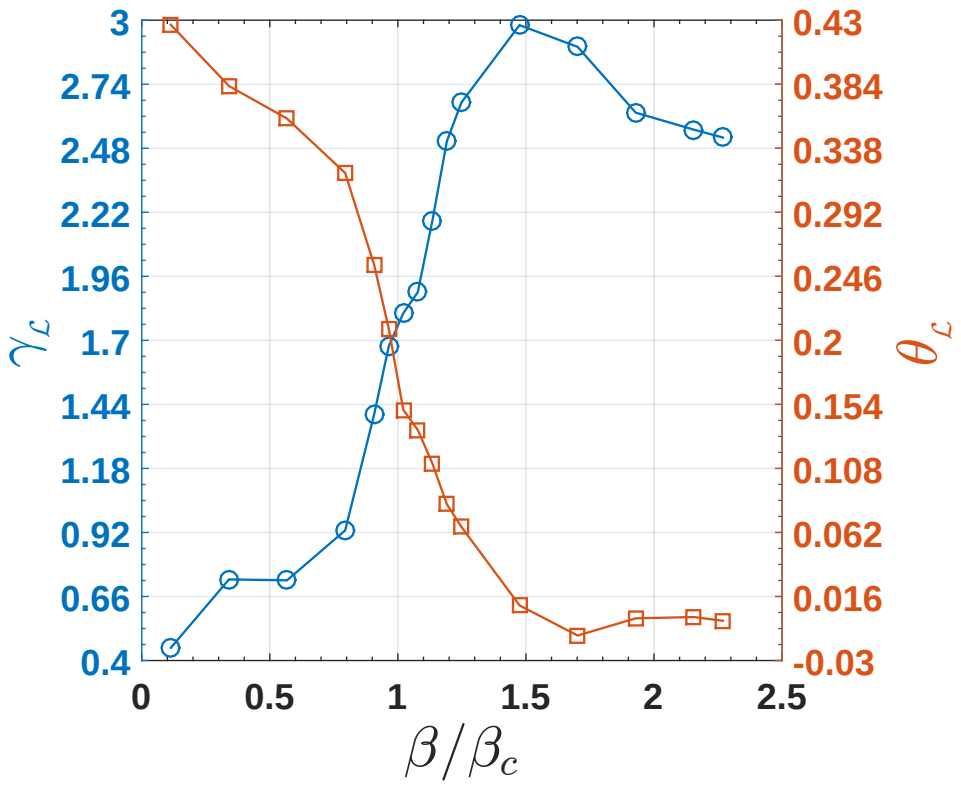


Figure 52.: The exponents of our fitting function $f.d.(\mathcal{L}) = \psi \mathcal{L}^{-\gamma_{\mathcal{L}}} e^{-\theta_{\mathcal{L}} \mathcal{L}}$ plotted as functions of the inverse temperature β. Blue circles are the values for $\gamma_{\mathcal{L}}$ and red squares are the values for $\theta_{\mathcal{L}}$. The lines have been included as a guide for the eye.

gests that a power law tail in the lifetime frequency distribution is caused by interactions between crowds being the dominant dynamic for changes.

In summary we found that the frequency of lifetimes decayed exponentially with their length at very high temperatures and as a power law at low temperatures. Analysis of intermediate temperatures showed us that distribution transitioned smoothly from one to the other and thus suggested a Gamma distribution. Attempts to fit the Gamma distribution failed and we use $f.d.(\mathcal{L}) = \psi \mathcal{L}^{-\gamma_{\mathcal{L}}} e^{-\theta_{\mathcal{L}} \mathcal{L}}$ instead.

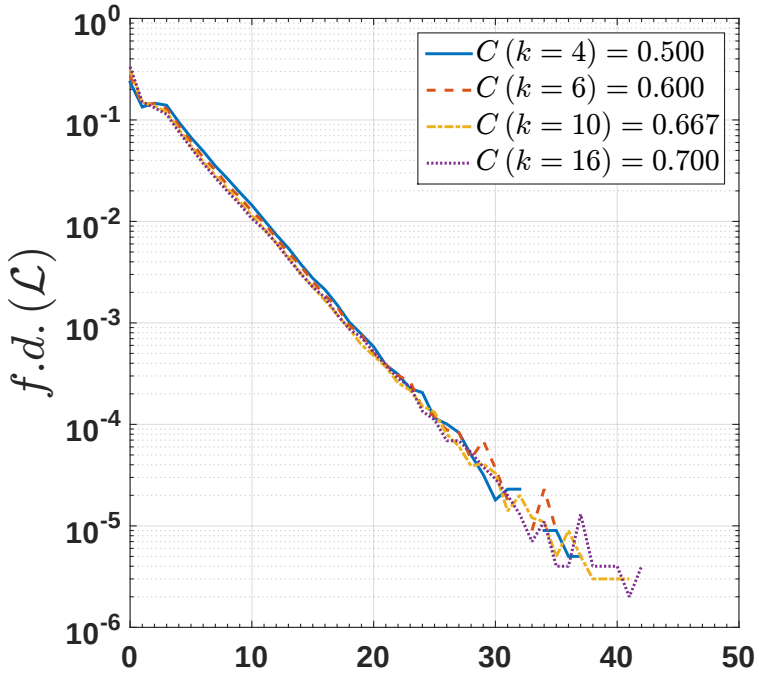
5.3 CIRCULAR LATTICE

The clustering in 1-dimensional circular lattice graph (CL) is dependent on its degree k, with the clustering coefficient defined as,

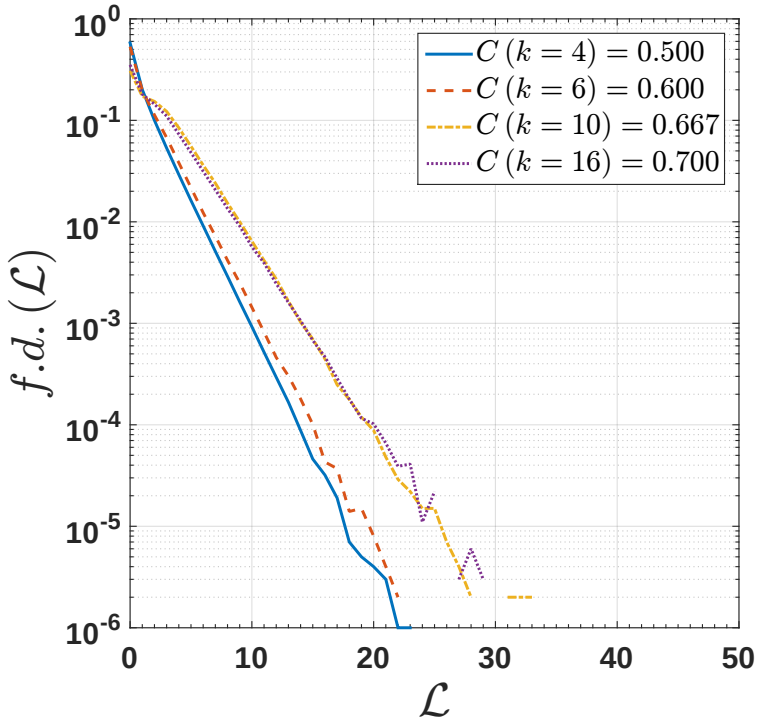
$$C(k) = \frac{3(k-2)}{4(k-1)}.$$

We studied the lifetimes of crowds on 7 circular lattices with a clustering coefficients $C(k=4) = 0.500$, $C(k=6) = 0.600$, $C(k=8) = 0.643$, $C(k=10) = 0.667$, $C(k=12) = 0.682$, $C(k=14) = 0.692$, and $C(k=16) = 0.700$, for more information see Section 2.3. The 1-d structure makes crowds weak to vertices behaving noisily, at low temperatures there should be less flipping of opinion and the reinforcement of opinions should become stronger.

Figure 53a shows the frequency density distribution of the crowd lifetimes $f.d.(\mathcal{L})$ for $\beta = 0.95$. At this temperature the lifetimes distributions for all the graphs are the same thus the processes which cause crowds to die are the same on all the graphs and occur with similar frequency. This means that crowd lifetimes at low temperatures are not dependent degree, clustering coefficient or graph size. This is similar to the results for the population frequency distributions in Section 4.3, where the $f.d.(\mathcal{P})$ was the same for all the graphs and limited only by the graph size. This suggests that at very low temperature crowd dynamics are the



(a) $\beta = 0.95$



(b) $\beta = 0.250$

Figure 53.: Frequency density distribution of the crowd lifetimes for 4 CL graphs with different clustering coefficients. Data has been plotted as a line to aid wit

Surprisingly the longest lifetime is approximately $\mathcal{L}^{\max} \approx 42$ which is very short compared to the 2000 time step interval being analysed. Clustering pro-

vides some reinforcement of opinions but it is insufficient to overcome noisy behaviour.

The inverse temperature in figure 53b is $\beta = 0.250$, we observe that the crowd lifetimes frequency distributions have narrowed for all the graphs and that the maximum observed lifetimes have decreased as well.

The distributions for the $k = 4$ and $k = 6$ graphs have narrowed the most and the maximum lifetimes for these graphs is $\mathcal{L}^{\max} \approx 22$. The majority of crowds on these graphs live for very short lifetimes and very few live as long as 22 time steps. The distributions for the $k = 10$ and $k = 16$ circular lattices has also narrowed but $\mathcal{L}^{\max} \approx 29$ is a little larger, so crowds in general live slightly longer on these graphs.

The difference in behaviour between the lower and higher clustering coefficient graphs indicates that crowd lifetimes is dependent on clustering at high temperatures $\beta \ll 1$.

At very high temperatures $\beta = 0.05$, figure 54, the lifetimes of crowds on the $k = 10$ and $k = 16$ graphs are found to be shorter than on the $k = 4$ and $k = 6$ graphs. As vertices are flipping opinions independently of their neighbours we can say that this is a consequence of the graph structure. Recall that for a crowd of size $\mathcal{P}_t$ can only lose a maximum of half its vertices $\mathcal{P}_{t+1} > \mathcal{P}_t/2$ or at most double in size, $\mathcal{P}_{t+1} < 2\mathcal{P}_t$, them during a single time step. At very high temperatures the a crowd can expect to lose half its vertices every during time step, or should expect half its neighbours to flip and join it. On graph with large degrees the connectivity allow for the formation of long chain like

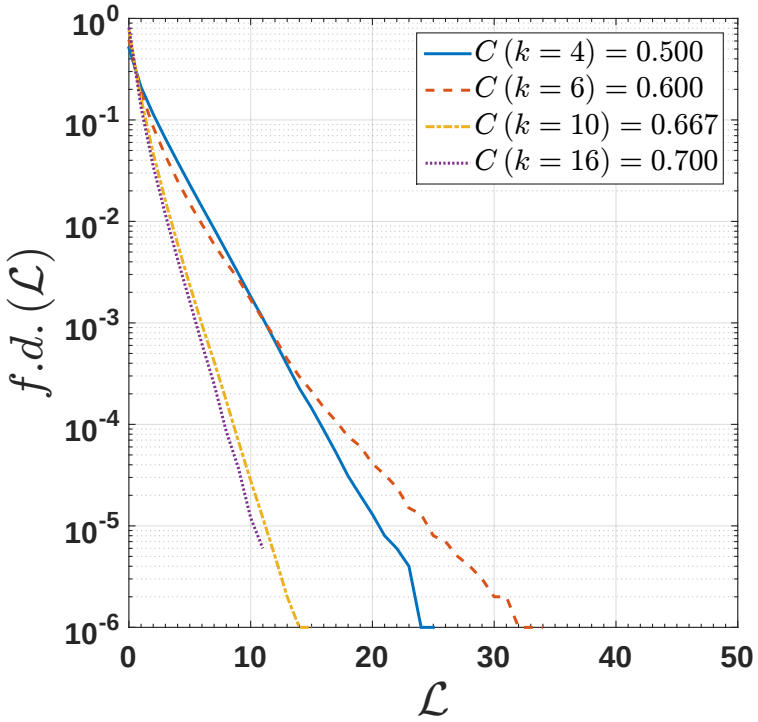


Figure 54.: The crowd lifetime frequency density distributions for $\beta = 0.05$. Results for several 1-d circular lattice graphs with different clustering coefficients are plotted together.

crowds, these crowds die due to vertices leaving but also kill smaller crowds when they merge. This results in all crowds having shorter lifetimes even if they are very large. On the low degree circular lattices crowds tend to be small as different crowds with the same opinion are unable to connect with each other, such crowds die more often by vertices leaving then due to merges with other crowds. Thus crowds have longer lifetimes at higher temperatures on these CL graphs with low degree.

The form of the crowd lifetimes frequency distribution was an exponential decay at all inverse temperatures. We used linear regression to fit $f.d.\,(\mathcal{L}) = \psi e^{-\theta_{\mathcal{L}}\mathcal{L}}$ to the distributions to obtain the exponent θ. In figure 55a we plot $\theta_{\mathcal{L}}$ as a function of β. Inspection of the plot tells us that the rate at which the

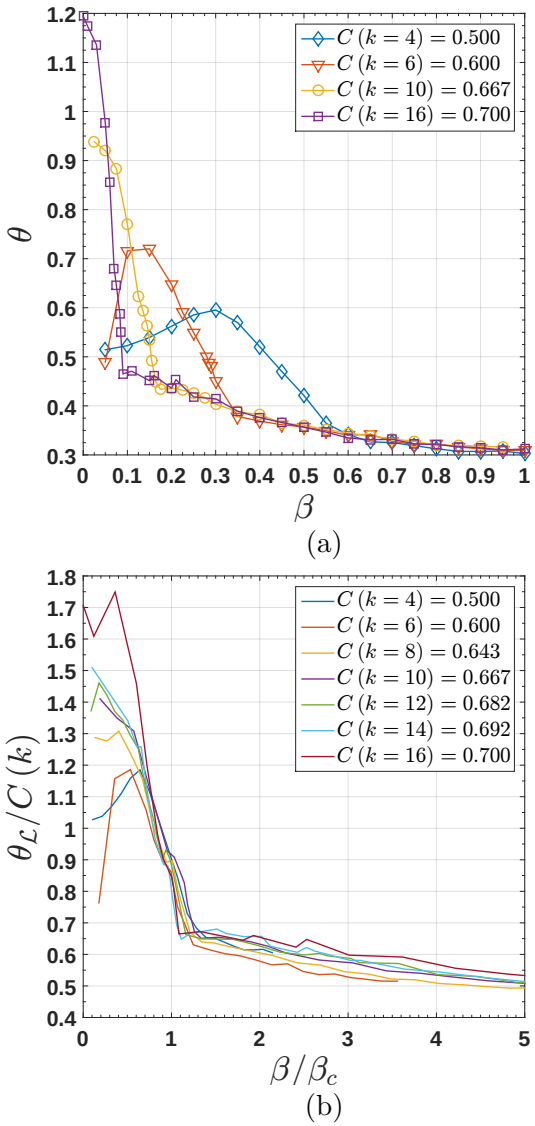


Figure 55.: The crowd lifetime frequency densities were fitted with the function $f.d.(\mathcal{L}) = \psi e^{-\theta_{\mathcal{L}}\mathcal{L}}$. The exponent of the fit $\theta_{\mathcal{L}}$ is plotted as a function of the inverse temperature β (top). A data collapse is performed by scaling the exponent and the inverse temperature by dividing them by the clustering coefficients $C(k)$ and critical inverse temperature β_c respectively (bottom).

lifetime distributions decay decreases as the temperature is lowered, i.e. longer lifetimes occur more frequently as noisy behaviour decreases.

Interestingly for the $k = 4$ and $k = 6$ graphs have exponents which are low at high temperatures ($\theta_{\mathcal{L}} \approx 0.5$), then increase as the temperature decreases reach a peak and then decrease with the temperature. This suggests that there

is a temperature β_1 unique to each graph for which longer lifetimes become significantly more improbable.

The exponents for the $k = 10$ and $k = 16$ graphs also respond similarly to changes in temperature. We perform a data collapse by scaling the inverse temperature by the critical inverse temperature β_c and the exponents by the clustering coefficients $C(k)$. Figure 55b shows the results of the data collapse for the exponents for all the graphs investigated. The fact that data collapse uses factors which are dependent only on properties of the graph and not crowds indicates that crowd lifetimes were independent of crowd-crowd interactions.

At very high temperatures $\beta/\beta_c \lesssim 0.75$ the scaling breaks down this suggest that crowd lifetimes are independent of the clustering coefficients of the graphs. $m_1 = -0.6 \pm 0.17$ and $m_2 = -0.03 \pm 0.02$ are the gradients in the intervals in the interval $0.75 \lesssim \beta \lesssim 1.1$ and $\beta/\beta_c \gtrsim 1.1$. As $|m_1| \gg |m_2|$ we can say that the crowd lifetimes are highly sensitive to noise for $\beta/\beta_c \in [0.75, 1.1]$ and far less sensitive to noise for $\beta \in [1.1, \infty]$.

In summary crowds at very high temperatures the crowds are created by chance, a larger degree makes big crowds possible but also make it easier for crowds to change by large amounts. Large changes kill crowds and create new ones. At lower temperatures still above the critical value crowd lifetimes are extremely sensitive to the temperature, as $\beta \to \beta_c$ longer lived crowds occur more frequently. Once $\beta \gtrsim \beta_c$ crowd lifetimes are less sensitive to the temperature. At low temperatures $\beta \to 1$ there is a maximum lifetime $\mathcal{L}^{\max} \approx$

42, the amount of clustering in a graph no longer has any affect on preventing a crowd from dying.

5.4 ERDŐS-RÉNYI GRAPHS

The vertices in an Erdős-Rényi (ER) graph are connected to a random selection of other vertices. This means the number of cycles and clustering is dependent entirely on the wiring probability p_w. We analysed the lifetimes of crowds on 6 ER graphs with $p_w = 0.0041$, 0.0057, 0.0074, 0.0089, 0.0109, and 0.0160, chosen such that the structural features in the graphs are independent of the number of vertices and the results should be true for all ER graphs in general, see Section 1.1.6 and 2.3 for more information.

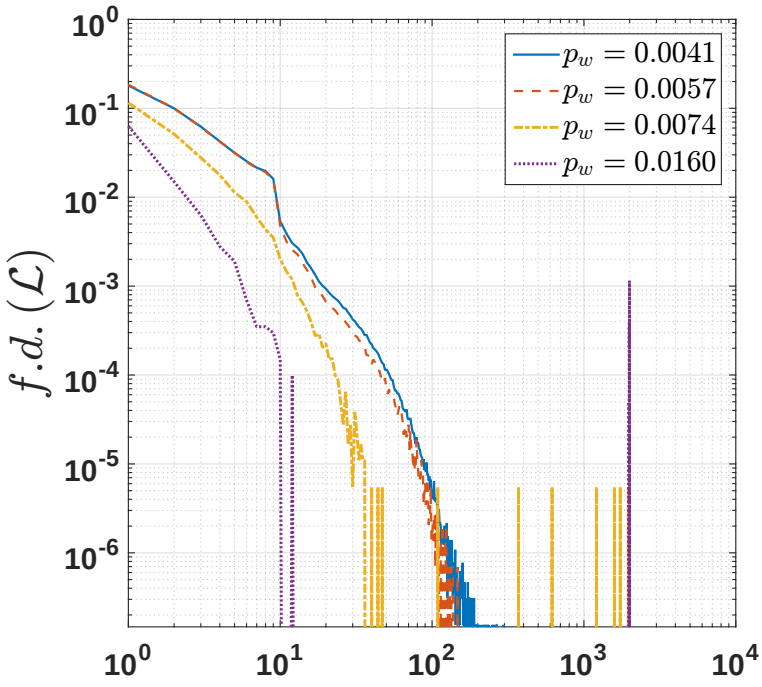
Erdős-Rényi graphs with low wiring probability have few neighbours and very little clustering, this means there is little reinforcement of opinions between neighbouring vertices thus their opinions are independent of one another. Crowd lifetimes on ER graphs with small $p_w \ll 1$ will be independent of crowd dynamics. On ER graphs with large $0 \ll p_w < 1$ vertices are connected and the opinion reinforcement will very strong consequently it is very likely for a global consensus to form. This means that there will be very few mesoscopic crowds on highly connected ER graphs.

Each of the distributions presented in this section consist of two parts. Crowds with very short lifetimes $\mathcal{L} \lesssim 10$ are considered to be created by noisy behaviour as they are quickly destroyed. The second part of the distribution are the crowds

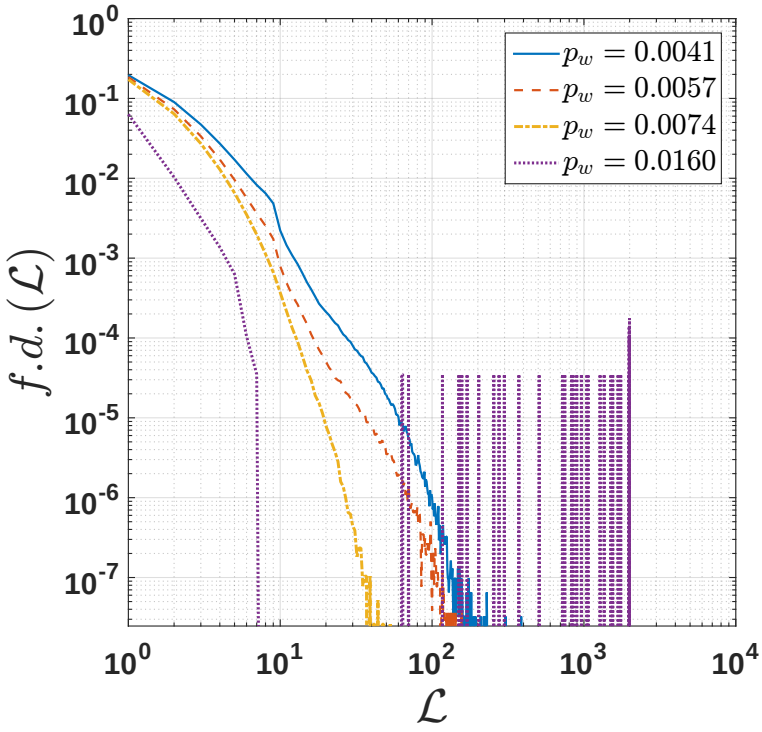
with lifetimes $\mathcal{L} \gtrsim 10$, these are robust enough to not be destroyed quickly and thus can be considered real crowds.

Figure 56a shows the crowd lifetime distributions for several ER graphs at low temperature ($\beta = 1.00$). There is a sharp change in frequency at $\mathcal{L} \approx 10$ for the $p_w = 0.0041$ and 0.0057 distribution. Comparing form with the distributions in the high temperature case (figure 56b) shows that more of the crowds created by noise are living up to 10 time steps. The low temperature coupled with the weak connectivity make it unlikely for noisy vertices to be influenced by neighbours, consequently vertices in crowds created by noise are less likely to be reverted by neighbours and thus killed quickly thus they live slightly longer.

Crowd lifetime frequency distribution at temperatures near the critical value are shown in figure 56b. The primary thing to note is that the lifetimes of all crowds on all the graphs has been affected by the increase in noisy behaviour of the vertices. The distributions for $p_w = 0.0041$, 0.0057, and 0.0074 have become narrower and the distributions for the $p_w = 0.0041$ and 0.0074 are no longer similar. The distribution of lifetimes are actually narrower for graphs with greater wiring probability. This seems counter to what one would expect to occur. However consider that a crowd dies when if it loses more than 50% of its vertices or it merges with a larger crowd. On a graph with a higher wiring probability when vertices that neighbour a crowd flip it is more likely to connect two or more crowds together causing them to merge. Mergers between crowds generally kill the smaller crowd. Furthermore the expected amount of vertices in a crowd of size $\mathcal{P}$ to change opinion during any time step is $\mathcal{P}/2$,



(a) $\beta = 1.00$



(b) $\beta = 0.000$

Figure 56.: Crowd lifetime frequency distributions, $f.d.\,(\mathcal{L})$, for low temperature (top) and at a high temperature near the critical value (bottom), The results are an Monte Carlo averages for several Erdős-Rényi graphs with different wiring probabilites p_w.

which also kills the crowd. On graphs with lower wiring probabilities mergers are extremely unlikely to occur thus crowds only die when half or more their vertices change opinion. Thus crowds on graphs with larger wiring probabilities have two processes which kill them which means in general it is less likely they will have long lifetimes.

The exception to the scenario is that if a graph is very highly connected like the $p_w = 0.0160$ ER graph. The only crowds on this graph are the crowds that are created by noisy vertices and the global consensus crowd (all vertices are part of the crowd). Vertices in crowds created by noise are quickly converted by the global consensus crowd and thus only live for very short periods of time. On the other hand the global consensus crowd is robust enough that it can live for the entire 2000 time steps we analyse, this exhibits as a Kronecker delta peak at $\mathcal{L} \approx 2000$. However there is sufficient noise that during some realisations the global consensus crowd is broken apart by noise for short periods of time, the pieces swiftly merge forming a new global consensus crowd which can have very long lifetimes. The breaking of the global consensus crowd causes the noisiness in the $p_w = 0.0160$ lifetime frequency distribution for $60 < \mathcal{L} \lesssim 2000$.

The high temperature ($\beta = 0.00$) results are given in figure 56b, vertices change opinions with a 50% probability. Thus crowd lifetime is independent of crowd-crowd interactions. The distributions have separated further based on the wiring probability. The crowd lifetimes on the $p_w = 0.0160$ are a result of the same processes as on the other more weakly connected graphs. The reason for crowds having narrower distributions is the same as stated for the $\beta = 0.200$

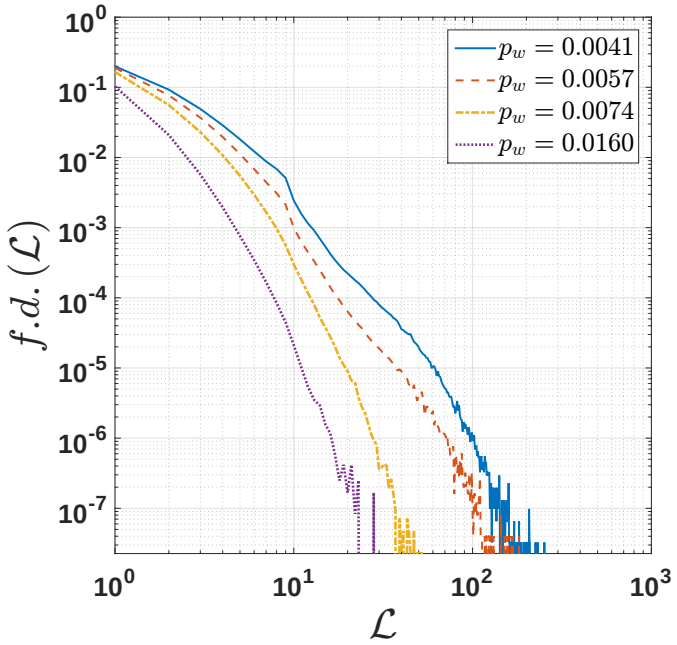


Figure 57.: Crowd lifetime frequency density distribution for the high temperature limit ($\beta = 0.00$). The distributions for 4 ER graphs have been plotted.

results earlier. At high temperatures crowds can be destroy by vertices leaving and by merging with other crowds. On graphs with greater wiring probabilities crowds have a much higher probability of merging thus crowds are more likely to die.

We fit the tails of the lifetime frequency distributions to an exponential decay function $f.d.(\mathcal{L}) = \psi e^{-\theta_{\mathcal{L}}\mathcal{L}}$. The Kronecker delta peaks in the distributions have been ignored. Figure 58 plots the exponential exponent θ as a function of the inverse temperature β.

There is a clear separation in the exponents for ER graphs with wiring probabilities $p_w \lesssim 0.0057$ and for $p_w \gtrsim 0.0074$. The formation of the global consensus completely changes the dynamics of the crowds as most of them are formed by noise and quickly reverted by the global consensus. As the temperature de-

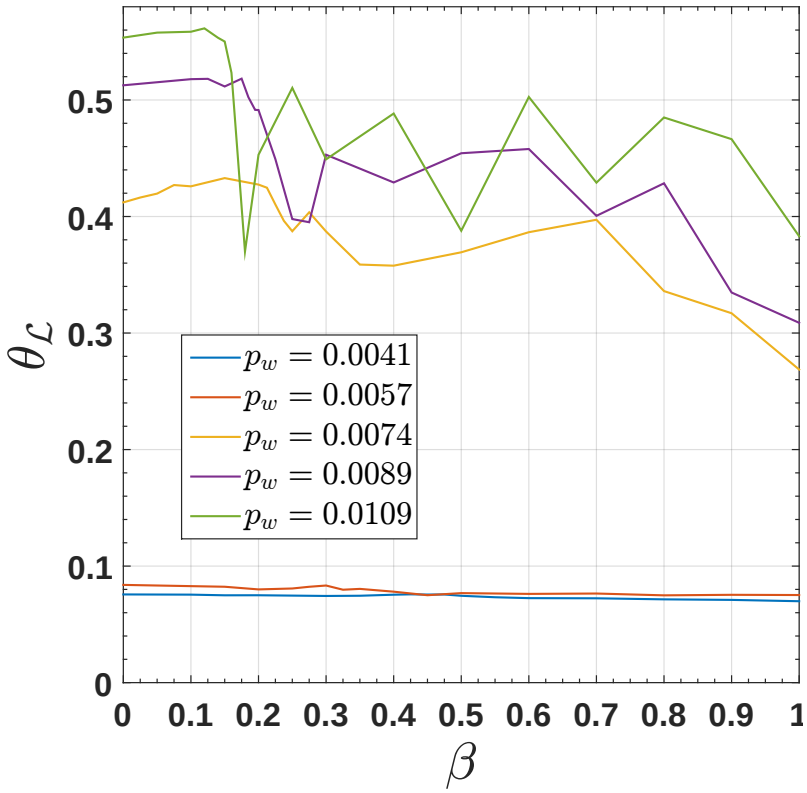


Figure 58.: The figure shows the exponent of the exponential fit to the tails of the lifetime frequency distributions.

creases the noise parts of the distributions widen as the lower temperature makes it harder for the global consensus crowd to revert their opinions.

On the $p_w \lesssim 0.0057$ no global consensus forms and the weak connectivity means that crowds behave independently at all temperatures thus the exponent θ barely change for these distributions as the temperature drops.

5.5 WATTS-STROGATZ GRAPHS

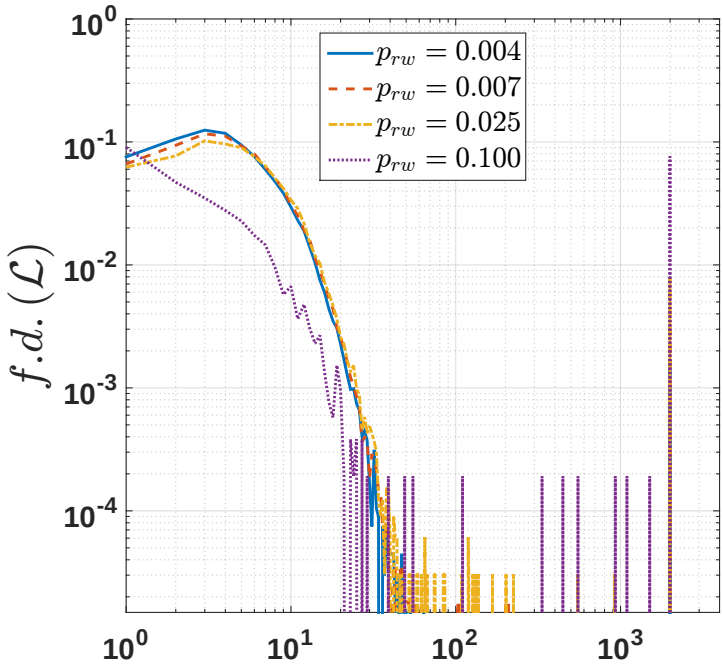
Watts-Strogatz graphs are circular lattices with a small number of edges rewired at random. This causes the graph to separate into communities. The small-world links allow regions that would be far apart on the CL to interact with

each other - at low temperatures this means that a global consensus can form, thus there are no crowds. On the CL crowds were easily broken up by noisy behaviour as there were only a small number of paths connecting different regions of the graph, on the WS small-world links can provide alternate paths which by pass noisy vertices. This means that crowds are not as easy to break up by a small number of noisy vertices.

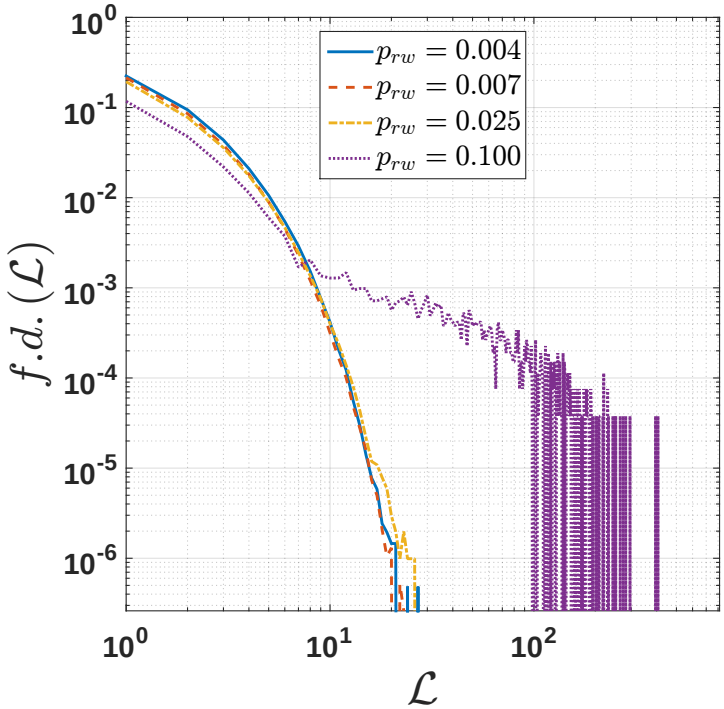
We see at $\beta = 1$ in figure 59a that most crowds live for lifetimes between 1 and 10 time steps, this indicates the majority of crowds are created by noise and are quickly converted back by the global consensus. Between $10 \leq \mathcal{L} \leq 100$ are the crowds which break away from the global consensus but are robust enough to resist being converted back by the global consensus, these occur far less frequently than crowds created by noise.

Very long lived crowds occur more frequently on the $p_w = 0.100$ graph. It consists of lots of small communities (between 30 to 50 vertices), the weak links between communities protect crowds within them from being converted back by the global consensus. At $\mathcal{L} = 2000$ the large Kronecker delta spike in the distribution indicates that the global consensus frequently lives for the entire time period analysed.

The distribution of the $p_w = 0.100$ in the interval $1 \leq \mathcal{L} \leq 10$ is less than that for the other graphs. These are the lifetimes of crowds which form due to vertices flipping opinion at random, their neighbours influence them to flip back.



(a) $\beta = 1.00$



(b) $\beta = 0.25$

Figure 59.: The frequency density of the crowd lifetimes for several Watts-Strogatz graphs with different rewiring probabilities. The top figure are the low temperature results $\beta = 1.00$ and the bottom figure is for a high temperature $\beta = 0.25$ which near to the critical value.

The $p_{rw} = 0.004$, 0.007, and 0.025 WS graphs have similar frequency distributions for $\mathcal{L} \lesssim 100$. The communities in these graphs can be very large (100 to 300) with structure similar to the circular lattice. Consequently the frequency distribution for these lifetimes is similar to that of CL graphs. While it is difficult to distinguish on these plot the lifetime frequency distributions also have Kronecker delta spikes at $\mathcal{L} \approx 2000$. Thus many crowds live for the entire span of the of the analysed time period, not all of them are due to a global consensus.

At temperatures near β_c the crowd sizes change super-diffusively, see Section 3.5. Small-world links allow crowds in different communities to connect and merge which results in crowds growing by large amounts over short periods of time. However the small-world links are weak points and when the vertices connected by them flip opinion this breaks the crowd and kills it. Consequently we do not observe very long lifetimes for crowds on the $p_w = 0.004$, 0.007 and 0.025 graphs. Their frequency distributions are still very similar, this suggests that there are not enough differences in the graph structure to cause the crowd lifetimes to behave differently

The $\mathcal{L} \lesssim 10$ part of the frequency distribution for the $p_{rw} = 0.1$ graph's is now similar to the others. However its tail ($10 \lesssim \mathcal{L} \lesssim 100$) is significantly different. Crowd population dynamics on this graph is different than on the other WS graphs. The diffusion exponents obtained for this graph in Section 3.5 indicate the crowd population dynamics are a normal diffusion process while on the other graphs they are super-diffusive. The tail of the distribution has a very

fat tail, many crowds have lifetimes between 10 and 100 time steps. For $\gtrsim$100 the number of crowds that live that long are rare, consequently the distribution becomes noisy and shows up as lots of Kronecker delta spikes. The reason for the difference is in the structure of the graph, the smaller communities means that crowds are more robust against noise and crowd-crowd interactions. The small size of the communities means the crowd that form are also smaller, consequently when crowds merge or break apart the change in size less thus crowds live for longer.

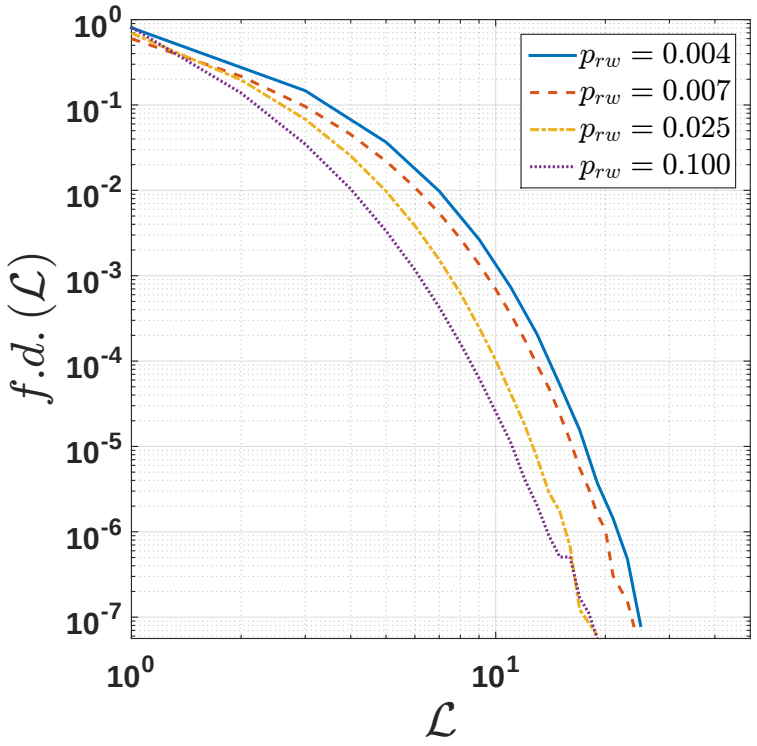
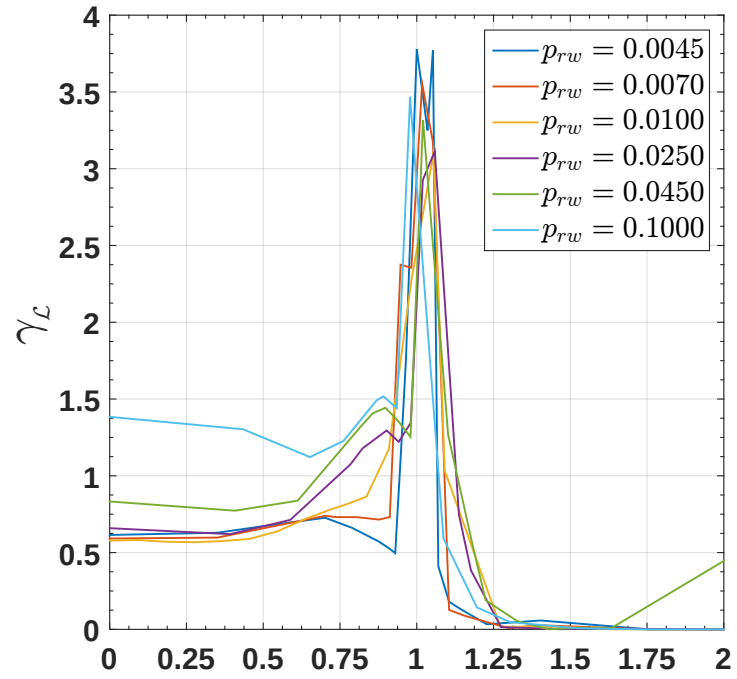
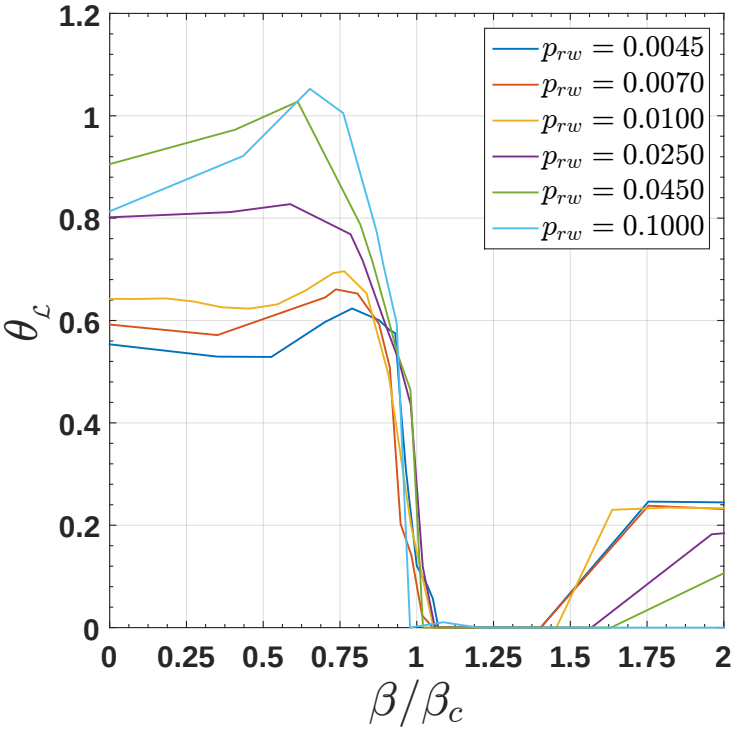


Figure 60.

At very high temperatures well above the critical temperatures the vertices choose one of the two opinions uniformly at random. Crowds forming are the results of chance as vertices do not reinforce each others opinions.



(a)



(b)

Figure 61.: The lifetime frequency distributions were fit with function $f.d.(\mathcal{L}) = \psi \mathcal{L}^{-\gamma_{\mathcal{L}}} e^{-\theta_{\mathcal{L}} \mathcal{L}}$, the exponent of the power law component $\gamma_{\mathcal{L}}$ is plotted in 61a and the exponent of the exponential decay component $\theta_{\mathcal{L}}$ in 61b.

We fit the function $f.d.(\mathcal{L}) = \psi \mathcal{L}^{-\gamma_\mathcal{L}} e^{-\theta_\mathcal{L} \mathcal{L}}$ to the tails of the lifetime frequency density distributions for all the Watts-Strogatz graphs we studied. The fit ignores the Kronecker Delta spike at $\mathcal{L} \approx 2000$. In figures 61a and 61b we plot the power law exponent $\gamma_\mathcal{L}$ and the exponential exponent $\theta_\mathcal{L}$ respectively as functions of β/β_c. The scaling of the inverse temperature is sufficient to collapse the power law exponent for $\beta/\beta_c \gtrsim 0.95$ and the exponential exponent for $\beta/\beta_c \gtrsim 0.85$.

For $\beta/\beta_c < 0.75$ (high temperatures) both the power law and exponential exponents are non-zero. As the temperature approached the critical value ($\beta/\beta_c \to 1$) the exponential exponent $\theta_\mathcal{L} \to 0$ and the power law exponent $\gamma_\mathcal{L} \to 3.5$. A transition from a mixture of exponential and power law to a pure power law has occurred in the temperature region where the crowd-crowd interactions dominate the crowd dynamics. However between $1 < \beta/\beta_c < 1.25$ the power law exponent rapidly decreases as the there is insufficient noisy behaviour to drive crowds to merge. $\gamma_\mathcal{L}$ then remains small for lower temperatures and the exponential exponent becomes non-zero for $\beta > 1.35$. The tail of the lifetime distribution has a strong exponential component when there is little crowd-crowd interactions but becomes a power-law when there are.

5.6 DISCUSSION AND SUMMARY

The tails of lifetimes f.d.s for crowds on the CL and ER graphs are exponential at all temperatures. If crowds are susceptible to being broken up by noise

with little crowd-crowd interactions the tails of the lifetime distributions decay exponentially. We also observe that at high temperatures the tails of the lifetime f.d.s are exponential, indicating that noisy behaviour determines crowd dynamics and thus lifetimes.

The tails of the f.d. on the RL transition from decaying exponentially to decaying as a power law as $\beta \to \beta_c$. A similar transition occurs for the WS graph f.d.. This suggests that crowd-crowd interactions are dominant and they lead to an increase in long lived crowds. On the RL the lifetime f.d. tail remains as a power law even after the crowd population dynamics becomes sub-diffusive. We know from previous analysis that crowds continue to interact with each other often in this regime. On the WS graph however the crowd population dynamics become non-diffusive and the tail of the distribution switches back to an exponential decay indicating that noise is once again the determining factor in the crowd lifetimes.

The exponents of the lifetime f.d. tails for the CL graphs were independent of the crowd-crowd interactions. By plotted $\theta_{\mathcal{L}}/C\left(k\right)$ as a function of β/β_c we showed that the lifetime f.d. on CL graphs was dependent on the critical temperature and the clustering coefficient of the graph for $\beta/\beta_c \gtrsim 0.75$. For $\beta/\beta_c \lesssim 0.75$ the lifetimes are no longer solely dependent on these factors.

The exponents of the ER graphs was divided into two groups, weakly connected graphs had much wider tails than those which were strongly connected.

The distribution for the WS graph consists of a short lifetime component which can be fitted by $f.d.\left(\mathcal{L}\right) = \psi\mathcal{L}^{-\gamma_{\mathcal{L}}}e^{-\theta_{\mathcal{L}}\mathcal{L}}$. By plotting the exponents $\theta_{\mathcal{L}}$

and $\gamma_{\mathcal{L}}$ as function of β/β_c we find that the transition from exponential decay to power law decay is independent of the rewiring probability and only depend on the critical temperature.

6

MAXIMUM POPULATIONS AND LIFETIMES

6.1 INTRODUCTION

This is a short chapter in which we discuss how the maximum crowd populations $\langle \mathcal{P}^{\max} \rangle_R$ and the maximum crowd lifetimes $\langle \mathcal{L}^{\max} \rangle_R$ as functions of the inverse temperature β, where the subscript R denotes the average is over the realisations. These results are of interest as the frequency distributions in Chapters 3 and 5 were strongly influenced by crowds created through noisy behaviour. $\langle \mathcal{P}^{\max} \rangle_R$ and $\langle \mathcal{L}^{\max} \rangle_R$ ignore the contributions due to noisy behaviour at high to low temperatures.

The maximum crowd population is not to be confused with magnetisation M given in Section 1.2.3, the former is a measure of the number of vertices in a cluster of magnetism and the latter is a measure of the number of vertices in the majority opinion state.

6.2 RECTANGULAR LATTICE

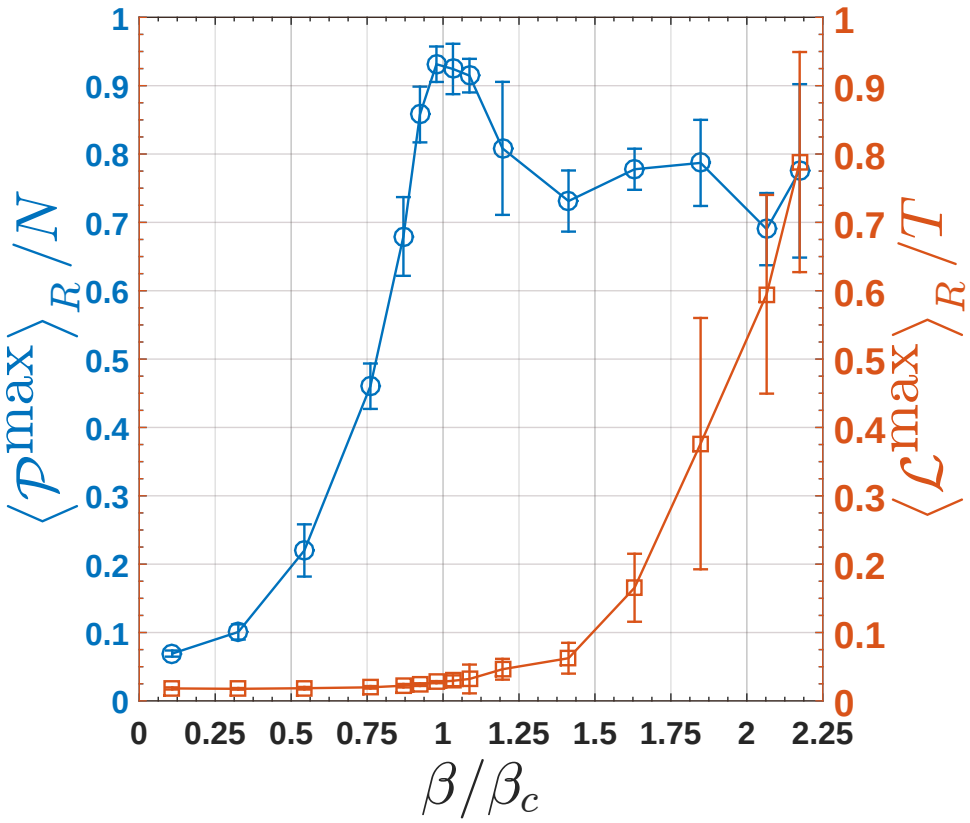


Figure 62.: The scaled average maximum crowd population $\langle \mathcal{P}^{\max} \rangle_R$ (blue circles) and the scaled average maximum crowd lifetime $\langle \mathcal{L}^{\max} \rangle_R$ (red squares) for the rectangular lattice plotted as functions of the scaled inverse temperature β/β_c. Error bars represent the standard deviation of the values used to calculate the averages.

Figure 62 shows the results for the rectangular lattice as a function of the scaled inverse temperature β/β_c. Both the values of the average maximum populations and lifetimes increase as the temperature decreases as do their standard deviations. At very low temperatures the crowds can become very large due to their increased robustness, as there are multiple large stable crowds same time which prevent each other from growing larger. Thus we do not see a global consensus forming and a $\langle \mathcal{P}^{\max} \rangle_R / N \approx 1$. Further the size of the

large crowds is dependent on their interactions with each other and results in a large range of sizes and larger standard deviation. Lifetimes are heavily dependent on interactions between crowds and thus on the conditions during a realisation this means that the $\mathcal{L}^{\max}$ is highly variable thus standard deviation of the lifetimes increases together with the mean.

Overall both $\langle \mathcal{P}^{\max} \rangle_R$ and $\langle \mathcal{L}^{\max} \rangle_R$ behave as we would expect. At high temperatures $\beta/\beta_c \to 0$ the noise prevents large crowds from forming and destroys them very quickly.

As $\beta/\beta_c \to 1$ the average maximum population increases to be on the order of the graph size $\mathcal{O}(N)$. The crowds are super-diffusive at these temperatures, growing very quickly over short periods of time, this is possible due to the crowds being sufficiently robust against noise that they can hold together long enough to merge frequently. However we see that is still $\langle \mathcal{L}^{\max} \rangle_R \ll 1$ all crowds at these temperatures are extremely unstable and easily broken up.

At low temperatures $\beta/\beta_c \gg 1$ both the average maximum population and lifetime are large, this is due to the noise being very low and crowds being very robust.

The results tell us that the rectangular lattice graph is conducive to the formation of large and stable crowds at low temperatures. While at temperatures near the critical value large crowds can form but they will not be stable.

6.3 CIRCULAR LATTICE

The circular lattice graph is of interest as clustering is an important part of its structure. To keep the average path length the same while altering the clustering coefficient we created circular lattices with degrees $k = 4$, 6, 8, 10, 12, 14, and 16 and graph sizes $N = 256$, 384, 512, 640, 768 896, and 1024 respectively. Thus the ratio of the degree and the graph size is the same on all the circular lattice graphs, $k/N = 0.0156$. In Figure 63a we have decided to scale $\langle \mathcal{P}^{\max} \rangle_R$ by N as it collapses the data and provides insight into how big crowds get compared to the graph size.

We found in Chapter 3 that the distribution of the population sizes was dependent only on the temperature and the degree of the graph. It is no surprise then that we find that the maximum crowd population is dependent on a N which is proportional to k.Figure 63a is the plot of $\langle \mathcal{P}^{\max} \rangle_R / N$ as a function of β/β_c. For very high temperatures ($\beta/\beta_c < 0.75$) the number of noisy vertices is large thus the maximum crowd sizes are independent of the graph structure. In the interval $0.75 \lesssim \beta/\beta_c \lesssim 1$ the scaled average maximum crowd size $\langle \mathcal{P}^{\max} \rangle_R / N$ is the same for the CL graphs with degree $k \leq 14$. As β/β_c approaches 1 the crowds have become more and more robust to noisy vertices this allows them to grow larger but are still susceptible enough to noise that it limits their maximum size. At $\beta/\beta_c = 1$ the average maximum size is close to N for all the graphs, crowds at this temperature are robust enough to prevent being broken apart by noise but weak enough to the Ising

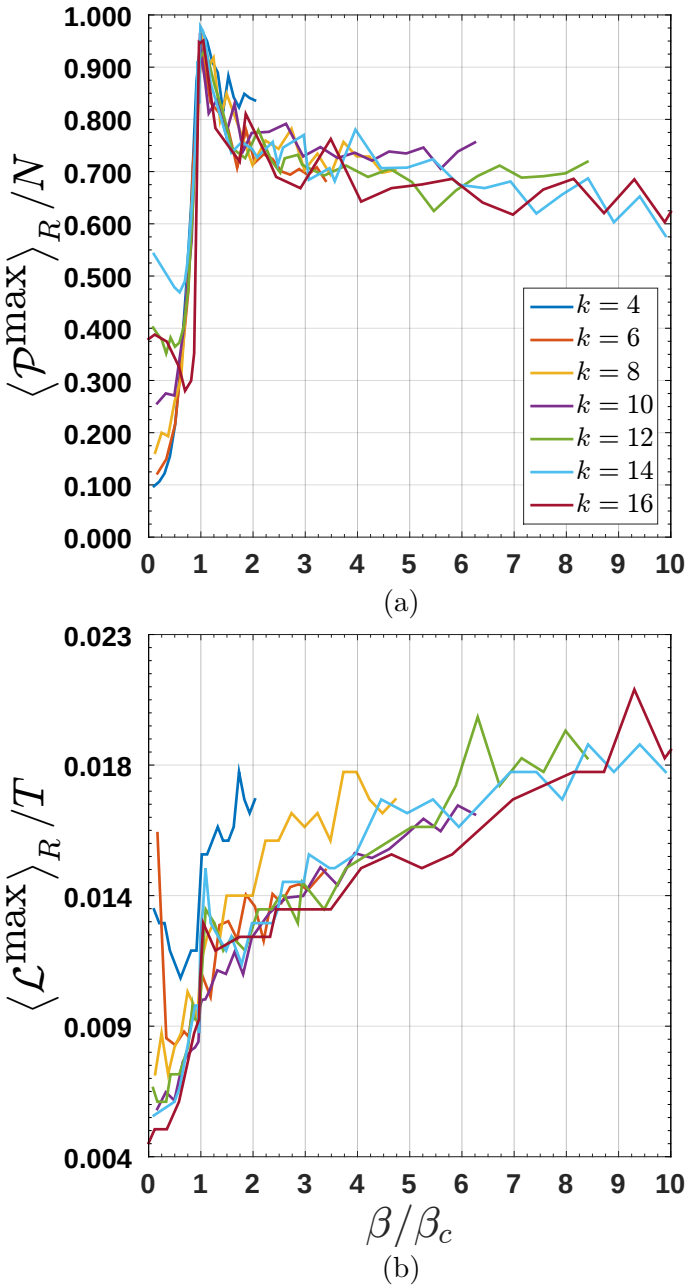


Figure 63.: The scaled average maximum crowd population $\langle \mathcal{P}^{\max} \rangle_R / N$ (top) and the scaled average maximum crowd lifetime $\langle \mathcal{L}^{\max} \rangle_R / T$ (bottom) as functions of the scaled inverse temperature β/β_c. These results are for the k-degrees circular lattice graphs with clustering coefficients $C(k = 4) = 0.500$, $C(k = 6) = 0.600$, $C(k = 8) = 0.643$, $C(k = 10) = 0.667$, $C(k = 12) = 0.681$, $C(k = 14) = 0.692$, and $C(k = 16) = 0.7$ and graph sizes $N = 256$, 384, 512, 640, 768 896, and 1024 respectively. The legend is appropriate for both plots.

dynamics that a majority of the vertices align and form a global consensus.

For $\beta/\beta_c > 1$ the average maximum size is still very large but less than when

$\beta/\beta_c = 1$. As crowds are more robust to noise and crowd-crowd interactions at low temperatures several large stable crowds ($0.25 \lesssim \mathcal{P}/N \lesssim 0.75$) can form, these prevent very large crowds $\mathcal{P}/N \gtrsim 0.75$ from growing larger which results in the smaller observed $\langle \mathcal{P}^{\max} \rangle_R$ at low temperatures.

The lifetime frequency distributions in Section 5.4 were dependent on the clustering coefficient however scaling only the inverse temperature β is sufficient to collapse the results for the graphs with degree $k > 4$. This suggests that while the lifetimes of crowds in general is controlled by the clustering coefficient the maximum lifetime is dependent only on the amount of noise. This is understandable as it is noisy behaviour which cause crowds to break apart on circular lattice graphs. The average maximum lifetime $\langle \mathcal{L}^{\max} \rangle_R$ has been normalised by diving by the size of the time period sampled, $T = 2000$. $\langle \mathcal{L}^{\max} \rangle_R \ll 1$ at all temperatures as crowds as crowds on the CL graph are not robust at all.

To summarise we have found that the maximum crowd size is dependent on the graph structure just like the crowd population frequency distribution. On the other hand the maximum lifetimes of the crowds depend only on the Ising models response to temperature on circular lattices. Having a greater degree or clustering coefficient does not make crowds more robust. It will however allow them to larger sizes.

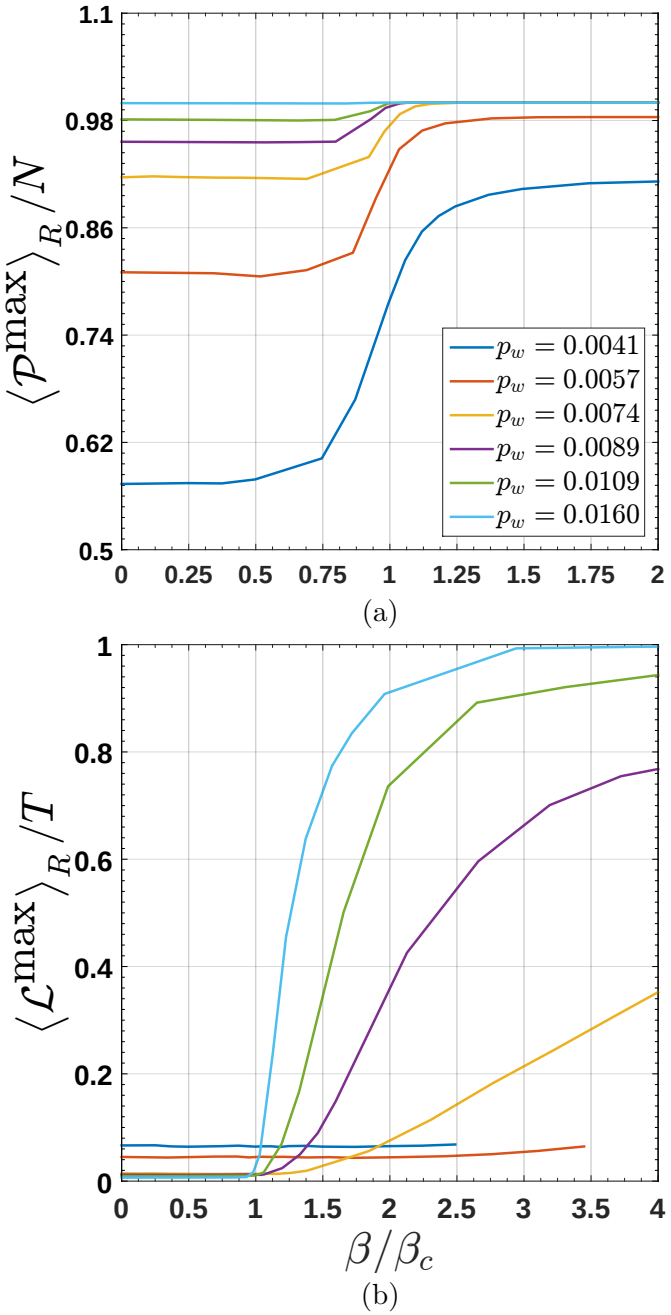


Figure 64.: The scaled average maximum crowd population $\langle \mathcal{P}^{\max} \rangle_R / N$ (top) and the scaled average maximum crowd lifetime $\langle \mathcal{L}^{\max} \rangle_R / T$ (bottom) as functions of the scaled inverse temperature β / β_c. These results are for Erdős-Rényi graphs with $N = 640$ vertices and different wiring probabilities p_w. The legend is appropriate for both plots.

6.4 ERDŐS-RÉNYI GRAPHS

The structure of Erdős-Rényi graphs does not lend itself to supporting meso-

scopic crowds, either crowds are very small ($\mathcal{P} < 10$) or they have sizes which

are on the order of the graph size $N = 640$. The wiring probability p_w controls the number of edges in the graph and thus the sensitivity of crowds to noisy behaviour. The values of the wiring probability were chosen using the formula $p_w = N^{-z}$, where z is the size invariant wiring parameter, this ensured that the structural features of the graphs will be independent of the graph size N, see Section 2.3.

In figure 64a we plot the average maximum crowd size normalised to the size of the graph $\langle \mathcal{P}^{\max} \rangle_R / N$ as a function of the inverse temperature β scaled by its critical value β_c. In Section 4.4 the exponent $\gamma_{\mathcal{P}}$ of the power law fit of the population frequency distribution for some graphs could be collapsed by scaling scaling the results by z. This suggested that for $p_w = 0.0074$, $p_w = 0.0089$, 0.0109 changes in the local structural features affected crowd sizes in a predictable manner. However attempting to collapse the $\langle \mathcal{P}^{\max} \rangle_R$ data using the average path length $\bar{l} \approx= \ln(N) / \ln(p_w N)$, the size invariant wiring parameter z and the wiring probability p_w were unsuccessful. As the maximum crowd sizes increase with the wiring probability we know that this is an important factor, the inability to collapse the data suggests that there are factors not associated with graph structure at play.

On graphs with low wiring probabilities ($p_w = 0.0041$ and 0.0057) the average maximum crowd size is smaller at all temperatures. For $\beta/\beta_c \ll 1$ the average maximum crowd size is $\mathcal{O}(N/2)$ and increases to $\mathcal{O}(N)$ for $\beta > 0.75$. Crowd sizes are very sensitive to noise on weakly connected ER graphs. The more

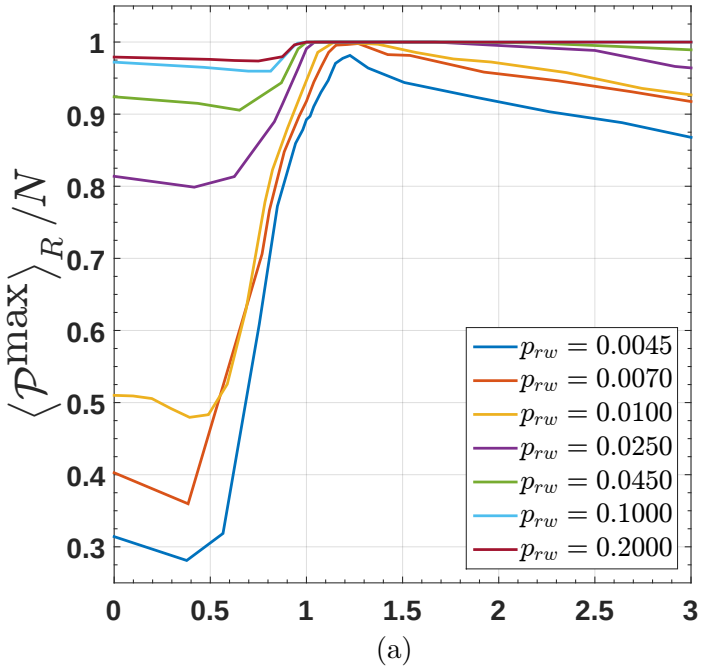
connected a graph is the less sensitive crowd size is to noisy behaviour of its vertices.

The normalised average maximum lifetimes $\langle \mathcal{L}^{\max} \rangle_R / T$ plotted as a function of β/β_c in figure 64b. On all the graph the average maximum lifetime is ≈ 0 for temperatures below the critical value $\beta/\beta_c \leq 1$. Above β_c the average maximum lifetimes of the $p_w \geq 0.0074$ show an increase. Greater increases are observe on graphs with larger wiring probabilities, indicating that crowds on ER graphs with lots of edges are more stable.

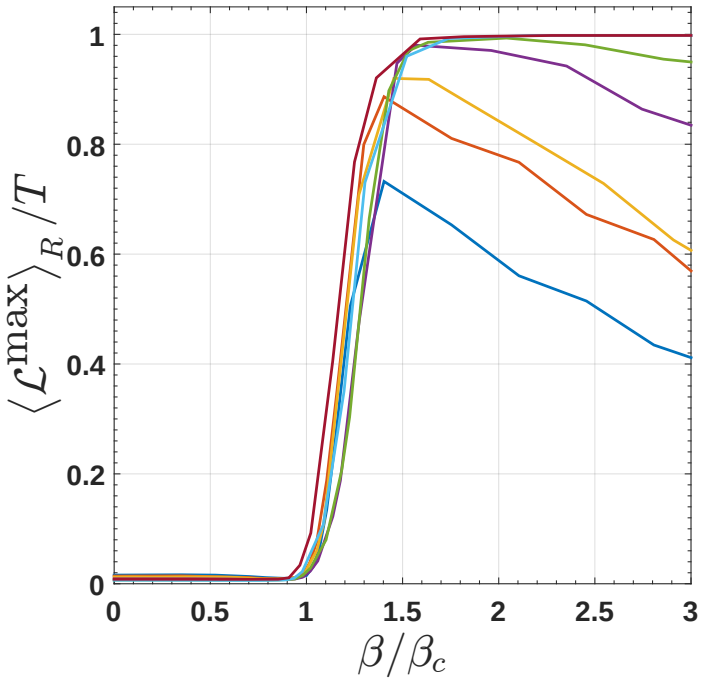
The average maximum lifetimes of crowds on the $p_w = 0.0041$ and 0.0057 graphs do not increase as the temperature decreases below the critical value. The lack of edges in these graphs make crowd extremely susceptible to being broken apart at all temperatures, even small amounts of noise will destroy crowds.

6.5 WATTS-STROGATZ GRAPHS

The Watts-Strogatz graph is a circular lattice which has had edges rewired at random, this creates small-world and communities (see Section 1.1.7). Vertices within the same community have greater influence on each other than vertices without. This means the opinions of crowds that form within a community will be reinforced strongly and be resistant to the influence of crowds in another community leading to larger sizes and longer lifetimes. The small-world links help connect distant parts of the graph; the greater the rewiring probability



(a)



(b)

Figure 65.: The average maximum crowd population $\langle \mathcal{P}^{\max} \rangle_R$ (top) and the average maximum crowd lifetime $\langle \mathcal{L}^{\max} \rangle_R$ (bottom) as functions of the inverse temperature β which have been scaled by the graph size $N = 640$, the time period $T = 2000$, and critical inverse temperature β_c. These results are for Watts-Strogatz graphs each with the same degree $k = 6$ and different rewiring probabilities p_{rw}. The legend given in (a) is appropriate for both plots.

the more small-world links are created in a graph. Thus crowds on graphs with lots of small-world links are able to have global influence as opposed to only local influence, which similar to what occurs in highly connected Erdős-Rényi graphs.

Figure 65a shows the average maximum crowd size $\langle \mathcal{P}^{\max} \rangle_R$ as a function of the inverse temperature β which have been scaled by the graph size N and the critical inverse temperature β_c to normalise them.

We find that for high temperatures, $\beta/\beta_c < 1$, that the average maximum crowd size behaves differently on graphs with different wiring probabilities. $\langle \mathcal{P}^{\max} \rangle_R = \mathcal{O}(N/2)$ for graphs with few small-world links ($p_{rw} \leq 0.01$) and $\langle \mathcal{P}^{\max} \rangle_R = \mathcal{O}(N)$ for graphs with lots of small-world links.

Near the critical inverse temperature, $\beta/\beta_c \to 1$, the average maximum crowd size is $\mathcal{O}(N)$ for all graphs regardless of small-world links. This is also the region of temperature for which we observe super-diffusive crowd dynamics (see Chapter 3).

As the temperature lowers further $\beta/\beta_c >> 1$ the average maximum size begins to decrease for graphs with low rewiring probabilities. As few edges have been rewired on these graphs their communities tend to be large thus their structure is very similar to the circular lattice. Crowds on such graphs are extremely robust to crowd-crowd interactions and thus tend to prevent each other from growing larger. On the graphs with lots of small-world links the entire graph is able to come to a global consensus consequently and is not a result of crowd dynamics.

The average maximum crowd lifetime $\langle \mathcal{L}^{\max} \rangle_R$ results are present in figure 65b. For $\beta/\beta_c < 1$ the average crowd lifetime is approximately 0. However for $1 \leq \beta/\beta_c < 1.5$ the average maximum lifetimes for crowds on all graphs become very long, the super-diffusive behaviour of the crowds allow them to become very big and the small-world links allow them to remain connected even though there is a lot of noisy vertices and crowd-crowd interactions occurring. For very low temperatures $\beta/\beta_c > 1.5$ the average maxim lifetime of crowds begins to decrease significantly for graphs with few small world links $p_{rw} \leq 0.01$. As large crowds form at lower temperatures they must span over multiple communities, vertices which have small-world link are weak points. If a vertex with small-world link(s) flips this can shatter a crowd resulting in its death. On graphs with lots of small-world links a crowd will have multiple paths connecting different regions thus even if one or two vertices small-world links flip opinion it does not shatter them. The difference in lifetime behaviour at low and high temperatures indicates that the differences in graph structure do not come into play until $\beta/\beta_c \gtrsim 1.3$.

7

CORRELATIONS

7.1 INTRODUCTION

In this chapter we explore whether a crowd's population size is correlated with its lifetime. We check for correlations between initial population size $\mathcal{P}^0$ and total lifetime $\mathcal{L}$ as well as between a crowd's current population $\mathcal{P}^t$ and remaining lifetime $\Delta\mathcal{L} = \mathcal{L} - t$. We use the Kendall's rank correlation coefficient, tau-B (τ_B) [59], as it makes no assumption on the underlying distribution of the variables and is less affected by anomalous data points.

We only analyse the data for crowds with initial sizes $\mathcal{P}^0 \in \left(\frac{1}{4}\mathcal{P}^{\max}, \frac{3}{4}\mathcal{P}^{\max}\right)$ and total lifetimes $\mathcal{L} > 10$, where $\mathcal{P}^{\max}$ is the largest crowd size in the data set. This removes crowds created by noise and very large crowds both of which have different behaviours than normal crowds.

7.2 INITIAL CROWD POPULATION SIZE AND LIFETIME

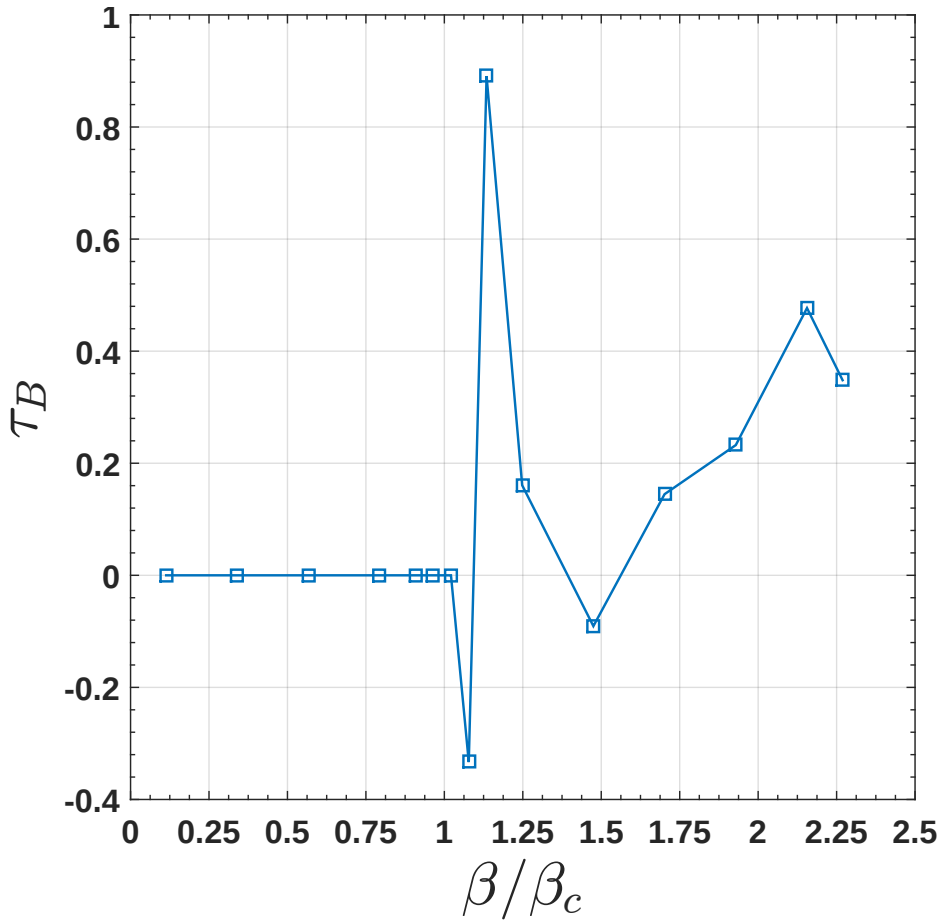


Figure 66.: The Kendall rank correlation coefficient plotted as a function of the scaled inverse temperature β/β_c for the initial population sizes $\mathcal{P}^0$ and total lifetimes $\mathcal{L}$ of crowds on the rectangular lattice.

Figure 66 shows the correlation coefficients for the initial population sizes $\mathcal{P}^0$ and total lifetimes $\mathcal{L}$ of crowds on the rectangular lattice. At high temperatures $\beta/\beta_c < 1$ the initial size of a crowd is uncorrelated with the lifetime. The lifetime of a crowd is independent of internal and external crowd dynamics.

Just below and near to the critical temperature ($\beta/\beta_c \approx 1.1$) there is moderately negative correlation. This indicates that crowds that are born large have shorter lives than those that are initially small.

At $\beta/\beta_c \approx 1.125$ the correlation suddenly become strongly positive. Crowds that start off large live longer lives than those that start of small. Between $1.125 < \beta/\beta_c < 1.5$ the correlation coefficient decreases rapidly till it is slightly negative. Then as the temperature lowers further, $\beta/\beta_c \to \infty$, it increases till it is moderately positive.

When the crowd population dynamics are super-diffusive the correlation between initial size and lifetime are extremely sensitive to the temperature. The sudden change occurs as small and large crowds are effected by differently be the temperature. Near the critical value noisy behaviour is frequent, this breaks up large crowds into smaller ones. Some of the smaller ones will be killed by noise but a few go on to merge and grow large before dying. However as the temperature drops the large crowds are less affected by noise and do not break up as quickly allowing them to absorb smaller neighbours. This simultaneously decreases the lifetime of small crowds and increases the lifetime of large ones. However as the temperature decreases even further the small crowds become more robust as well and the large ones lose their advantage.

The population dynamics then switches to super-diffusive, at these temperatures noisy behaviour is infrequent and so crowds are very stable. Small crowds occur at boundaries between larger crowds or are created by noise within a crowd. Consequently small crowds are either absorbed by their larger neighbours, albeit slowly, or reverted. Large crowds mainly gain and lose vertices with their similarly sized neighbours, changing very slowly thus leading to long lifetimes.

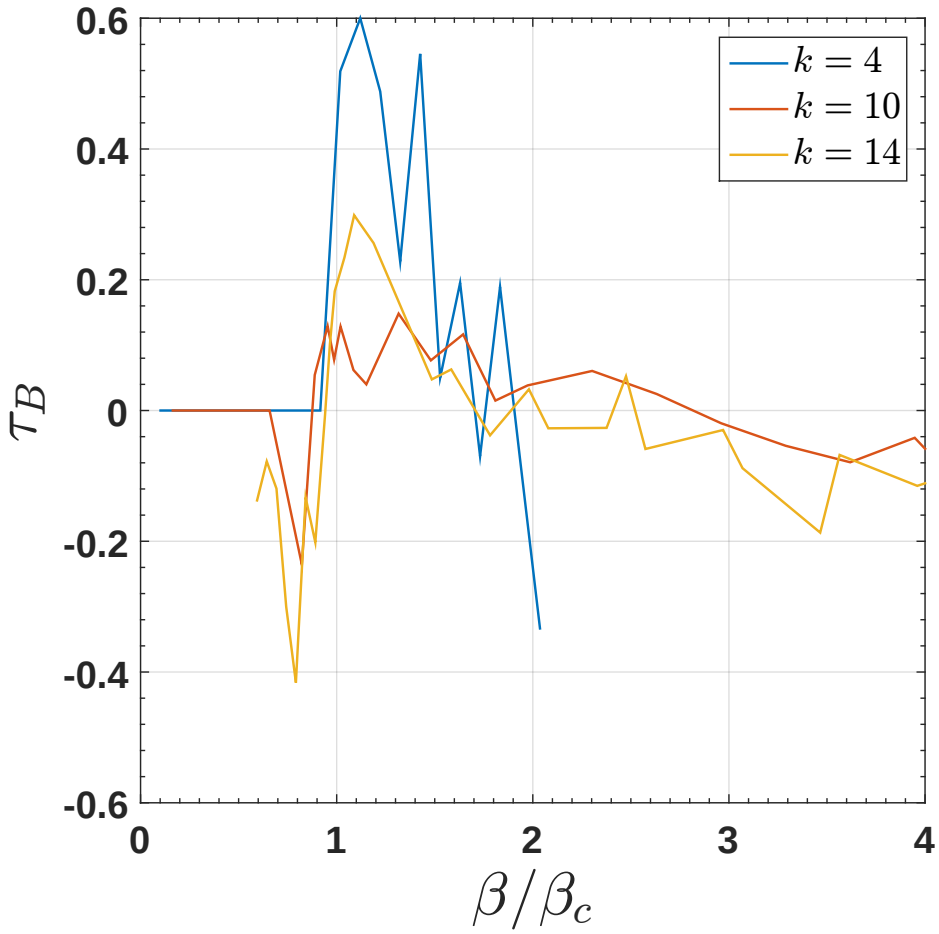


Figure 67.: The Kendall rank correlation coefficient plotted as a function of the scaled inverse temperature β/β_c for the initial population sizes $\mathcal{P}^0$ and total lifetimes $\mathcal{L}$ of crowds on the circular lattice with degrees $k = 4$, 10 and 14.

We present the correlation results of the circular lattice graphs in figure 67. Only the results for $k = 4$, $k = 10$ and $k = 14$ have been given as otherwise the results were too noisy to distinguish features.

At high temperatures $\beta/\beta_c < 1$ the initial size is uncorrelated for the $k = 4$ graph and correlates negatively for the $k = 10$ and 14 graphs. Large crowds on circular lattices tend to be long and thin, thus when vertices flip the crowd breaks apart into lots of smaller crowds. The small crowds on the other hand survive because they are just as likely to gain vertices due to noisy behaviour

as they are to lose them, consequently they can live for long periods and change slightly each time.

For temperatures in the interval $1 \lesssim \beta/\beta_c \lesssim 1.5$ there is a positive correlation between initial size and lifetime. As the temperature decreases further the correlation coefficient become slightly negative. The decrease in noisy behaviour as the temperature drops allows large crowds to remain whole for longer while small crowds get converted by their larger neighbours, this results in the positive correlation. At even lower temperatures the small crowds become robust too and resist being absorbed by a larger crowd. Over time large crowds will collect lots of small crowds within them, this eventually shatters them. Small crowds do not undergo this process thus large crowds are destroyed by multiple processes causing them to die quicker.

On Watt-Strogatz graphs with low and high rewiring probabilities $p_{rw} \leq 0.010$ and $p_{rw} \geq 0.100$ the initial crowd size and total lifetime of a crowd are uncorrelated at all temperatures. However the graphs with medium amounts of rewiring exhibit strong correlations near the critical temperature $\beta/\beta_c \approx 1$, at lower temperatures they are mildly negatively correlated.

At temperatures near the critical value the noisiness is high enough to drive super-diffusive behaviour but low enough that large crowds do not shatter. Large crowds span multiple communities and so small-world links allow them to keep connected and not break apart into several pieces if a single vertex or group of vertices flip opinion. Small crowds on the other hand tend to be converted by the large crowds. This results in longer lifetimes for large crowds

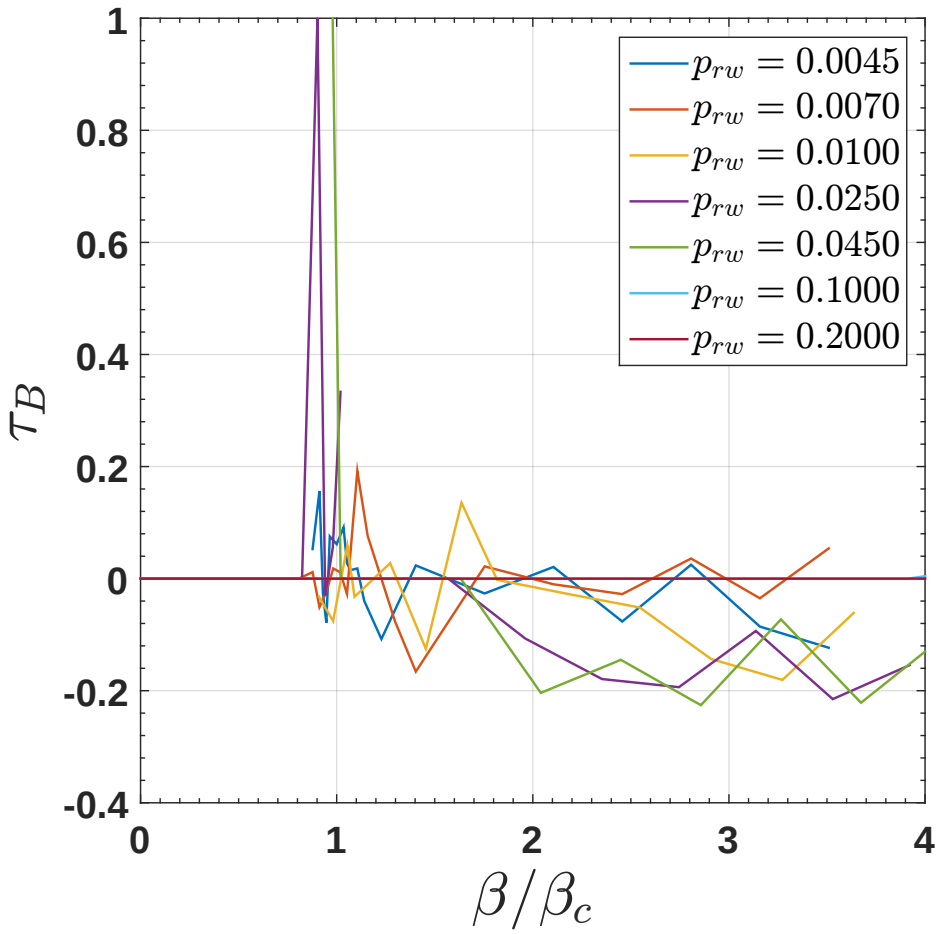


Figure 68.: The Kendall rank correlation coefficient plotted as a function of the scaled inverse temperature β/β_c for the initial population sizes $\mathcal{P}^0$ and total lifetimes $\mathcal{L}$ of crowds on Watts-Strogatz graphs, p_{rw} is the rewiring probability.

and shorter lifetimes for small ones. Thus starting with large results in longer lifetimes.

Once again at lower temperatures the small crowds become robust to both noise and being converted by larger crowds. Over time large crowds will gain a collection of small crowds within them which will eventually cause the large crowd to break apart. Consequently small crowds have long lifetimes and large crowds have short lifetime compared to their size.

In summary at high temperatures there is either no correlation or a negative one. In the region near the critical value large crowds feel the effects of a decrease in noisiness before small crowds thus they live longer. At lower temperatures small crowds become robust as well which allows them to live longer. Small crowds normally form due to noisy behaviour, by living longer large crowds are more likely to collect lots of small crowds this destroys them. This process does not occur on the rectangular lattice where the large crowds are very stable.

7.3 CURRENT CROWD POPULATION SIZE AND REMAINING LIFETIME

Figure 69 shows the Kendall rank correlation coefficient plotted as a function of the scaled inverse temperature β/β_c for the current population sizes $\mathcal{P}^t$ and remaining lifetimes $\Delta\mathcal{L} = \mathcal{L} - t$. The correlation coefficient is strongly negative for high temperatures $\beta/\beta_c \ll 1$ and increases linearly with the inverse temperature.

This suggests that at high temperatures crowds with a large size are more likely to undergo a process that causes them to change too much to continue to be considered the same crowd. Interestingly near the critical temperature $\beta/\beta_c \approx= 1$ the current size is uncorrelated with remaining lifetime suggesting size is not the determining factor in whether a crowd lives for a long time.

This runs contrary to the results in the previous section where the initial size definitely mattered.

At low temperatures $\beta/\beta_c \gg 1$ current size and remaining lifetime are moderately correlated. Crowds that start off small or become small are unlikely to live very long. Similarly crowds that are large or become large have a greater chance of living for a long time.

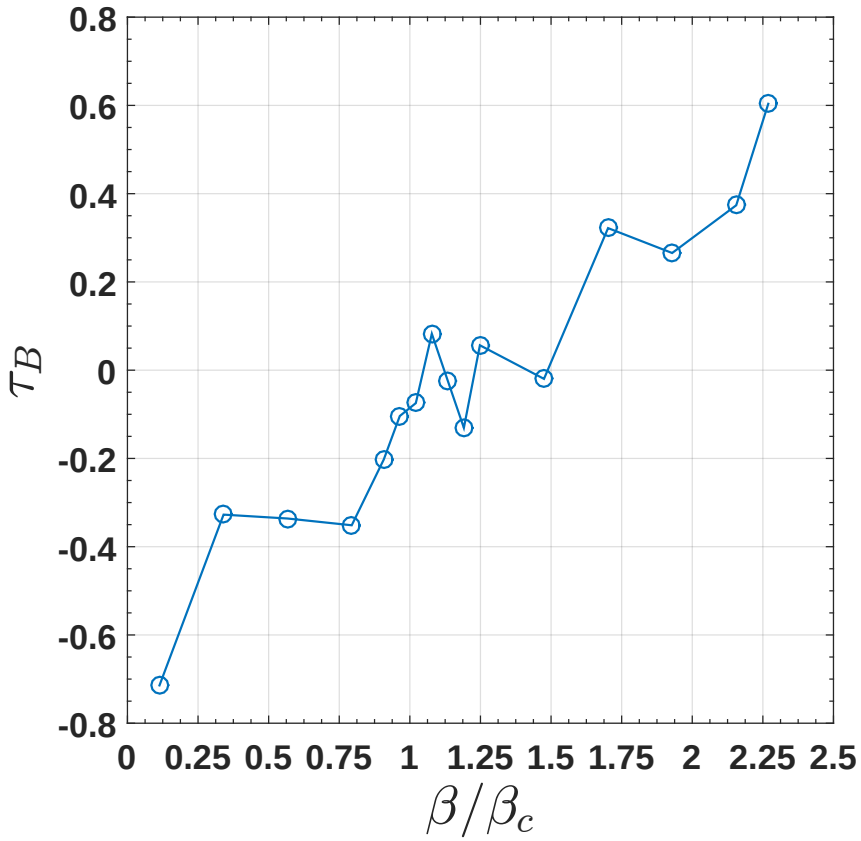


Figure 69.: The Kendall rank correlation coefficient plotted as a function of the scaled inverse temperature β/β_c for the current population sizes $\mathcal{P}^t$ and remaining lifetimes $\Delta\mathcal{L} = \mathcal{L} - t$ of crowds on the rectangular lattice.

The results for the circular lattice in figure 70 show that the current size and remaining lifetime is uncorrelated at all temperatures. Indicating that the current size provides no advantage for survival.

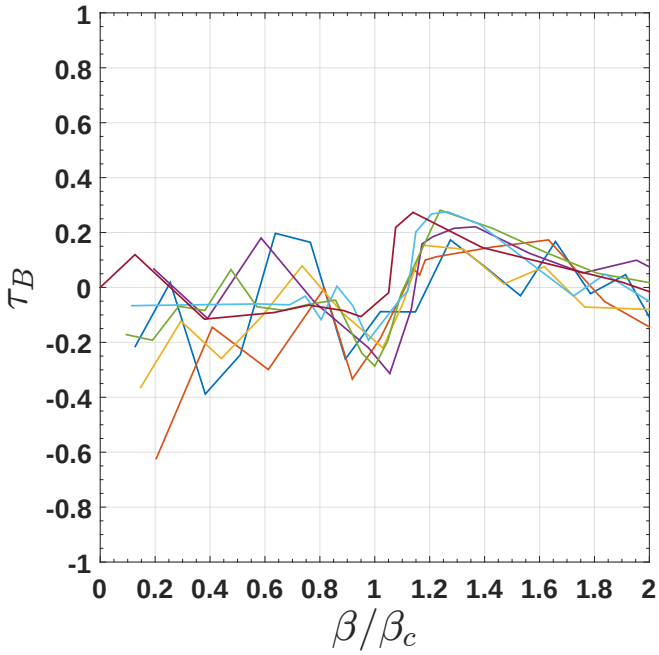
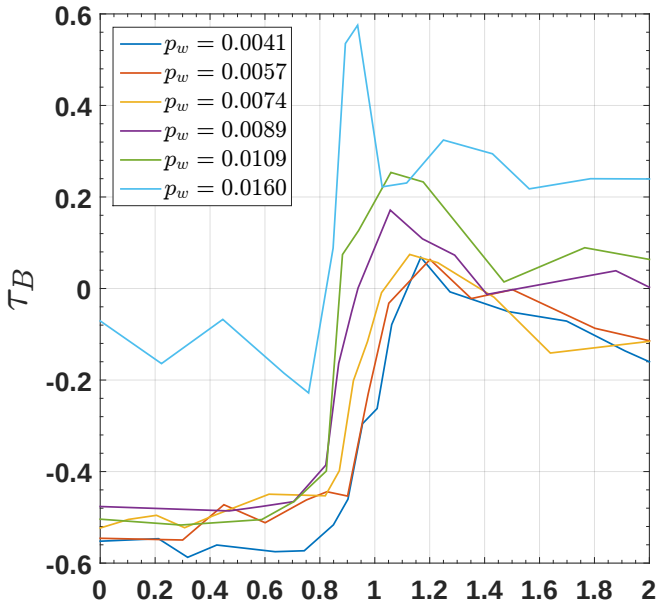


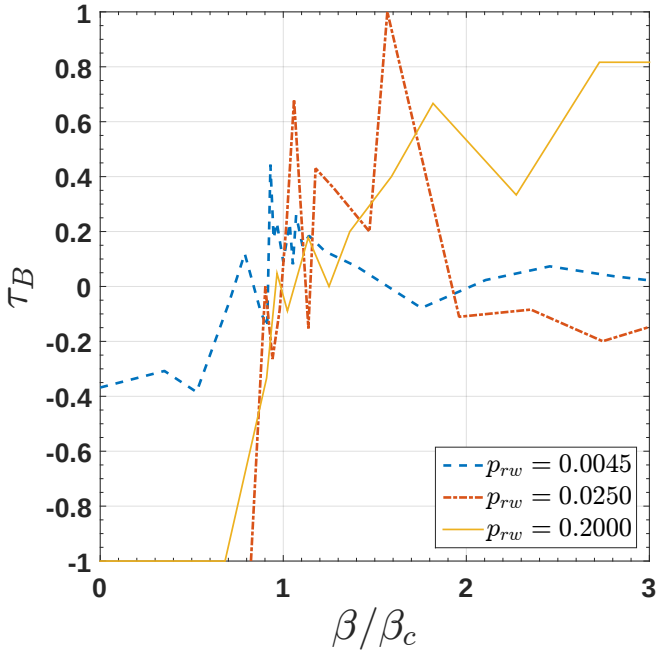
Figure 70.: The Kendall rank correlation coefficient plotted as a function of the scaled inverse temperature β/β_c for the current population sizes $\mathcal{P}^t$ and remaining lifetimes $\Delta\mathcal{L} = \mathcal{L} - t$ of crowds on the circular lattice graph. The results for the graphs with degrees k = 4,6, 8, 10, 12, 14, 16 been plotted together.

Figure 71a shows the results for the Erdős-Rényi graphs. At high temperatures the current size is moderately negatively correlated with the remaining lifetime. Thus large crowds live shorter lives. As $\beta/\beta_c \to 1$ the correlation coefficient rises sharply to 0. Thus for $\beta/\beta_c \gtrsim 1$ size does not determine lifetime. The $p_w = 0.0160$ behaves differently from the other graphs. As it is so highly connected there exists an unstable global consensus for $\beta/\beta_c < 0.8$ and a stable one for $\beta/\beta_c > 0.8$. Thus sizes do not matter for lifetimes at high temperatures but do for low ones.

Crowd sizes are moderately negatively correlated with remaining lifetime on Watts-Strogatz graphs with low wiring probabilities, see figure 71b, for $\beta/beta_c < 1$. For $\beta/\beta_c \geq 1$ they are uncorrelated. The structure of weakly



(a)



(b)

Figure 71.: The Kendall rank correlation coefficient plotted as a function of the scaled inverse temperature β/β_c for the current population sizes $\mathcal{P}^t$ and remaining lifetimes $\Delta\mathcal{L} = \mathcal{L} - t$ of crowds on the Erdős-Rényi graph (top) and Watts-Strogatz graph (bottom). p_w is the wiring probability and p_{rw} is the rewiring probability.

rewired WS graphs is similar to that of a circular lattice thus current size does impact the longevity of a crowd.

On WS graphs with larger rewiring probabilities $p_{rw} = 0.0250$ and 0.2000 the correlation coefficient is -1 for $\beta/\beta_c \lesssim 0.8$. A crowd that becomes large on such graphs are almost certain to die quickly. However at $\beta/\beta_c \to 1$ the correlation coefficients increase to 0 indicating there is no correlation at the critical temperature. For $\beta/\beta_c \gg 1$ the current size and remaining lifetimes are uncorrelated on the $p_{rw} = 0.0250$ graph but strongly correlated on the $p_{rw} = 0.2000$ graph.

As the wiring probability increases the graph become less like a CL and more like an ER graph. Larger crowds on such graphs span multiple communities and have lots of small-world links. At high temperatures where the majority of the crowds are small this allows large crowds to form but they are quickly destroyed by noise behaviour. Small crowds on the other hand can survive for longer as their lifetimes are independent of their interactions with neighbours.

At lower temperature the small-world links and small communities make large crowds robust against noise and interactions with neighbours as there are many ways for a large crowd to remain connected when vertices flip opinions. Small crowds do not span multiple communities thus do not have the same benefits. Consequently being large makes a crowd more stable and thus results in greater longevity.

To summarise becoming large provides a survival benefit on the rectangular lattice and Watts-Strogatz graph.

8

CONCLUSION AND FUTURE WORK

8.1 THESIS SUMMARY

In Chapter 1 we introduced the concept of opinion formation in groups of people as phenomenon which could be modelled using graphs and spin models. This was followed by a discussion of the literature were such models were successfully applied. To conclude we discussed the formation of consensus in a social network and why clusters of consensus are interesting and important to understand. We then outline the toy model we used to investigate the properties and behaviours of crowds.

The rest of the chapter covered the basic theory pertaining to this thesis. First we covered the definitions of the properties used to categorize graphs and then discussed the properties of the rectangular lattice, circular lattice, Erdős-Rényi, and Watts-Strogatz graph. We also defined the basic Ising and the more general Potts spin models. In the final section we explain the concept of communities in graph structure and methods of identifying them.

Chapter 2 provided further definitions, the key part is the definition of a crowd and its properties. The chapter also has details the exact properties of the systems we study and validate our implementation of the Ising model by comparing the critical values of the inverse temperature (β_c) we obtain against results found in the literature. We found that our implementation had good agreement with established results in all cases except for the circular lattice where our results were larger than the analytical results.

Starting with the third chapter we present the results of our study. The first property of we discuss is the root mean square change in crowd population size $[\Delta\mathcal{P}]_{\text{rms}}$ as a function of the crowd lifetime $\mathcal{L}$ for a range of inverse temperatures (β). These results indicated whether the crowd size changes were non-diffusive, sub-diffusive, diffusive or super-diffusive. We found that on the rectangular lattice crowds population dynamics ranged from non-diffusive at high temperatures, super-diffusive near the critical temperature and sub-diffusive at low temperatures. On the circular lattice the population sizes changed sub-diffusively at all temperatures while on the Erdős-Rényi graph they were non-diffusive at all inverse temperatures. Watts-Strogatz graphs had a Goldilocks region $0.2 \lesssim \beta \lesssim 0.35$ within which crowd populations changed ballistically and super-diffusively, at all other temperatures the dynamics were non-diffusive.

In the fourth and fifth chapters we analyse the frequency density distributions of the crowd population sizes $f.d.\,(\mathcal{P})$ and their lifetimes $f.d.\,(\mathcal{L})$. We found that the tails of the distributions crossed over from an exponential decay to a power law during temperatures where crowd-crowd interactions were dominant

and had a strong impact on the sizes and lifetimes of crowds. For crowds on the circular lattice and Erdős-Rényi graphs their population and lifetime frequency distributions were found to be dependent purely on the temperature and properties of the graph structure.

Chapter 6 we further analysed the maximum population size and lifetimes averaged over the simulation realisations. Our results for this section were mainly qualitative. The maximums were clearly influenced by the temperature and the general graph structure but we did not find good analytical functions which their response the temperature properly.

In the final results chapter we reported on the correlations between initial population size $\mathcal{P}^0$ of a crowd and its total lifetime $\mathcal{L}$, and the current population size $\mathcal{P}^t$ of a crowd and its remaining lifetime $\Delta\mathcal{L}$. To do this we used Kendall's τ-B correlation. The results indicated that crowds that started off large tended slightly to have short lifetimes at most temperatures. However near the critical value where crowds are behaving super-diffusively crowds with large initial populations tended to live longer.

In contrast, on the rectangular lattice at high temperatures analysis of the correlations between the current population size and remaining lifetime indicated that large crowds died quickly. The correlation coefficient τ_B increases linearly with β/β_c, thus as the temperature cools the current size of a crowd is a good indicator of long it would live for. Current population sizes did not correlate strongly with remaining lifetime on circular lattice graphs at all temperatures. The results for the ER graphs showed that at high temperatures the

correlation was moderately negative, at temperature near the critical value and blow it was uncorrelated on most the graphs. On the Watts-Strogatz graph large sizes at high temperatures meant short lifetimes, at the critical temperature there was no correlation and for lower temperatures it depended on the rewiring probability.

This work gives a description of how mesoscopic consensuses opinion interacts with each other in different artificial environments. It showed that they exhibit volatile and non-volatile changes in size while remaining well defined on the rectangular lattice. Further it found that the circular-lattice and Erdős-Rényi graphs were did not produce novel behaviour while the Watts-Strogatz graph did. Together the results suggest that crowds will show the most interesting behaviour on graphs where they will have lots of redundant routes of opinion reinforcement internally. Consequently when reinforcement paths are broken by vertices flipping opinion there are still other routes which allow vertices within a crowd to continue reinforcing each other. Such crowds will be more robust and thus longer lived allowing more time for interactions with neighbours. Ultimately this thesis provides a launching pad for more in depth studies which will be able to choose graphs with better suited structures to investigate.

8.2 RECOMMENDATIONS FOR FUTURE WORK

8.2.1 *Alternative Regular Graph Structures*

We have learned that the rectangular graph provided the greatest range of crowd dynamics. The next step would be to explore how other 2-d lattices would impact the crowd behaviour. The first choice is the triangular lattice, it has a clustering coefficient of $\frac{2}{7}$ but should increase the amount of reinforcement of opinions within a crowd and therefore their robustness to noise. On the other hand we also suggest using the hexagonal lattice which reduces the degree of the vertices making them more susceptible to noisy behaviour at lower temperatures. This may allow super-diffusive changes in crowd size to continue at even lower temperatures or make crowds too fragile to live long enough to interact.

Along the same lines 3-dimensional lattices would be a natural progression of this work. The boundaries between crowds would be much larger and would facilitate lots of boundary interactions. It would be much more difficult for crowds to settle into an equilibrium state which lead to different behaviours than what we have observed on the 2-d rectangular lattice.

8.2.2 *Alternative Modelling Approaches*

The concept of crowds is not limited to just the Ising model. The Potts model is a more general version of the Ising model has similar opinion forming mechanics but more than 2 opinion states. Introducing more opinion states into the system would make far more difficult for crowds of similar opinion to merge. An interesting question to answer is how many opinions need to be introduced before super-diffusive behaviour stops occurring on various lattices. There are also models to consider where a vertex can have varying levels of belief in competing opinions. For these models the definition of a crowd would have to be altered to allow for analysis. More abstractly we could also attempt to model crowds as area or volume taken up by immiscible fluids in a 2 or 3 dimensional container.

8.2.3 *Real World Data*

The last suggestion is to obtain data from real world social networks and analyse the comments to determine opinions and the consensuses that form. A network could be built to represent friendships based on frequent communication between users. A better source would be social media websites, these often have voting mechanics and users are encouraged share their opinions on topics posted. By analysing their past posts we can link users based on whether they frequently post in the same thread - weighting these links more heavily if they

communicate with each other often. In both cases the user opinions on a topic can be roughly determined by using a bag-of-words model to look for positive or negative reactions. There are other options also available: Massively Multi-player Online games provide a microcosm of the real world economy and social interactions however all the data can be made available for analysis; and census type data would be invaluable as we would be able to analyse whether crowd like behaviour occurs for education, religion, salary and ethnicity.

Appendices

A

THE HURST EXPONENT

A.1 INTRODUCTION

The Hurst exponent H can be used to categorise the dynamics of quantities which change over time and as a measure of the smoothness of a fractal time series [60, 61]. When $H < 1/2$ the time series is anti-persistent (the time series is likely to oscillate about a mean), if $H > 1/2$ then the time series is persistent (large values are more likely to be followed by large values while low values are more likely to be followed by low values), and when $H = 1/2$ the time series is Brownian. However there are issues with using the Hurst exponent it requires that time series used for analysis be fairly long, at least 128 time steps, and also that the smallest time slice be at least 8 time steps.

An estimate of the Hurst exponent can be made by splitting the time series up into n smaller time slices of length $T(n)$, $P = \{P_1(t), \ldots, P_i(t), \ldots, P_n(t)\}$, and calculating,

$$H = \frac{\ln(\mathrm{E}[R_i(n)/S_i(n)])}{\ln(T(n))}, \tag{78}$$

where $R_i(n)$ is the range and $S_i(n)$ is the standard deviation for the time series $P_i(t)$, thus $\mathrm{E}[R(n)/S(n)]$ is the expected value of the ratio of the rescaled range for time slices of length $T(n)$.

To calculate the range of a time series $P_i(t)$ we define the cumulative deviate series as,

$$Q_i(t) = \sum_{\tau}^{t} P_i(\tau) - \bar{P}_i, \tag{79}$$

where $\bar{P}_i = \frac{1}{T(n)} \sum_{t}^{T} (n) P_i(t)$ is the mean of the time slice i. Then we define the rescaled range for the time slice i as,

$$\begin{aligned} R_i(n) = &\max[Q_i(t=1), \ldots, Q_i(t=T(n))] \\ &- \min[Q_i(t=1), \ldots, Q_i(t=T(n))]. \end{aligned} \tag{80}$$

The standard deviation for a time slice is given by,

$$S_i(n) = \sqrt{\frac{1}{T(n)} \sum_{t}^{T(n)} (P_i(t) - \bar{P}_i)^2}. \tag{81}$$

We rescale the range by diving the range by the standard deviation, then the expected value for the rescaled range is,

$$\mathrm{E}\left[R\left(n\right)/S\left(n\right)\right] = \frac{1}{n}\sum_{i}^{n}\frac{R_i\left(n\right)}{S_i\left(n\right)}. \tag{82}$$

This is performed for each $n = 1, 2, 3, \ldots, \left\lfloor \frac{T}{8} \right\rfloor$.

While this is the simplest method it is not the only one nor is it always suitable. Estimates can also be found using wavelet packets [60].

A.2 RESULTS FOR THE RECTANGULAR LATTICE

We use the rescaled range method outlined in the introduction to estimate the Hurst exponents of the population size time series of individual crowds and aggregated them into frequency density plots. This analysis was only possible for a small range of inverse temperatures on the rectangular lattice as there were an insufficient number of crowds on the other graphs with long lifetimes.

In Figure 72 we show the frequency distribution of the Hurst exponent estimates over a range of inverse temperatures. At $\beta \approx \beta_c$ the majority of the crowds have $H \approx 0.5$ which indicates that their populations change diffusively. There are also a few crowds which are anti-persistent ($H < 0.5$), this gives further evidence to them undergoing frequent changes in population size. It does not however indicate anything about the size of the changes which should

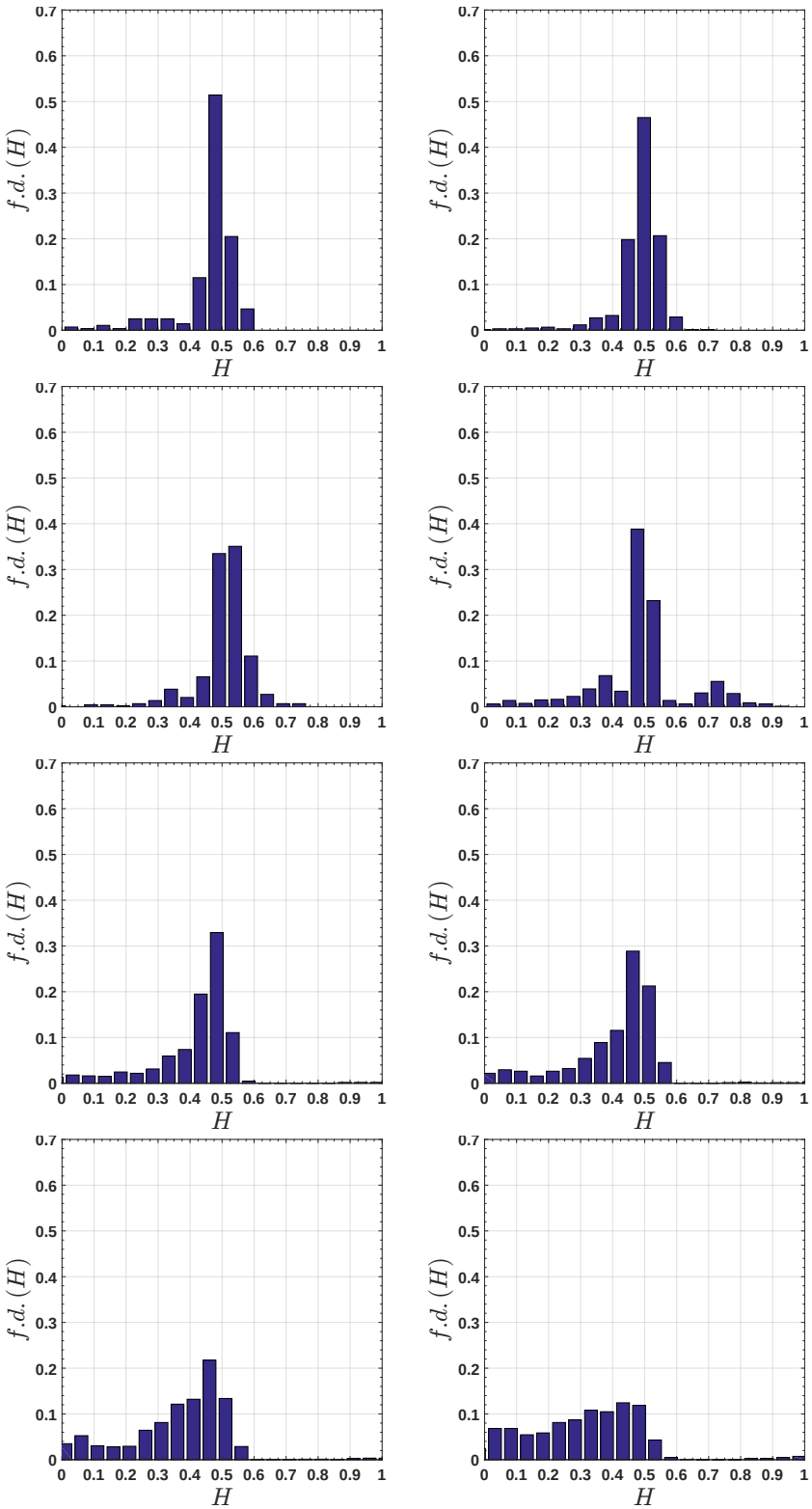


Figure 72.: The frequency density distributions of the estimated Hurst exponents $f.d.(H)$ for different inverse temperatures β. From left to right and top to bottom: $\beta = 0.450$, 0.475, 0.500, 0.550, 0.650, 0.750, 0.850, and 0.950.

are likely large as we know from Chapter 3 the population dynamics are super-diffusive.

As the inverse temperature increases the distribution spreads out and while the majority remain diffusive there are more crowds which are anti-persistent and persistent. This indicates that population size is still volatile at these β but some crowds are becoming more stable and do not change in size frequently.

At high inverse temperatures, $\beta \to 1$, we do not observe more persistent behaviour but instead more anti-persistent behaviour. This may seem counter intuitive until we consider what is occurring to the crowds over time. After quenching the crowds quickly reach unstable equilibriums with each other. Most of the changes in population occur at borders and they tend to move back and forth, this creates an oscillating population size which we observe as Hurst exponents that are less than 0.5.

The Hurst exponent on its own does not tell us much about how crowds behave but in conjunction with the results in Chapter 3 we can determine more without making assumptions.

B

GRAPH GENERATION ALGORITHMS

B.1 RECTANGULAR LATTICE

The rectangular lattice consists of vertices arranged into a Cartesian grid formation and edges are created between a vertex v and those immediately above, below, right, and left of v. To determine which vertices are neighbours of v we need to first identify its position in the grid thus we map the vertex id $v \in [0, W \cdot H)$ to 2-dimensional co-ordinates (x, y) where $x \in [0, W)$ and $y \in [0, H)$. The functions 83 and 84 return the column (x co-ordinate) and row (y co-ordinate) of a vertex v.

$$\mathrm{col}\,(v, W, H) = \{v\,(\mathrm{mod} H \cdot W)\}\,(\mathrm{mod}\ W)\,, \tag{83}$$

$$\mathrm{row}\,(v, W, H) = \left\lfloor \frac{v\,(\mathrm{mod}\ H \cdot W)}{W} \right\rfloor, \tag{84}$$

where H and W are the height and width of the lattice and $\lfloor x \rfloor = \max\{y \leq x \mid y \in \mathbb{Z}\}$ rounds the real number x down to the nearest integer y.

The non-periodic version of the graph can then be created by adding edges between vertices as long as they are adjacent in the same row,

$$\begin{aligned} \exists \{v, w\} \in G : (\mathrm{col}\,(v, W, H) = \mathrm{col}\,(w, W, H) \pm 1) \\ \wedge (\mathrm{row}\,(v, W, H) = \mathrm{row}\,(w, W, H))\,, \end{aligned} \tag{85}$$

or in the same column,

$$\begin{aligned} \exists \{v, w\} \in G : (\mathrm{row}\,(v, W, H) = \mathrm{row}\,(w, W, H) \pm 1) \\ \wedge (\mathrm{col}\,(v, W, H) = \mathrm{col}\,(w, W, H))\,. \end{aligned} \tag{86}$$

In the periodic case columns 1 and W are considered adjacent as are rows 1 and H, consequently we need to account for this. Thus equation 85 becomes,

$$\begin{aligned} \exists \{v, w\} \in G : [\mathrm{col}\,(v, W, H) = (\mathrm{col}\,(w, W, H) \pm 1) \bmod (W)] \\ \wedge (\mathrm{row}\,(v, W, H) = \mathrm{row}\,(w, W, H))\,, \end{aligned} \tag{87}$$

and equantion 86 becomes,

$$\begin{aligned} \exists \{v, w\} \in G : [\mathrm{row}\,(v, W, H) = (\mathrm{row}\,(w, W, H) \pm 1) \bmod (H)] \\ \wedge (\mathrm{col}\,(v, W, H) = \mathrm{col}\,(w, W, H))\,. \end{aligned} \tag{88}$$

Algorithm 1: Rectangular_Lattice(W,H, Periodic). W and H are positive integers and 'Periodic' is either true or false.

```
1  A ← 0_{N×N}
2  for i ← 0 to N − 1 do
3      for j ← 0 to N − 1 do
4          if Periodic then
5              if row(j, W, H) = { row(i, W, H) ±1 } (mod H ) then
6                  if col(j, W, H) = col(i, W, H) then
7                      A_ij ← 1, A_ji ← 1
8              if row(j, W, H) = row(i, W, H) then
9                  if col(j, W, H) = { col(i, W, H) ±1 } (mod W ) then
10                     A_ij ← 1, A_ji ← 1
11         else
12             if row(j, W, H) = row(i, W, H) ±1 then
13                 if col(j, W, H) = col(i, W, H) then
14                     A_ij ← 1, A_ji ← 1
15             if row(j, W, H) = row(i, W, H) then
16                 if col(j, W, H) = col(i, W, H) ±1 then
17                     A_ij ← 1, A_ji ← 1
18 return A.
```

B.2 CIRCULAR LATTICE

The circular lattice is simple to generate. Vertices are placed in a circle and edges exist between a vertices $v, w \in [0, N)$ if w is one of the K nearest neighbours of v,

$$\begin{aligned} \exists \{v, w\} \in G : & |v - w| \leq K/2 \\ & \vee |N + v - w| \leq K/2 \\ & \vee |v - (N + w)| \leq K/2. \end{aligned} \tag{89}$$

The pseudocode for this procedure is given in algorithm 2.

Algorithm 2: Circular_Lattice(N,K). Where N is the number of vertices and K is the number of nearest neighbours each vertex has.

```
A ← 0_{N×N}
for i ← 0 to N − 1 do
    for k ← 1 to K/2 do
        j ← (i + k) (mod N)
        A_ij ← 1, A_ji ← 1
return A.
```

B.3 ERDŐS-RÉNYI

There are two approaches to generating Erdős-Rényi graph, see Section 1.1.6. The first method samples graphs from the set of all graphs with N vertices and m edges and the other creates graphs with N vertices where each pair of vertices are connected by an edge with probability p_w. We implement the second generative method, however we use the parameter Z instead of p_w. By setting $p_w = N^{-Z}$ we can control the graph structure independently of its size N. Below is the pseudocode for generating Erdős-Rényi graphs.

Algorithm 3: Erdős_Rényi(N, Z)

```
1 A ← 0_{N×N}
2 p ← N^{-Z}
3 for i ← 0 to N − 1 do
4     for j ← i + 1 to N − 1 do
5         r ← U_ℝ [0, 1]
6         if r ≤ p then
7             A_ij ← 1, A_ji ← 1.
8 return A.
```

B.4 WATTS-STROGATZ GRAPHS

The Watts-Strogatz graph begins by creating a circular lattice and then half the edges of each vertex is rewired with probability p_{rw}. Rewiring creates small-world links in the graph and also breaks up the graph into communities. Algorithm 4 is the pseudo-code for generating the Watts-Strogatz graphs.

Algorithm 4: Watts_Strogatz(N,K,p_{rw})

```
1  A ←CircularLattice(N, K)
2  for i ← 0 to N − 1 do
3      for k ← 1 to K do
4          r ← U_ℝ [0, 1]
5          if r < p_rw then
6              A_ij ← 0, A_ji ← 0.
7              m ← i.
8              while m = i or A_im = 1 do
9                  m ← U_ℤ[0, N)
10             A_im ← 1, A_mi ← 1.
11 return A.
```

C

GRAPH ANALYSIS ALGORITHMS

C.1 BREADTH FIRST SEARCH

One of the most useful algorithms we came across was the Breadth First Search. Starting from a single vertex i it visits every vertex j which is reachable which means it is ideal for identifying graph components and with some small modifications it can also be used to find the lengths of the shortest paths, the number of shortest paths and crowds.

Given a graph $G(V, E)$ where V is the set of vertices in the graph and E the set of edges, let M be the set of marked vertices and N be the set of neighbours of the vertices in M that are not also in M,

$$N = \{w \mid w \notin M \wedge \exists v \in M : \{v, w\} \in E\}. \tag{90}$$

The procedure for the BFS is,

1. Begin with no marked vertices, $M = \emptyset$.

2. Visit some vertex i and mark it, $M = M \cup \{i\}$.

3. Identify the unvisited neighbours of the visited vertices, $N = \Big\{ j \mid \exists \{i, j\} \in E : i \in M, j \in V \backslash M \Big\}$.

4. Visit all the unvisited neighbours. $M = M \cup N$.

5. Repeat steps 3 and 4 until there are no more unvisited neighbours.

This will identify all the vertices that are in the same component as vertex i.

The pseudo-code given algorithm 5 executes these steps but also keeps track of the shortest distances and the number of them from the starting vertex s in the matrices $\boldsymbol{D}$ and $\boldsymbol{T}$ respectively. Further it also labels each vertex with a given component id c.

Algorithm 5: BFS($\boldsymbol{A}$, $\boldsymbol{D}$, $\boldsymbol{T}$, $\overrightarrow{C}$, c, s). $\boldsymbol{A}$ is the adjacency matrix, $\boldsymbol{D}$ is the shortest path length matrix, $\boldsymbol{T}$ is the number of shortest paths matrix, $\overrightarrow{C}$ is the component id vector, c is the component id, and s is the starting vertex.

```
1  Q ← ∅
2  Q push s
3  C_s ← c
4  D_ss ← 0
5  while Q ≠ ∅ do
6      v pull Q
7      for w ← 0 to N − 1 do
8          if A_vw = 1 then
9              C_w ← c
10             if D_sw ≥ D_sv + 1 then
11                 D_sw ← D_sv + 1
12                 T_sw ← T_sw + 1
13 return D, T, C.
```

Algorithm 6: CompleteBFS($\boldsymbol{A}_{N\times N}$)

```
1  c ← 0
2  C⃗ ← −1_{N×1}
3  D ← −1_{N×N}
4  T ← −1_{N×N}
5  for s ← 0 to N − 1 do
6      if C⃗_s = −1 then
7          c ← c + 1
8          D, T, C⃗ ← BFS(A, D, T, C⃗, c, s)
9      else
10         D, T, C⃗ ← BFS(A, D, T, C⃗, C⃗_s, s)
```

C.2 GIRVAN-NEWMAN

The Girvan-Newman algorithm, see Section 1.3, is used to identify communities in the graph structure, its procedure is relatively simple [47, 48]:

1. Compute the edge-betweenness of all edges in the graph.
2. Remove the edge with largest value of edge-betweenness.
3. Recompute the edge-betweenness of all edges effected by the removal of the edge.
4. Repeat steps 2 and 3 until no edges remain.

The edge-betweenness is defined as,

$$B_e = \sum_{i \neq j} \frac{g_{iej}}{g_{ij}},$$

where $g_{ij} = |\{\rho^*(i,j) \mid i,j \in G\}|$ the size of the set of all paths between vertices i and j and $g_{iej} = |\{\rho^*(i,j) \mid i,j \in G \wedge \exists v_x, v_{x+1} \in \rho i,j : v_x \in e, v_{x+1} \in e \backslash v_x\}|$ is the size of the set of all paths between i and j that uses the edge $e = \{v,w\}$. Notice that it needs to be recalculated each time an edge is removed, this is required as traffic gets rerouted through the graph in an unpredictable manner. Algorithm 7 is the pseudo-code for calculating th edge-betweenness for every edge in the graph.

The algorithm produces a dendrogram, where the root at the top represents the graph as a whole, each branch is the graph being split and the leaves at

Algorithm 7: Edge_Betweenness($\boldsymbol{A}$, $\boldsymbol{B}$, $\boldsymbol{D}$, $\boldsymbol{T}$, Ψ, s). $\boldsymbol{A}$ is the adjacency matrix, $\boldsymbol{B}$ is the matrix of edge-betweenness', $\boldsymbol{D}$ is the matrix of shortest path lengths, $\boldsymbol{T}$ is the matrix of number of shortest path lengths, $\Psi \in [-1, +1]$ determines whether a contribution the edge-betweenness is added or subtracted, s is the vertex for which the edge-betweenness is being calculated.

```
1 for d ← max(D_s1, ..., D_sj, ..., D_sN) to 0 do
2     for i ← 1 to N do
3         if D_si = d then
4             for j ← 1 to N do
5                 if A_ij = 1 and D_si = D_sj + 1 then
6                     B_ij ← B_ij + Ψ · T_sj / T_si
7 return B.
```

the bottom the individual vertices. A horizontal cut along any point of the dendrogram produces a partition of the graph into communities, by calculating the modularities of such partitions after each branching we can determine the best partition.

C.3 CNM

The CNM algorithm is a greedy algorithm for identifying communities in a graph's structure, see Section 1.3, its algorithmic procedure is:

1. Put each vertex into its own community.

2. Calculate the modularity of the current set of communities.

3. Calculate the change in modularity if a pair of communities were merged, do this for all possible pairs.

4. Merge the pair of communities with the largest positive change in modularity and repeat steps 2 and 3, otherwise if there are no pairs that can be merged which results in a positive change in modularity stop.

Where the modularity is defined as $Q = \sum_i \left(\boldsymbol{\mathcal{E}}_{ii} - a_i^2\right)$, with $\boldsymbol{\mathcal{E}}_{ij}$ being the fractional number of edges between communities i and j, and $a_i = \sum_j \boldsymbol{\mathcal{E}}_{ij}$ being the fraction of all edges connected to community i. The result is a dendrogram where the at the top it consists of as many roots as there are vertices and at the bottom is a partition of the graph into its communities.

D

ISING MODEL AND CROWD ALGORITHMS

D.1 ISING MODEL

Using the Hamiltonian function,

$$H(\sigma) = -\frac{1}{2}\sum_{i=1}^{N}\sum_{j=1}^{N} \boldsymbol{A}_{ij}\boldsymbol{J}_{ij}^{\text{int}}\sigma_i\sigma_j - \mu\sum_{i=1}^{N} J_i^{\text{ext}}\sigma_i$$

we can model a ferromagnetic material's spin configuration over time with two approaches. The first is a macroscopic method where spin configuration of the entire system is chosen during each time step at random according the probabilities given by equation 38. The procedure is,

1. Set $t = 0$.
2. Let $\sigma^{t=0}$ be a randomly chosen spin configuration.
3. Uniformly at random select one of the 2^N spin configurations, let it be referred to as σ^{pot}.

4. Uniformly at random pick a real number $r \in [0, 1)$.

5. If $r < P\left(\sigma^{\text{pot}}, \sigma^t\right)$ then go to step 6, otherwise go to step 3.

6. Set $\sigma^{t+1}\sigma^{\text{pot}}$ and set $t = t + 1$.

7. If $t \leq T$ go to step 3 otherwise stop.

By controlling the temperature one can cause the system to settle in a spin configuration with a low energy where the spins are all aligned. For a material with such spin configuration it would be magnetic. We shall discuss this further in Section 1.2.3. The second approach is microscopic where each vertex picks its spin state independently from the others during each time step where its procedure is,

1. Set t = 0.

2. Let $\sigma^{t=0}$ be a randomly chosen spin configuration.

3. Set i = 0;

4. Uniformly at random pick a real number $r \in [0, 1)$.

5. If $r < P\left(\sigma_i^{t+1} = -\sigma_i^t, \sigma_i^t\right)$ then set $\sigma_i^{t+1} = -\sigma_i^t$ otherwise set $\sigma_i^{t+1} = \sigma_i^t$.

6. If $i < N$ set $i = i + 1$ and go to step 4, otherwise continue.

7. If $t \leq T$ set $t = t + 1$ and go to step 3, otherwise stop.

In theory the results of the microscopic approach should be the similar to that of the macroscopic approach and what we choose depends on what level of detail we wish to observe. However this is only true when considering averages

of quantities and not in terms of configuration states of the system over time. In a macroscopic implementation as long as the energies of σ^t and σ^{t+1} are similar the configurations states themselves do not. This can be used to find or study the average properties of a system but is not useful if the time evolution is important. The microscopic approach allows each vertex to choose its spin consequently consecutive configuration states of the system tend to be very similar. Such an implementation would allow the study of properties which evolve over time but this can lead to more outlier results thus requiring more realisations than a macroscopic implementation.

During a time step each vertex chooses its spin state based only on the opinions of its neighbours in the previous time step. Thus we can compute the new opinions simultaneously, this requires thousands of float operations - something GPUs are very good at. We implement our Ising Model opinion function as a CUDA *kernel* which is executed on the GPU.

In our implementation we use equation 42 to calculate the probability of a vertex v flipping its opinion. The equation is reproduced here with a minor adjustments to the indexing,

$$P\left(\sigma_v^t = -\sigma_v^{t-1}, \sigma_v^{t-1}\right) = \frac{e^{-2\beta\left(2S_v^{t-1} - k_v\right)}}{1 + e^{-2\beta\left(2S_v^{t-1} - k_v\right)}}, \tag{91}$$

where $S_v^t = \sum_{j=1}^{N} \boldsymbol{A}_{vj} \delta\left(\sigma_v^t, \sigma_j^t\right)$ is the number of nearest neighbours with same opinion as v and k_v is v's degree.

Once we have obtained $p = P\left(\sigma_v^t = -\sigma_v^{t-1}, \sigma_v^{t-1}\right)$ we use generate a random number to see if the flip occurs. To do this a pseudo-random number generator

$\mathrm{U}_{\mathbb{R}}[0,1]$ picks a real number r between 0 and 1 uniformly at random. If $r \leq p$ then the opinion has flipped and if $r > p$ then the opinion stays the same. The pseudo-code is given in algorithm 8.

Algorithm 8: IsingModel($\boldsymbol{A}$, $\overrightarrow{k}$, $\boldsymbol{\Sigma}$, v, t, β). $\boldsymbol{A}$ is the adjacency matrix, $a\,\overrightarrow{k}$ is a vector containing the degrees of each vertex, $\boldsymbol{\Sigma}$ is the matrix of configuration spins, v is the vertex id, t is current time step, and β is the inverse temperature.

$S \leftarrow 0$
for $i \leftarrow 0$ **to** $N-1$ **do**
    if $\boldsymbol{A}_{vi} = 1$ **then**
        if $\boldsymbol{\Sigma}_{v,t-1} = \boldsymbol{\Sigma}_{i,t-1}$ **then**
            $S \leftarrow S + 1$
$H \leftarrow 2S - k_i$
$p \leftarrow exp(-2\beta H) / (1 + exp(-2\beta H))$
$r \leftarrow \mathrm{U}_{\mathbb{R}}[0,1]$
$\boldsymbol{\Sigma}_{vt} \leftarrow \boldsymbol{\Sigma}_{v,t-1}$
if $r \leq p$ **then**
    $\boldsymbol{\Sigma}_{vt} \leftarrow -\boldsymbol{\Sigma}_{v,t-1}$
return $\boldsymbol{\Sigma}$.

Algorithm 9: ClusterBFS($\boldsymbol{A}_{N\times N}$, $\boldsymbol{Z}_{N\times T}$, $\overrightarrow{P}_{N\times 1}$, t). $\boldsymbol{A}$ is the adjacency matrix, $\boldsymbol{Z}$ is the matrix of spin configurations, $\overrightarrow{P}$ is a vector containing crowd partitions for time step t, and t is the time step for which the graph is being partitioned.

```
1  c ← 0
2  for s ← 0 to N − 1 do
3      if P⃗_s = −1 then
4          Q⃖ ← ∅
5          Q⃖ push s
6          c ← c + 1
7          P⃗_s ← c
8          while Q⃖ ≠ ∅ do
9              v pull Q⃗
10             for w ← 0 to N − 1 do
11                 if A_vw = 1 and Z_vt = Z_wt and P⃗_w = −1 then
12                     Q⃖ push w
13                     P⃗_w ← c
14 return P⃗
```

D.2 CROWD EXTRACTION

Crowds are clusters of consensus on a graph which change over time, to be able to analyse them we need to extract individual crowds using the spin configuration $\boldsymbol{Z}_{N\times T}$ and adjacency matrix $\boldsymbol{A}_{N\times N}$.

The first step is to create graphs G^t for each time step where the edges between vertices with different spins have been removed, their adjacency matrices are defined as,

$$\boldsymbol{A}_{ij}^t = \boldsymbol{A}_{ij}\delta\left(\boldsymbol{Z}_{it}, \boldsymbol{Z}_{jt}\right), \tag{92}$$

where δ is the Kronecker delta function. Each graph G^t consists of a finite set of components $\left\{K_1^t, \ldots, K_i^t, \ldots\right\}$. The pseudo-code for partition a graph, $\boldsymbol{A}_{N\times N}$, into components using the spin configuration of the vertices $\boldsymbol{Z}_{N\times T}$ at time t is given in algorithm 9. The elements of the partition vector $\overrightarrow{P}_{N\times 1}$ are such that if $i = \overrightarrow{P}_v = \overrightarrow{P}_w$ then they are in the same component K_i^t.

Components K_i^t and K_j^{t+1} are part of the same crowd if more than 50% of their vertices are the same, i.e. $\Phi\left(K_i^t, K_j^{t+1}\right) > 0.7071$. Thus we define a matrix,

$$\boldsymbol{S}_{it} = (j+1)\,\mathcal{H}\left(\Phi\left(K_i^t, K_j^{t+1}\right) - 0.7071\right) - 1 : i, j \in \mathcal{Z}^+, \tag{93}$$

The i-th element $\boldsymbol{S}_{it} = j$ is the component in the next time step, K_j^{t+1}, which has more than 50% of the same vertices as K_i^t. If there is no component in the next time step which satisfies our conditions $\boldsymbol{S}_{it} = -1$. Algorithm 10 is the pseudo-code for computing the elements in the t-th column of $\boldsymbol{S}$, notice that the size of the matrix is $N \times T$, we use N as it is the maximum number of components a graph with N vertices can be partitioned into.

Our penultimate step is to collect components that are in the same crowd together. The matrix $\boldsymbol{S}_{N\times T}$ tells us which components in consecutive time

Algorithm 10: ComponentLinks($\boldsymbol{P}_{N\times T}$, t). $\boldsymbol{P}$ is the matrix of components, if elements $i = \boldsymbol{P}_{vt} = \boldsymbol{P}_{wt}$ then vertices v and w are in the same component i during time step t.

$\overrightarrow{S} \leftarrow \overrightarrow{-1}_{N\times 1}$

$\overrightarrow{K}^{t} \leftarrow \overrightarrow{0}_{N\times 1}$

$\overrightarrow{K}^{t+1} \leftarrow \overrightarrow{0}_{N\times 1}$

$\boldsymbol{R} \leftarrow \boldsymbol{0}_{N\times N}$

for $i \leftarrow 0$ **to** N **do**

  $c1 \leftarrow \boldsymbol{P}_{it}$

  $c2 \leftarrow \boldsymbol{P}_{i,t+1}$

  $\overrightarrow{K}^{t}_{c1} \leftarrow \overrightarrow{K}^{t}_{c1} + 1$

  $\overrightarrow{K}^{t+1}_{c2} \leftarrow \overrightarrow{K}^{t+1}_{c2} + 1$

  $\boldsymbol{R}_{c1,c2} \leftarrow \boldsymbol{R}_{c1,c2} + 1$

for $c1 \leftarrow 0$ **to** N **do**

  for $c2 \leftarrow 0$ **to** N **do**

    $\boldsymbol{R}_{c1,c2} \leftarrow \boldsymbol{R}_{c1,c2} / \left(\overrightarrow{K}^{t}_{c1} + \overrightarrow{K}^{t+1}_{c2} - \boldsymbol{R}_{c1,c2}\right)$

    if $\boldsymbol{R} > 0.7071$ **then**

      $\overrightarrow{S}_{c1} = c2$

return $\overrightarrow{S}$

steps are in the same crowd we can then define an intermediary matrix $\boldsymbol{L}_{N\times T}$ where every component that is part of the same crowd is given the same unique

Algorithm 11: CrowdLinksRec($\boldsymbol{S}$, $\boldsymbol{L}$, i, t, c). $\boldsymbol{S}$ is the matrix of component links, $\boldsymbol{L}$ is the matrix of crowd links, i is the component id, t is the time step, and c is the crowd id.

```
1 L_it ← c
2 if S_it > −1 then
3     j ← S_it
4     L ←CrowdLinksRec(S, L, j, t + 1, c)
5 return L
```

integer id. The procedure for this is recursive and is given in algorithm 11. The algorithm 12 initiates the recursive function.

Algorithm 12: CrowdLinks($\boldsymbol{S}$, $\boldsymbol{P}$). $\boldsymbol{S}$ is the matrix of component links and $\boldsymbol{P}$ is the matrix of consensus cluster components.

```
1 L ← −1_{N×T}
2 c ← 0
3 for t ← 0 to T − 1 do
4     for i ← 0 to max(P_{[0,N),t}) − 1 do
5         if S_it > −1 then
6             if L_it = −1 then
7                 c ← c + 1
8                 L ←CrowdLinksRec(S, L, i, t, c)
9 return L
```

Finally we define a matrix $bmC_{N\times T}$ where the element $c = \boldsymbol{C}_{vt}$ is the id of the crowd a vertex v is in during time step t,

$$\boldsymbol{C}_{vt} = \boldsymbol{L}_{it} \tag{94}$$

where $i = \boldsymbol{P}_{vt}$. The matrix $\boldsymbol{C}$ can then be used to analyse the properties of the crowds overt time. Algorithm 13 is the pseudo-code for the whole procedure and incorporates algorithms 9, 10 and 12. Large parts of the algorithm is parallelizable and this can reduce execution time at the expense of memory usage.

Algorithm 13: CrowdExtraction($\boldsymbol{A}_{N\times N}$, $\boldsymbol{Z}_{N\times T}$). $\boldsymbol{A}$ is the adjacency matrix, and $\boldsymbol{Z}$ is the matrix of spin configurations.

$\boldsymbol{P} \leftarrow -\mathbf{1}_{N\times T}$

$\boldsymbol{S} \leftarrow -\mathbf{1}_{N\times T}$

$\boldsymbol{L} \leftarrow -\mathbf{1}_{N\times T}$

$\boldsymbol{C} \leftarrow -\mathbf{1}_{N\times T}$

for all $t \in [0, T)$ **do in parallel**

  $\boldsymbol{P}_{[0,N),t} \leftarrow$`ClusterBFS(`$\boldsymbol{A}$, $\boldsymbol{Z}$`)`

for all $t \in [0, T)$ **do in parallel**

  $\boldsymbol{S}_{[0,N),t} \leftarrow$`ComponentLinks(`$\boldsymbol{P}$`)`

$\boldsymbol{L} \leftarrow$`CrowdLinks(`$\boldsymbol{S}$, $\boldsymbol{P}$`)`

for all $t \in [0, T)$ **do in parallel**

  for $v \leftarrow 0$ **to** $N - 1$ **do**

    $p \leftarrow \boldsymbol{P}_{vt}$

    $\boldsymbol{C}_{vt} \leftarrow \boldsymbol{L}_{pt}$

return $\boldsymbol{C}$

BIBLIOGRAPHY

[1] Matt J Keeling and Ken TD Eames. Networks and epidemic models. *Journal of the Royal Society Interface*, 2(4):295–307, 2005.

[2] Francisco C Santos, JF Rodrigues, and Jorge M Pacheco. Epidemic spreading and cooperation dynamics on homogeneous small-world networks. *Physical Review E*, 72(5):056128, 2005.

[3] Xuetao Wei, Nicholas Valler, B Aditya Prakash, Iulian Neamtiu, Michalis Faloutsos, and Christos Faloutsos. Competing memes propagation on networks: a case study of composite networks. *ACM SIGCOMM Computer Communication Review*, 42(5):5–12, 2012.

[4] Lilian Weng, Filippo Menczer, and Yong-Yeol Ahn. Virality prediction and community structure in social networks. *Scientific reports*, 3, 2013.

[5] Noah E Friedkin. Norm formation in social influence networks. *Social networks*, 23(3):167–189, 2001.

[6] Claudio Castellano. Social influence and the dynamics of opinions: The approach of statistical physics. *Managerial and Decision Economics*, 33 (5-6):311–321, 2012.

[7] Katarzyna Sznajd-Weron and Józef Sznajd. Opinion evolution in closed community. *International Journal of Modern Physics C*, 11(06):1157–1165, 2000.

[8] Americo T Bernardes, Dietrich Stauffer, and Janos Kertész. Election results and the sznajd model on barabasi network. *The European Physical Journal B-Condensed Matter and Complex Systems*, 25(1):123–127, 2002.

[9] Clément Sire and Satya N Majumdar. Coarsening in the q-state potts model and the ising model with globally conserved magnetization. *Physical Review E*, 52(1):244, 1995.

[10] Somendra M Bhattacharjee and Avinash Khare. Fifty years of the exact solution of the two-dimensional ising model by onsager. *Current science*, 69(10):816–821, 1995.

[11] Paulo RA Campos, Viviane M de Oliveira, and FG Brady Moreira. Small-world effects in the majority-vote model. *Physical Review E*, 67(2):026104, 2003.

[12] FWS Lima, UL Fulco, and RN Costa Filho. Majority-vote model on a random lattice. *Physical Review E*, 71(3):036105, 2005.

[13] Claudio Castellano, Santo Fortunato, and Vittorio Loreto. Statistical physics of social dynamics. *Reviews of modern physics*, 81(2):591, 2009.

[14] Sinan Aral and Dylan Walker. Identifying influential and susceptible members of social networks. *Science*, 337(6092):337–341, 2012.

[15] Thomas W Valente. Social network thresholds in the diffusion of innovations. *Social networks*, 18(1):69–89, 1996.

[16] Sergey N Dorogovtsev, Alexander V Goltsev, and José FF Mendes. Critical phenomena in complex networks. *Reviews of Modern Physics*, 80(4):1275, 2008.

[17] AK Nandi and SS Manna. A transition from river networks to scale-free networks. *New Journal of Physics*, 9(2):30, 2007.

[18] Peter Sheridan Dodds and Daniel H Rothman. Geometry of river networks. i. scaling, fluctuations, and deviations. *Physical Review E*, 63(1):016115, 2000.

[19] Peter Sheridan Dodds and Daniel H Rothman. Geometry of river networks. ii. distributions of component size and number. *Physical Review E*, 63(1): 016116, 2000.

[20] Steven H Strogatz. Exploring complex networks. *Nature*, 410(6825):268–276, 2001.

[21] Mark EJ Newman. Scientific collaboration networks. i. network construction and fundamental results. *Physical review E*, 64(1):016131, 2001.

[22] Benno Schwikowski, Peter Uetz, and Stanley Fields. A network of protein–protein interactions in yeast. *Nature biotechnology*, 18(12):1257–1261, 2000.

[23] BY ALBERT-LÁSZLÓ BARABÁSI and Eric Bonabeau. Scale-free. *Scientific American*, 2003.

[24] Réka Albert and Albert-László Barabási. Statistical mechanics of complex networks. *Reviews of modern physics*, 74(1):47, 2002.

[25] David Joyner, Minh Van Nguyen, and Nathann Cohen. Algorithmic graph theory. *Google Code*, 2010.

[26] Fan RK Chung and Linyuan Lu. *Complex graphs and networks*, volume 107. American mathematical society Providence, 2006.

[27] Philippe Blanchard and Dimitri Volchenkov. *Random Walks and Diffusions on Graphs and Databases: An Introduction*, volume 10. Springer Science & Business Media, 2011.

[28] Alain Barrat and Martin Weigt. On the properties of small-world network models. *The European Physical Journal B-Condensed Matter and Complex Systems*, 13(3):547–560, 2000.

[29] Stefano Boccaletti, Vito Latora, Yamir Moreno, Martin Chavez, and D-U Hwang. Complex networks: Structure and dynamics. *Physics reports*, 424 (4):175–308, 2006.

[30] Mark EJ Newman. The structure and function of complex networks. *SIAM review*, 45(2):167–256, 2003.

[31] Edgar N Gilbert. Random graphs. *The Annals of Mathematical Statistics*, 30(4):1141–1144, 1959.

[32] Paul Erdős and Alfréd Rényi. On random graphs. *Publicationes Mathematicae Debrecen*, 6:290–297, 1959.

[33] Duncan J Watts and Steven H Strogatz. Collective dynamics of 'small-world'networks. *nature*, 393(6684):440–442, 1998.

[34] Mark EJ Newman and Duncan J Watts. Scaling and percolation in the small-world network model. *Physical Review E*, 60(6):7332, 1999.

[35] Mark EJ Newman, Steven H Strogatz, and Duncan J Watts. Random graphs with arbitrary degree distributions and their applications. *Physical Review E*, 64(2):026118, 2001.

[36] Agata Fronczak, Piotr Fronczak, and Janusz A Hołyst. Average path length in random networks. *Physical Review E*, 70(5):056110, 2004.

[37] Stanley Milgram. The small world problem. *Psychology today*, 2(1):60–67, 1967.

[38] Lars Onsager. Crystal statistics. i. a two-dimensional model with an order-disorder transition. *Physical Review*, 65(3-4):117, 1944.

[39] J Viana Lopes, Yu G Pogorelov, JMB Lopes Dos Santos, and Raul Toral. Exact solution of ising model on a small-world network. *Physical Review E*, 70(2):026112, 2004.

[40] M Gitterman. Small-world phenomena in physics: the ising model. *Journal of Physics A: Mathematical and General*, 33(47):8373, 2000.

[41] RJ Baxter. Onsager and kaufman's calculation of the spontaneous magnetization of the ising model. *Journal of Statistical Physics*, 145(3):518–548, 2011.

[42] Daniel S Fisher and David A Huse. Equilibrium behavior of the spin-glass ordered phase. *Physical Review B*, 38(1):386, 1988.

[43] Fa-Yueh Wu. The potts model. *Reviews of modern physics*, 54(1):235, 1982.

[44] Rodney J Baxter. Potts model at the critical temperature. *Journal of Physics C: Solid State Physics*, 6(23):L445, 1973.

[45] Jordi Delgado. Emergence of social conventions in complex networks. *Artificial intelligence*, 141(1):171–185, 2002.

[46] Luiz FC Pereira and FG Brady Moreira. Majority-vote model on random graphs. *Physical Review E*, 71(1):016123, 2005.

[47] Mark EJ Newman and Michelle Girvan. Finding and evaluating community structure in networks. *Physical review E*, 69(2):026113, 2004.

[48] Michelle Girvan and Mark EJ Newman. Community structure in social and biological networks. *Proceedings of the National Academy of Sciences*, 99(12):7821–7826, 2002.

[49] Huawei Shen, Xueqi Cheng, Kai Cai, and Mao-Bin Hu. Detect overlapping and hierarchical community structure in networks. *Physica A: Statistical Mechanics and its Applications*, 388(8):1706–1712, 2009.

[50] Aaron Clauset, Mark EJ Newman, and Cristopher Moore. Finding community structure in very large networks. *Physical review E*, 70(6):066111, 2004.

[51] Gabor Csardi and Tamas Nepusz. The igraph software package for complex network research. *InterJournal*, Complex Systems:1695, 2006. URL `http://igraph.org`.

[52] Hung T Diep. *Frustrated spin systems*. World Scientific, 2004.

[53] A Messager and S Miracle-Sole. Equilibrium states of the two-dimensional ising model in the two-phase region. *Communications in Mathematical Physics*, 40(2):187–196, 1975.

[54] Ralf Metzler and Joseph Klafter. The random walk's guide to anomalous diffusion: a fractional dynamics approach. *Physics reports*, 339(1):1–77, 2000.

[55] Loukas Vlahos, Heinz Isliker, Yannis Kominis, and Kyriakos Hizanidis. Normal and anomalous diffusion: A tutorial. *arXiv preprint arXiv:0805.0419*, 2008.

[56] Dirk P Kroese, Thomas Taimre, and Zdravko I Botev. *Handbook of Monte Carlo Methods*, volume 706. John Wiley & Sons, 2013.

[57] Andrzej Pękalski. Ising model on a small world network. *Physical Review E*, 64(5):057104, 2001.

[58] MATLAB. *Version 8.5.0.197613 (R2015a)*. The MathWorks Inc., 2015.

[59] Allen Rubin. *Statistics for evidence-based practice and evaluation*. Cengage Learning, 2012.

[60] Zhiguo Wang, Dechun Guo, Xi Li, and Yuanchun Fei. Estimating hurst exponent with wavelet packet. In *Computer-Aided Industrial Design and Conceptual Design, 2006. CAIDCD'06. 7th International Conference on*, pages 1–4. IEEE, 2006.

[61] Ludmila Kirichenko, Tamara Radivilova, and Zhanna Deineko. Comparative analysis for estimating of the hurst exponent for stationary and nonstationary time series. *Information Technologies & Knowledge*, 5(1):371–388, 2011.